UNIVERSIDADE ESTADUAL DE CAMPINAS
INSTITUTO DE QUÍMICA

CARLOS MARROTE MANZANO

NEW METAL COMPLEXES WITH ANTHRANILIC ACID DERIVATIVES AND CYCLOSERINE: SYNTHESIS, CHARACTERIZATION AND EVALUATION OF THEIR BIOLOGICAL ACTIVITIES.

NOVOS COMPLEXOS METÁLICOS COM DERIVADOS DO ÁCIDO ANTRANÍLICO E CICLOSERINA: SÍNTESE, CARACTERIZAÇÃO E AVALIAÇÃO DE SUAS ATIVIDADES BIOLÓGICAS.

CAMPINAS
2022

CARLOS MARROTE MANZANO

NEW METAL COMPLEXES WITH ANTHRANILIC ACID DERIVATIVES AND CYCLOSERINE: SYNTHESIS, CHARACTERIZATION AND EVALUATION OF THEIR BIOLOGICAL ACTIVITIES.

NOVOS COMPLEXOS METÁLICOS COM DERIVADOS DO ÁCIDO ANTRANÍLICO E CICLOSERINA: SÍNTESE, CARACTERIZAÇÃO E AVALIAÇÃO DE SUAS ATIVIDADES BIOLÓGICAS.

Tese de Doutorado apresentada ao Instituto de Química da Universidade Estadual de Campinas como parte dos requisitos exigidos para a obtenção do título de Doutor em Ciências

Doctor's thesis presented to the institute of Chemistry of the University of Campinas as part of the requirements to obtain the title of Doctor in Sciences

Supervisor: Prof. Dr. Pedro Paulo Corbi

O arquivo digital corresponde à versão final da Tese defendida pelo aluno Carlos Marrote Manzano e orientada pelo Prof. Dr. Pedro Paulo Corbi

CAMPINAS

2022

Ficha catalográfica
Universidade Estadual de Campinas
Biblioteca do Instituto de Química
Simone Luiz Alves - CRB 8/9094

M319n

Manzano, Carlos Marrote, 1993-
New metal complexes with anthranilic acid derivatives and cycloserine : synthesis, characterization and evaluation of their biological activities / Carlos Marrote Manzano. – Campinas, SP : [s.n.], 2022.

Orientador: Pedro Paulo Corbi.
Tese (doutorado) – Universidade Estadual de Campinas, Instituto de Química.

1. Prata. 2. Cobre. 3. Paládio. 4. Agentes antiinfecciosos. 5. Compostos antitumorais. I. Corbi, Pedro Paulo, 1974-. II. Universidade Estadual de Campinas. Instituto de Química. III. Título.

Informações para Biblioteca Digital

Título em outro idioma: Novos complexos metálicos com derivados do ácido antranílico e cicloserina : síntese, caracterização e avaliação de suas atividades biológicas
Palavras-chave em inglês:
Silver
Copper
Palladium
Anti-infective agents
Antitumoral compounds
Área de concentração: Química Inorgânica
Titulação: Doutor em Ciências
Banca examinadora:
Pedro Paulo Corbi [Orientador]
Paulo Cesar de Sousa Filho
Wdeson Pereira Barros
Flávia Aparecida Resende Nogueira
Alexandre Cuin
Data de defesa: 21-02-2022
Programa de Pós-Graduação: Química

Identificação e informações acadêmicas do(a) aluno(a)
- ORCID do autor: https://orcid.org/0000-0002-0969-223X
- Currículo Lattes do autor: http://lattes.cnpq.br/2313056299380984

BANCA EXAMINADORA

Prof. Dr. Pedro Paulo Corbi (Orientador - IQ/ UNICAMP)

Prof. Dr. Paulo Cesar de Sousa Filho (IQ/ UNICAMP)

Prof. Dr. Wdeson Pereira Barros (IQ/ UNICAMP)

Dra. Flávia Aparecida Resende Nogueira (Universidade de Araraquara)

Dr. Alexandre Cuin (Universidade Federal de Juiz de Fora)

A Ata da defesa assinada pelos membros da Comissão Examinadora consta no SIGA/Sistema de Fluxo de Dissertação/Tese e na Secretaria do Programa da Unidade.

Este exemplar corresponde à redação final da Tese de Doutorado defendida pelo aluno Carlos Marrote Manzano, aprovada pela Comissão Julgadora em 21 de fevereiro de 2022

Agradecimentos

À minha familia e amigos pelo apoio ao longo desses anos, especialmente meus pais, irmãos e minha querida companheira;

Ao meu orientador Prof. Dr. Pedro Paulo Corbi, meu pai científico e querido amigo ao qual serei sempre grato;

A todos os meus colegas de laboratório que estiveram comigo ao longo dos últimos 10 anos e que fizeram o ambiente de trabalho sempre mais agradável;

Ao Prof. Dr. Wilton R. Lustri pela longa e produtiva colaboração científica, especialmente em relação aos ensaios antibacterianos;

À Profa. Dra. Flávia Resende Nogueira pela colaboração nos experimentos de avaliação de mutagenicidade e atividade antitumoral;

Ao Prof. Dr. Fernando Pavan pela colaboração no desenvolvimento dos ensaios antimicobacterianos;

Ao Prof. Dr. Douglas Nakahata e Dr. Raphael Enoque, não somente pelas colaborações nesse trabalho, mas também pela parceria em outros projetos que enriqueceram minha formação;

Ao Instituto de Química da UNICAMP e os técnicos que me auxiliaram nesse trabalho, entre eles Acacia Salomão, Diego Campaci, Anderson Santos, Gustavo Shimamoto, Déborah Simoni, Sonia, Fabi, Cláudia Martelli, Raquel Miller, Carol Galuppo, Priscila, entre outros.

Aos professores do IQ da UNICAMP com os quais tive o prazer de aprender, seja em aulas, laboratórios ou bancas;

À Fundação de Amparo à Pesquisa do estado de São Paulo (FAPESP) pela bolsa concedida. Processo: 2017/25995-6

Ao apoio da Coordenação de Aperfeiçoamento de Pessoal de Nível Superior – Brasil (CAPES) – Código de Financiamento 001

Resumo

A tuberculose é a doença infecciosa que mais mata no mundo e a crescente resistência de bactérias aos mais diversos antibióticos torna essa doença, causada pelo patógeno *Mycobacterium tuberculosis*, um problema urgente de saúde global. Uma estratégia para superar esse desafio é o desenvolvimento de novos complexos metálicos com atividade antibacteriana, pois os íons metálicos tem o potencial de atuar com eficácia em diversos alvos moleculares da bactéria. Para isso foram sintetizados e caracterizados complexos de Ag(I) com ligantes isômeros de ácidos fluoroantranílicos, cuja a atividade contra cepas de *M. tuberculosis* resistentes e formadoras de biofilme é reportada na literatura. Quatro complexos denominados de Ag4fa, Ag5fa, Ag6fa e Ag4,5fa foram caracterizados por análises elementar e termogravimétrica, espectrometria de massas (EM), espectroscopia no infravermelho (IV) e de ressonância magnética nuclear (RMN) de ^{1}H, ^{13}C e {^{15}N,^{1}H}, que revelaram uma proporção 1:1 metal:ligante e coordenação pelos átomos de nitrogênio do grupo amina e de oxigênio do carboxilato. A estrutura cristalina do complexo Ag5fa resolvida por difração de raios X (DRX) de monocristal confirma esses resultados e revela uma estrutura polimérica do complexo. Foi observada pronunciada atividade *in vitro* dos complexos Ag4fa, Ag5fa e Ag6fa frente a *M. tuberculosis* (MIC90 entre 2,6 e 4,2 μg/mL) e moderada contra outras bactérias Gram positivas e Gram negativas. Além disso, esses complexos também exibiram citotoxicidade *in vitro* para diversas células tumorais, em especial para adenocarcinoma epitelial colorretal (IC_{50} = 2,1 μg/mL e SI >3) e não foram capazes de causar mutagenicidade como evidenciado pelo teste de Ames. Os ligantes fluoroantranílicos também foram um objeto de estudo teórico por DFT, relacionando os resultados dos cálculos com as suas propriedades espectroscópicas de fluorescência e também por *docking* molecular afim de prever interações distintas de cada isômero fluoroantranílico com proteínas alvo pertencentes à via de biossíntese do triptofano em bactérias *M. tuberculosis*. Além disso, uma série de complexos de Cu(II) com 6fa e ligantes auxiliares (bipiridina, fenantrolina e 4,4'-dimetilbipiridina) e um complexo de Pd(II) com o fármaco antimicobacteriano cicloserina também foram sintetizados. Apesar da atividade biológica desses complexos ainda não ter sido avaliada, a caracterização dos mesmos é apresentada com uma perspectiva de novos trabalhos para investigá-los com mais detalhes não só na parte estrutural, mas também como potencial aplicação na química medicinal.

Abstract

Tuberculosis is a disease caused by the pathogen *Mycobacterium tuberculosis*. It is one of the infectious diseases that most kills worldwide and the emerging bacterial resistance to the most diverse antibiotics makes it an urgent global health problem. One strategy to overcome this challenge is the development of new metal complexes with antibacterial activity, as metal ions have the potential to effectively affect several molecular targets inside the bacterial cell. For this purpose, fluoroanthranilic acid isomers were selected as ligands due to their activity against resistant and biofilm-forming *M. tuberculosis*. Four complexes identified as Ag4fa, Ag5fa, Ag6fa and Ag4,5fa were characterized by elemental and thermogravimetric analysis, mass spectrometry (MS), infrared (IR) and ^{1}H, ^{13}C and {^{15}N,^{1}H} nuclear magnetic resonance (NMR) spectroscopy, which revealed a 1:1 metal:ligand ratio and coordination by the nitrogen atoms of the amine moiety and oxygen atoms of the carboxylate group. The crystal structure of the Ag5fa complex was determined by single crystal X-ray diffraction (XRD) confirming the proposed structure and revealing a polymeric structure for this complex. Significant *in vitro* activity of Ag4fa, Ag5fa and Ag6fa complexes was observed against *M. tuberculosis* (MIC90 between 2.6 and 4.2 μg/mL), while the activity was lower against other Gram-positive and Gram-negative bacteria. In addition, the complexes also exhibited *in vitro* cytotoxicity against several tumor cells, especially colorectal epithelial adenocarcinoma (IC50 = 2.1 μg/mL and SI >3) and were not mutagenic according to Ames test. Fluoroanthranilic ligands were also object of theoretical study by density functional theory (DFT) by comparing the calculated data with their spectroscopic properties of fluorescence, and also by molecular docking in order to predict distinct interactions of each fluoroanthranilic isomer with target proteins of the tryptophan biosynthesis pathway in *M. tuberculosis* bacteria. Furthermore, a series of Cu(II) complexes with 6fa and auxiliary ligands (bipyridine, phenanthroline and 4,4'-dimethylbipyridine) and one complex of Pd(II) with the antimycobacterial drug cycloserine were also synthesized. Although the biological activity of these complexes has not yet been evaluated, their characterization is presented here as a perspective for new projects, as such complexes could be further investigated, not only structurally, but also as potential active compounds in medicinal chemistry.

List of Figures

List of Tables

Summary

I. Introduction

1. General aspects

Tuberculosis (TB) is an infectious disease caused by the bacteria *Mycobacterium tuberculosis*, that affects the lungs and causes intense coughing, fever, weight loss and can lead to death [1,2]. It is believed that one third of the world population have latent tuberculosis, meaning that these people are infected with the bacteria but do not feel the symptoms nor are able to transmit the disease. However, about 10% of the latent tuberculosis cases are at risk of becoming active. That risk is much higher in individuals with deficient immunologic systems, as HIV positive, diabetics, smokers or undernourished [1,3].

According to the most recent Tuberculosis Report (2020) from World Health Organization (WHO), the investments in treatment and prevention of tuberculosis are insufficient to surpass the global epidemic [4,5], as TB is the infectious disease that most kills worldwide, even more than AIDS. There was a cumulative reduction of cases between 2015 and 2019 of only 9%, which is far from the necessary 20% reduction expected by WHO. In 2019, an estimated 10.0 million people fell ill with TB and about half a million new cases of rifampicin-resistant TB were registered (of which 78% had multidrug resistant TB) and 17.7% of previously treated cases evolved to multidrug resistant TB or rifampicin-resistant TB (MDR/RR-TB).[5] Similarly, the cumulative reduction in deaths between 2015 and 2019 was 14% while the milestone set by WHO was of 35% for 2020.

This increasing acquired resistance is associated with the hard treatment of TB, which takes 6 months and requires 4 to 5 antibiotics[6] that have to be meticulously administrated. The patients that abandon the treatment, or have their health impaired by other factors, end up collaborating to the increase of the bacterial resistance to commercial drugs, which then become ineffective[7]. Another important factor to be highlighted is the treatment cost worldwide as, according to the WHO, 49% of people with TB and 80% of people with drug-resistant TB face catastrophic costs (when the total cost of treatment is equivalent to more than 20% of annual household income). [5]

Currently, the first line drugs for TB are rifampicin and isoniazid, while the class of the fluoroquinolones and injectables, such as amikacin, kanamycin and capreomycin, are considered second line drugs. The classification of resistance is based in these drugs, once MDR-TB strains are resistant to at least two first line drugs and XDR-TB strains are resistant not only to the first line drugs, but also to one fluoroquinolone and one injectable drug from the second line collection [8]. For that reason, in the MDR-TB and XDR-TB

cases the use of second line drugs are of great importance. Also, the role of the second line drugs, and also newly developed drugs, is expected to be essential in the near future when we consider the increasing of bacterial resistance [6,9].

The scenario of emerging multiresistant bacterial strains due to uncontrolled usage of antibiotics is a global case of concern. A strategy to overcome resistance mechanisms is to combine bioactive compounds and metal ions with well-known antimicrobial activities to synthesize new metal complexes. The novel molecules, which may present new mechanisms of action and additive or synergic effects[10], may interfere in different phases of cell growth or division, avoiding the emergence of resistance of the bacterial strains against the coordination compound[11,12]. So, metal compounds have been considered to overcome the bacteria multiresistance [13].

In 2020 is also important to consider the impact of the COVID-19 pandemic in other diseases, such as TB. The number of TB deaths could increase significantly due to the health service disruption in many countries and also the reallocation of human, financial and other resources from TB to the COVID-19 response, as for example the use of GeneXpert machines for COVID-19 testing instead of diagnostic testing for TB.[5] One immediate consequence of this scenario is that in India, Indonesia and the Philippines, the reported number of people diagnosed with TB between January and June 2020 dropped more than 50% as shows Figure 1, which was extracted from the Global Tuberculosis Report 2020 (WHO).[5]

It is possible that between 200,000 and 400,000 excess TB deaths could be observed in 2020, setting back the fight against this disease in 5 to 7 years, without considering the risk of increase in bacteria resistance. [5] Therefore, more than ever, it is imperative to develop new and more efficient drugs, not only against TB and resistant-TB, but all kind of bacterial infections[14].

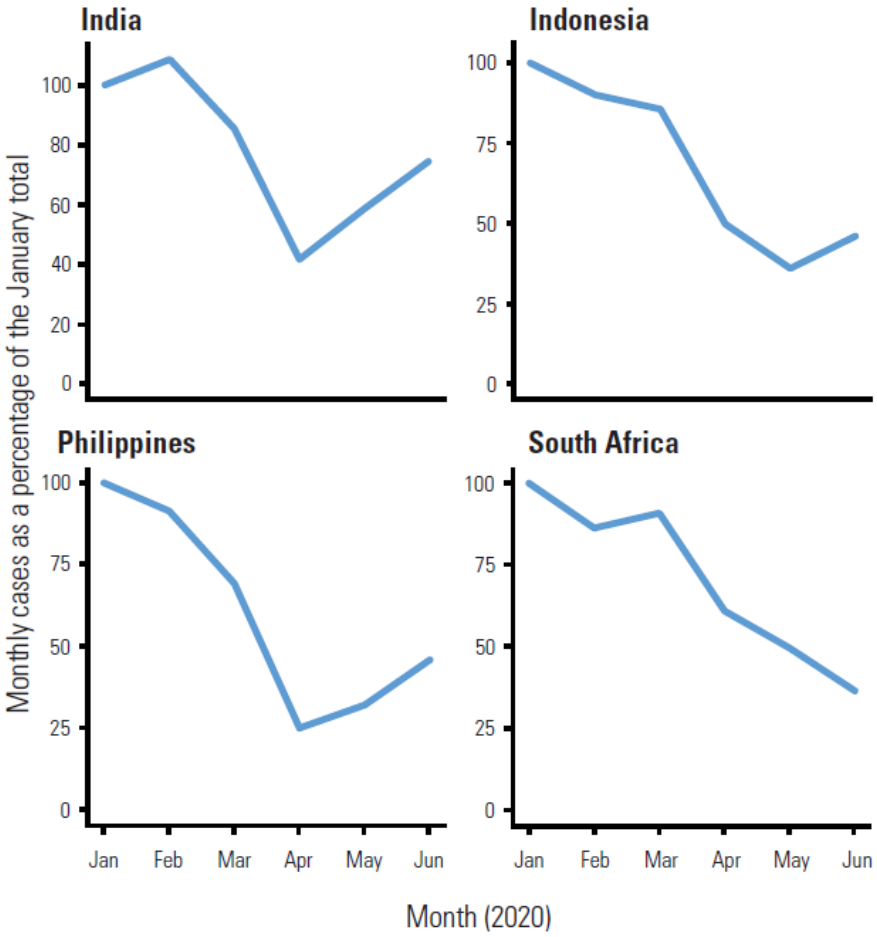

Figure 1. Trends in monthly notifications of people diagnosed with TB in the four highest TB burden countries in the world, January–June 2020. Image from the Global Tuberculosis Report 2020 (WHO).

The development of new drugs is expected to be essential in the near future when considering the increase of bacterial resistance to *M. tuberculosis* [6,9]. One strategy to overcome the resistance mechanisms is to combine bioactive compounds and metal ions with well-known antimicrobial activity [13]. Novel coordination compounds may be designed to have new mechanisms of action and additive or synergic effects [10], or interfere in different phases of bacterial growth and division [11,12].

2. Metals in Medicine

The use of metals in medicine is not a new concept. Ancient Greek, Egyptian and Chinese civilizations used metals such as silver, copper and gold empirically for medicinal purposes [15,16]. In special, the antimicrobial activity of silver is well established.[17] There are records of its usage in the 17th century, when silver nitrate was prescribed against ulcers and skin wounds [18]. Later, in the 1960's, silver nitrate solutions (0.5%) were used in conjunction to α-amino-p-toluenosulfonamide monoacetate (sulfamylon/mafenide) to treat infections in skin burns[19]. A few years later, silver sulfadiazine was synthesized and a remarkable improvement in the way that skin infections were treated was achieved. Nowadays, silver sulfadiazine is still frequently prescribed for the treatment of severe burns [20].

The success of silver sulfadiazine encouraged the scientific community to study new Ag(I) complexes for medicinal purposes. Recently, many examples of Ag(I) complexes active against Gram-positive and Gram-negative bacteria were reported[15,21–27]. In addition, the Ag(I) complexes have also being evaluated for their antitumoral activities due to their capacity to selectively inhibit the growth of certain cancer cell strains[22,25,27–32].

Another milestone of the history of inorganic chemistry in medicine is the discovery of the antitumoral activity of cisplatin, or cis-diamminedichloridoplatinum(II). In the 1960's, Barnett Rosenberg *et al*. showed that cisplatin was able to inhibit cell division in *Escherichia coli* strains[33]. Later, the same group discovered its remarkable antitumoral activity [15,34]. Nowadays, cisplatin and their derivatives (carboplatin and oxaliplatin) are used in 50% of all anticancer chemotherapies worldwide and are particularly important against lung, head, neck, testicle and ovary cancers [15,34–36].

Complexes with Pd(II) have also being considered as new antitumoral and antibacterial agents due to their structural similarity to Pt(II) complexes and their high antitumor and antimicrobial activities *in vitro* and *in vivo* [37]. Usually, Pd(II) complexes have a faster ligand exchange rate than the Pt(II) analogs. This may cause early hydrolysis of the complex, leading to higher toxicity and poorer biological distribution of the compound. Therefore, chelating ligands are usually chosen to stabilize the Pd(II) complexes [15,38].

Although Pt(II) and Pd(II) complexes are frequently associated with antitumor rather than antibacterial activity, it is worth to notice their antibacterial activities [39–41],

especially when dealing with the problem of bacterial multiresistance. In this case, the Pt(II) and Pd(II) ions may offer different mechanisms to overcome bacterial infections (similarly to what is observed for silver complexes). However, the high toxicity of such compounds is the main challenge when searching for new Pd(II) and Pt(II) complexes against infectious diseases.

Coordination compounds have been studied regarding their activity against *M. tuberculosis*. Recent examples are metal complexes of Pd(II) and Pt(II) with thioureas [42,43] that showed good antimycobacterial activity, as well as three platinum complexes with fluoroquinolones that showed activity in the μM range against drug-resistant tuberculosis[44]. Moreover, other metal ions such as Cu(II)[45,46], Mn(II)[46] and Ru(II)[47] have also being considered against *M. tuberculosis.*

Copper is another important metal in biological systems that is involved in many processes such as redox homeostasis, enzyme function, free radical scavenging and DNA cleavage.[48] It also plays an important role in cancer as concentration of copper in cancerous tissues is elevated,[49] which suggests that complexes of that metal may show some selectivity towards cancer cells.[50]

Copper Casiopeinas® are one of the most emblematic examples of Cu(II) complexes for the treatment of cancer. They are a class of mixed chelate copper(II) compounds of general formula $[Cu(N\text{-}N)(O\text{-}O)]NO_3$ or $[Cu(N\text{-}N)(O\text{-}N)]NO_3$, where N-N is a bipyridine derivative. The compounds have been extensively tested *in vitro* and *in vivo*, showing great antitumor activities.[51–55] The extended aromatic rings in the Casiopeinas allow them to bind to DNA by intercalative and non-intercalative modes either as free ligands or in metal complexes and also to favor the cis-configuration around the metal ion. Indeed, ligands such as 2,2'-bipyridine, phenanthroline and 4,4'-dimethyl-2,2'-bipyridine have relatively high affinity for copper due to their nitrogen-donor bidentate moiety.[56]

Casiopeinas also showed remarkable effect against resistant strains of *M. tuberculosis*. The MIC of the Casiopeinas CasIIIia, CasIIIEa, and CasIIgly against 7 resistant isolates ranges from 0.78 to 12.50 μg/mL and the synergistic activity with ethambutol was very pronounced.[57] The regulation of copper inside *M. tuberculosis* seems to be very important and Cu-mediated antibacterial toxicity may lead to novel strategies against tuberculosis. For example, the antimycobacterial activity of 8-hydroxyquinoline (MIC = 0.16 μmol/L in the presence of Cu) was found to be dependent on the presence of extracellular Cu and to be related to an increase in cell-associated labile

Cu ions.[58] The results suggest that specific ionophores for Cu ions have potential toxicity over *M. tuberculosis*.

Copper complexes can also be designed as artificial nucleases that are able to interact with DNA by intercalation or groove binding and then cleave the DNA phosphate ester bonds.[45] The bis-(1,10-phenanthroline)copper(I) complex, $[Cu(I)(phen)_2]^+$ was the first copper-based artificial nuclease reported in the literature.[59] The Cu(I) species is generated from $[Cu(II)(phen)_2]^{2+}$ which is reduced in the presence of molecular oxygen, and therefore, produces reactive oxygen species (ROS) which are also very toxic to the cells.[45,60]

Recently, a review was published about the "bioinorganic chemistry perspective on the roles of metals as drugs and targets against *Mycobacterium tuberculosis*". [61] One of the highlights of the article is a pentacyanidoferrate(II) complex with isoniazid (identified as IQG607).[62] The mechanism of action of isoniazid (a first line drug for TB) involves its oxidation by the enzyme catalase-peroxidase KatG, producing an isonicotinoyl radical intermediate that reacts with NAD(H) yielding a NAD-INH adduct. The NAD-INH adduct is responsible by the inhibition of an enoyl-ACP reductase enzyme (InhA) involved in one of the steps of mycolic acid biosynthesis, an essential element in the bacterial cell wall formation. Since isoniazid-resistant strains have exhibited mutations or deletions on the katG gene, IQG607 was developed as an alternative to produce the isonicotinoyl radical *in situ* with oxidation promoted by the Fe(II)/Fe(III) redox process, triggered by reactive oxygen species (ROS).[61]

The review also mentions 1-oxido-5-R-pyridin-2-yl-imidothiocarbamate derivatives that were able to inhibit Mtb strains by drastically increasing the concentration of copper inside the cell. The strains treated with these compounds overexpressed genes involved specifically in copper detoxification, supporting the theory that the mechanism involves the accumulation of copper ions and not iron, nickel, cobalt or zinc.[61,63]

These findings encouraged the investigation of Cu(II) complexes against Mtb, as not only the intracellular concentration of copper is especially toxic to the *M. tuberculosis* cell, but also because redox active copper complexes may trigger similar mechanisms of action like observed for the Fe(II)/Fe(III) pair in the IQG607 complex.

3. The anthranilic acid derivatives

Anthranilic acid derivatives are known since the 1950's for inhibiting the tryptophan synthesis pathway in bacteria[64]. It was suggested that the mechanism of inhibition of triptophan, which is essential to bacterial survival, occur by counter-selection of genes that codify proteins responsible for the convertion of anthranilic acid in tryptophan.[65–67]

The presence of fluorine atoms can alter the electronic, lipophilic and steric parameters of molecules, which can be engineered to enhance thermal stability, increase lipophilicity, improve bioavailability or better mimic enzyme substrates[68,69]. There are reports in the literature about studies with 5-fluoroanthranilic acid (5fa) and 6-fluoroanthranilic acid (6fa) (Figure 2) and its action against *M. tuberculosis*, with minimum inhibitory concentration (MIC) of 19.4 mg/L. [70] However, the most promising result of the fluoroantranilic acids was the ability to inhibit the growth of *M. tuberculosis* that can produce biofilm (MIC = 19.4 mg/L) in a more efficient way than pirazinamide (MIC > 1000 mg/L), isoniazid (MIC > 256 mg/L), streptomycin (CBM = 1000 mg/L) and amikacin (MIC = 1000 mg/L). The bacterial phenotype that produces biofilm is known to be more resistant to antibiotic treatment as they form interfaces between a surface and the surrounding air or liquid, considerably difficulting the treatment of the infection.[70,71]

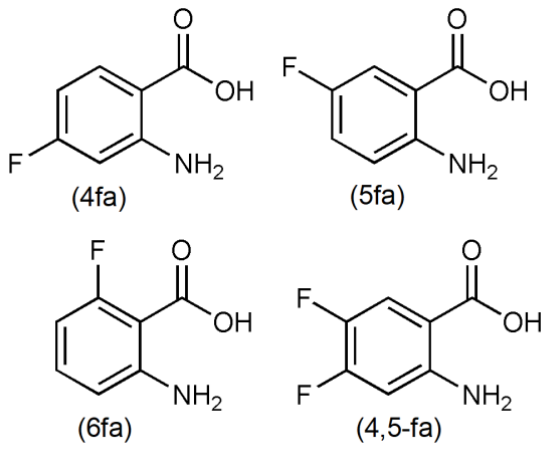

Figure 2. Structures of 4-fluoroanthranilic acid (4fa), 5-fluoroanthranilic acid (5fa), 6-fluoroanthranilic acid (6fa) and 4,5-difluoroanthranilic acid (4,5-fa).

3.1.The tryptophan biosynthetic pathway in *M. tuberculosis*

The discovery of anti-tubercular agents inhibiting tryptophan synthase highlights the therapeutic potential of this enzyme and draws attention to the prospect of other amino acid biosynthetic pathways as future Mtb drug targets.[72]

Reports in the literature suggest that the tryptophan biosynthetic pathway is conditionally essential for *M. tuberculosis* survival during infection.[72–75] In fact, this pathway is important for many bacteria whenever L-tryptophan it is not available from the environment. The pathway for L-Trp biosynthesis is typically organized in a single strictly regulated trp operon, including the genes trpE, trpG, trpD, trpF, trpC, trpB and trpA.[73]

Tryptophan synthase (TrpA/TrpB) was identified as an target in different studies[72,75] especially against *M. Tuberculosis*, as the inhibition of this enzyme prevent the tryptophan synthesis. TrpE, or anthranilate synthase, converts chorismate to anthranilate in the first committed step of tryptophan biosynthesis. The next enzyme in the pathway, TrpD, converts anthranilate to N-(5′-phosphoribosyl)-anthranilate. The deletion of trpE or trpD genes in *M. tuberculosis* causes the bacteria to be a tryptophan auxotroph that fails to survive in ambient of tryptophan starvation.[76] Tryptophan auxotroph mutants of *M. tuberculosis* are avirulent[77], even in immunocompromised hosts, and were also considered as potential vaccine candidates.[78]

In the case of the fluoroanthranilic acids, they do not inhibit the pathway. Instead they act as an antimetabolite and are incorporated in the biosynthesis by the anthranilate phosphoribosyltransferase (TrpD) that usually recognizes an anthanilate molecule in the beginning of the pathway of tryptophan synthesis (Figure 3). It leads to the synthesis of fluortryptophan that will eventually be used for the synthesis of other proteins in the bacteria and, therefore, causing toxicity, as mycobacteria have been reported not to catabolize tryptophan.[77] Also, it has been reported that fluorotryptophan molecules (with fluorine substituents in position 5 or 6) are able to inhibit bacterial growth in a dose dependent manner.[77]

Moreover, allosteric regulation of the pathway is provided by feedback inhibition of tryptophan binding to a regulatory site in the TrpE protein, as a way of activating the biosynthesis of this amino acid only when it is not readily available.[75]

It was shown that the toxicity of fluorotryptophan is due to its incorporation in bacterial proteins rather than depletion of tryptophan by feedback inhibition of the synthetic pathway.[77]

The lack of an equivalent biosynthetic pathway for tryptophan in mammals makes host toxicity less likely when this is the target in bacteria. [75]

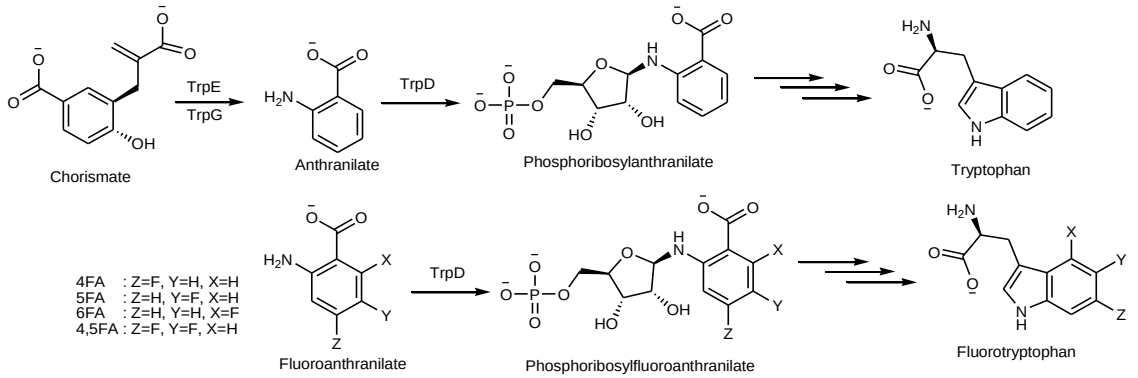

Figure 3. The simplified tryptophan biosynthetic pathway in *M. tuberculosis* (top) and possible alternative products by the incorporation of fluoroanthranilic acid isomers in the pathway (bottom). Clique ou toque aqui para inserir o texto. [75,79]

3.2. Fluoroanthranilic acids in inorganic chemistry

Due to the amino acid function in the structures of the anthranilic acid derivatives, many metal complex were synthesized with them, including Co(II), Ni(II), Cu(II), Cd(II), Cr(III), Pb(II), Sn(II) and Zn(II) [80–83]. Most of the complexes showed some antibacterial activity *in vitro*. The most recent report of metal complexes (Ag/Zn/Fe/Cu/Mn/Sn/Mg/Co/Ni) with anthranilic acid derivatives (with halogen-F/Cl/Br/I and nitro substitutions) in the literature describes 16 new coordination compounds that were able to strongly inhibit the enzyme α-glucosidase (IC_{50} in the nmol/L range). This enzyme is a carbohydrate-hydrolase that is a relevant target for the treatment of diseases involving glycogen storage, diabetes and also AIDS, as inhibition of α-glucosidase can prevent fusion of HIV and secretion of HBV [81,84]. Among the complexes, there is a silver(I) one with 5-fluoroanthranilic acid that inhibited α-glucosidase with IC_{50} = 4.30 nmol/L, but no further studies about biological activity or interaction with biomolecules were reported[81].

There are examples in the literature of copper(II) complexes with Schiff bases derived from fluoroanthranilic acids with remarkable biological activities. Xin Li et al. synthesized a copper(II) complex with Schiff base derived from 4fa and salicylaldehyde that was active against MDA-MB-231 breast cancer cells (IC_{50} = 14 μmol/L).[85] They identified the tumor proteasome as a target for the complex, which triggered apoptosis in the cultured MDA-MB-231 cells.

Another publication presents the synthesis, characterization and biological activity of three ternary copper(II) complexes with Schiff bases derived from 4fa and 4,5-fluoroanthranilic acid (4,5-fa).[86] The complexes were able to moderately interact with DNA and inhibit the growth of *Escherichia coli* and *Staphylococcus aureus* bacterial strains and the cancer cell lines A549 (lung cancer), HepG-2 (liver cancer) and Jurkat (leukemia derived T lymphocyte). The Cu(II) complex with the ligand derived from 4,5-fa and salicylaldehyde was the most active against A549 (IC_{50} = 1.42 μmol/L), HepG-2 (IC_{50} = 1.22 μmol/L) and Jurkat (IC_{50} = 7.09 μmol/L) and was the one that showed the highest inhibition halos for *E. coli* (19.0 mm) and *S. aureus* (21.5 mm). The authors suggest that the number of fluorine substituents in the structure of the ligands interfere in the biological activity of the Cu(II) complexes because of the electron withdrawing effect on the aromatic ring,[86] which may be directly related to DNA interaction.[87]

II. Objectives

The objective of this work was the synthesis of novel Ag(I), Cu(II), Pd(II) and Pt(II) complexes with fluoroanthranilic acid isomers and cycloserine and their biological evaluation *in vitro* for the treatment of tuberculosis and over a panel of cancer cell lines.

Specific goals are to determine the composition, coordination sites and chemical structure of the complexes obtained. For that goal, techniques such as X-ray diffraction, NMR, mass spectrometry, infrared spectroscopy, elemental analysis and others should be used.

Besides the antimycobacterial activity, it is intended to also evaluate the potential of these complexes and ligands as active species against other bacteria and also their toxicity against cancer cell lines in comparison to normal healthy cells

III.Materials and methods

1. Materials

Silver nitrate (≥ 99 %), K_2PtCl_4, K_2PdCl_4, $Cu(NO_3)_2$, 2-amino-4-fluorobenzoic acid (97%) (4fa), 2-amino-5-fluorobenzoic acid (97%) (5fa), 2-amino-6-fluorobenzoic acid (98%) (6fa) and 2-amino-4,5-difluorobenzoic acid (97%) (4,5-fa), 2,2'-bipyridine (bipy), 4,4'-dimethyl-2,2'-bipyridine (4,4'-Me bipy), phenanthroline (phen), D-Cycloserine (≥ 96.0%) (dcs) and potassium hydroxide (≥ 85.0%) were acquired from Sigma-Aldrich/Merck.

2. Synthesis

2.1. Synthesis of the Ag(I) complex with 4fa.

Silver nitrate (0.67 mmol) was dissolved in 5 mL of an ethanol/water mixture (1:1 v/v) and 4fa (0.67 mmol) was also dissolved in 5 mL of another ethanol/water mixture with 0.60 mmol of KOH. Then the alkaline 4fa solution was slowly added to the $AgNO_3$ solution. Immediately after the addition of 4fa, the precipitation of a white solid started and the suspension was kept under stirring for 2 hours. Then, the white solid obtained was separated by filtration, washed with water and dried with P_4O_{10} in the dark. Calcd. for $[Ag(C_7H_5FNO_2)]_n$ (%): C, 32.09; H, 1.92; N, 5.35. Experimental (%): C, 31.94; H, 1.79; N, 5.33. NMR ^{1}H (400 MHz, DMSO): δ 7.74 (dd, *J* = 8.9, 7.0 Hz, 1H), 6.50 (dd, *J* = 11.9, 2.6 Hz, 1H), 6.31 (td, *J* = 8.6, 2.6 Hz, 1H). NMR ^{13}C (101 MHz, DMSO) δ 172.0 (s), 164.8 (d, $J^1_{C,F}$ = 243.5 Hz), 152.6 (d, $J^4_{C,F}$ = 12.5 Hz), 135.1 (d, $J^3_{C,F}$ = 10.9 Hz), 114.5 (s), 101.5 (d, $J^2_{C,F}$ = 21.6 Hz), 101.0 (d, $J^2_{C,F}$ = 23.9 Hz). Yield: 92%.

2.2. Synthesis of the Ag(I) complex with 5fa.

Silver nitrate (0.60 mmol) was dissolved in 6 mL of an ethanol/water mixture (1:1 v/v) and 5fa (0.60 mmol) was also dissolved in 6 mL of another ethanol/water mixture with 0.60 mmol of KOH. Then the alkaline 5fa solution was slowly added to the $AgNO_3$ solution. Precipitation of a white solid started, and the suspension was kept under stirring for 4 hours. Finally, the white solid obtained was collected by filtration, washed with water and dried with P_4O_{10} in the dark. Calcd. for $[Ag(C_7H_5FNO_2)]_n$ (%): C, 32.09; H, 1.92; N, 5.35. Experimental (%): C, 32.02; H, 1.63; N, 5.32. NMR ^{1}H (500 MHz, DMSO) δ 7.48 (dd, *J* = 10.3, 3.2 Hz, 1H), 6.93 (td, *J* = 8.5, 3.2 Hz, 1H), 6.63 (dd, *J* = 8.9, 4.9 Hz, 1H), 6.56 (s, 1H). NMR ^{13}C (126 MHz, DMSO) δ 171.1 (s), 152.7 (d, $J^1_{C,F}$ = 229.2 Hz),

146.7 (s), 118.1 (d, $J^2_{C,F}$ = 22.7 Hz), 117.9 (d, $J^3_{C,F}$ = 5.6 Hz), 116.8 (d, $J^2_{C,F}$ = 18.7 Hz), 116.7 (d, $J^4_{C,F}$ = 3.6 Hz). Yield: 90%. Single crystals of $[Ag(5fa)]_n$ were obtained by the slow evaporation of a diluted ethanol solution of the complex.

2.3. Synthesis of the Ag(I) complex with 6fa.

Silver nitrate (1.00 mmol) was dissolved in 5 mL of an ethanol/water mixture (1:1 v/v) and 6fa (1.00 mmol) was also dissolved in 5 mL of another ethanol/water mixture with 1.00 mmol of KOH. Then the alkaline 6fa solution was slowly added to the $AgNO_3$ solution. As occurred for the other fluoroanthranilic ligands, precipitation of a white solid started, and the suspension was kept under stirring for 5 hours. Then, the white solid was separated by filtration, washed with water and dried with P_4O_{10} in the dark. Calcd. for $[Ag(C_7H_5FNO_2)]_n \cdot H_2O$ (%): C, 30.03; H, 2.52; N, 5.00. Experimental (%): C, 30.38; H, 2.51; N, 4.84. NMR ^{1}H (400 MHz, DMSO) δ 6.96 (td, J = 8.1, 6.2 Hz, 1H), 6.43 (d, J = 8.1 Hz, 1H), 6.20 (ddd, J = 10.7, 8.0, 0.9 Hz, 3H). NMR ^{13}C (101 MHz, DMSO) δ 169.3 (s), 162.4 (d, $J^1_{C,F}$ = 246.5 Hz), 150.5 (d, $J^2_{C,F}$ = 6.1 Hz), 130.2 (d, $J^2_{C,F}$ = 11.5 Hz), 111.3 (d, $J^4_{C,F}$ = 2.4 Hz), 110.4 (d, $J^3_{C,F}$ = 15.6 Hz), 102.5 (d, $J^3_{C,F}$ = 23.8 Hz). Yield: 78%.

2.4. Synthesis of the Ag(I) complex with 4,5-fa.

The silver complex with 4,5-fluoroanthranilic acid (4,5-fa) was prepared in a similar procedure early described for the silver complexes with 4fa, 5fa and 6fa. The complex was prepared as follows: first, $AgNO_3$ (1.0 mmol) was dissolved in 5 mL of an ethanol/water mixture (1:1 v/v) and 4,5-fa (1.0 mmol) was also dissolved in 5 mL of another ethanol/water mixture with 1.0 mmol of KOH. The ligand solution was slowly added to the $AgNO_3$ solution. Immediately after, the precipitation of a white solid started and the suspension was kept under stirring for additional 2 hours. Then, the white solid was separated by filtration, washed with water and dried under P_4O_{10} in the dark. Calcd. for $AgC_7H_4F_2NO_2$ (%): C, 30.03; H, 1.44; N, 5.0. Experimental (%): C, 29.94; H, 1.01; N, 4.84. Total yield of the synthesis: 98.2%.

2.5. Synthesis of Cu(II) complex with 6fa and 2,2'-bipyridine (Cu1)

First, 0.20 mmol of $Cu(NO_3)_2$ were dissolved in 10 mL of methanol, then 0.20 mmol of 2,2'-bipyridine (bipy) were added. After 30 min of stirring, 0.40 mmol of 6fa and 300 μmol of triethylamine were added and the mixture was kept under stirring for 3 hours. A green solid was separated by filtration, washed with methanol and dried under

P_4O_{10} in reduced pressure. Calcd. for $CuC_{24}H_{18}F_2N_4O_4$ (%): C, 54.60; H, 3.44; N, 10.61. Experimental (%): C, 54.4; H, 3.47; N, 10.5. Total yield of the synthesis: 45.7 %.

2.6. Synthesis of Cu(II) complex with 6fa and 4,4'-dimethyl-2,2'-bipyridine (Cu2).

In a flask containing 15 mL of methanol were added 0.26 mmol of $Cu(NO_3)_2$ and 0.26 mmol of 4,4'-dimethyl-2,2'-bipyridine. After 30 min of stirring, 0.52 mmol of 6fa and 200 µmol of triethylamine were added and the mixture was kept under stirring for 4 hours. A green solid precipitated and it was collected by filtration, washed with methanol and dried under P_4O_{10}. Calcd. for $CuC_{26}H_{22}F_2N_4O_4$ (%): C, 56.1; H, 3.99; N, 10.1. Experimental (%): C, 55.7; H, 3.89; N, 9.70. Total yield of the synthesis: 74.3%.

2.7. Synthesis of Cu(II) complex with 6fa and phenanthroline (Cu3)

First, 0.40 mmol of $Cu(NO_3)_2$ and 0.40 mmol of phenanthroline were added to a round bottom flask with 10 mL of methanol. After 30 min of stirring, 0.80 mmol of 6fa and 300 µmol of triethylamine were added and the mixture was kept under stirring for 4 hours. A light green solid precipitated and it was collected by filtration, washed with methanol and dried under P_4O_{10} in reduced pressure. Calcd. for $CuC_{26}H_{18}F_2N_4O_4$ (%): C, 56.6; H, 3.29; N, 10.1. Experimental (%): C, 56.4; H, 3.36; N, 9.93. Total yield of the synthesis: 43.3%.

2.8. Synthesis of Pd(II) complex with dcs and 2,2'-bipyridine (Pdbdcs).

First, 0.30 mmol of K_2PdCl_4 was dissolved in 6 mL of distilled water then 0.30 mmol of 2,2'-bipyridine (bipy) and 40 uL of HCl (30% v/v in H_2O) were added. The mixture was stirred for 4 hours at 70 °C and the resulting solid $[Pd(bipy)]Cl_2$ was separated by filtration, washed with water and immediately suspended again in deionized water. Following, 0.30 mmol of Ag_2SO_4 was added and after 2 hours of stirring, the white solid ($AgCl + Ag_2SO_4$) formed was removed by filtration and a yellow solution was reserved. Then, 0.60 mmol of dcs in alkaline medium (0.30 mmol of KOH) was added to the yellow solution and kept under stirring for 2 hours. Finally, 0.30 mmol of NH_4PF_6 was added. The resulting yellow compound was collected by filtration, washed with cold water and dried under P_4O_{10}. Calcd. for $[Pd(C_{16}H_{19}N_6O_4)]PF_6$ (%): C, 31.5; H, 3.14; N, 13.8. Experimental (%): C, 30.6; H, 3.26; N, 13.2. Total yield of the synthesis: 25 %. Inductively coupled plasma optical emission spectrometry (ICP-OES) measurements

showed 34.7 ± 0.3 % of Pd(II) in the sample solution while the calculated value was 34.9%.

2.9. Synthesis of Pt(II) complex with 6fa.

This complex was prepared as follows: in a round bottom flask, a solution containing 1.0 mmol of 6fa in 5mL of water:ethanol (70:30 v/v) was prepared and a KOH solution was used to adjust the pH to 7.0. This solution was added dropwise to a solution of K_2PtCl_4 (0.50 mmol) also in water:ethanol (70:30 v/v) and it was kept under stirring for 24h. The resulting purple solution was reserved for slow evaporation for several days until purple crystals were formed. Single crystals could be isolated and analyzed by X-ray diffraction to determine the structure of the Pt(II) complex

3. Equipment

Elemental analyses were performed on a Perkin Elmer 2400 CHNS/O Analyzer. Infrared spectroscopic measurements were performed on an Agilent Cary 630 FTIR spectrometer, using the Attenuated Total Reflectance (ATR) method equipped with a diamond cell. The spectra were recorded from 4000-400 cm^{-1}, with 64 scans and 2 cm^{-1} resolution. Thermogravimetric and differential thermal analyses (TGA/DTA) were performed on a simultaneous TGA/DTA SEIKO EXSTAR 6000 thermal analyzer, using the following conditions: synthetic air, flow rate of 50 $cm^3 \cdot min^{-1}$ and heating rate of 10 ºC min^{-1}, from 25 ºC to 900 ºC. The NMR spectra in solution (^1H, ^{13}C, ^1H,-^{13}C, ^1H-^{15}N, ^{19}F) were recorded in Bruker Avance III spectrometers of either 400 or 500 MHz in DMSO-d^6 at 298K. The ^{13}C and ^{15}N solid-state NMR (SSNMR) spectra were recorded in a Bruker 300 MHz spectrometer, using the combination of cross-polarization, proton decoupling and magic angle spinning techniques (CP/MAS) at 10 kHz and temperature of 298K. High resolution electrospray ionization quadrupole time-of-flight mass spectrometric (ESI-QTOF-MS) measurements were carried out in a Waters Quattro Micro API. The samples were evaluated in the positive mode. Samples of the complexes were diluted to the appropriate concentration in water:methanol (1:1 v/v) with 0.1% of formic acid. Each solution was directly infused into the instrument's ESI source with 30 $\mu L \cdot min^{-1}$ of infusion rate, capillary potential of 3.75 kV, cone voltage of 30 V, source temperature of 120 °C and desolvation temperature of 150 °C. UV-Vis spectrometer Agilent HP 8453 was used for UV-Vis measurements with optical path length of 1 cm.

Electrophoresis system BIO-RAD® (Sub-Cell® GT) was used for the agarose gel electrophoresis studies. The pGEX-4T1 plasmid DNA was kindly provided by Prof. Dr. Wilton R. Lustri from UNIARA, Araraquara, Brazil, and used in the experiments of DNA interaction with the compounds. The samples were electrophoresed by 2 hours and the gel was further colored by using 1 x SYBR green and finally photodocumented in a UVDoc 400i Delpho equipment. Fluorescence measurements were performed on a Cary Eclipse fluorescence spectrophotometer using a quartz cuvette of four clear windows and optical path length of 1.0 cm. Excitation and emission windows were set to allow a 5 nm slit.

4. Single crystal X-ray diffraction method

Crystallographic data for the Ag5fa, Pt6fa, 4fa and 6fa were collected on a Bruker APEX II Duo diffractometer at a temperature of 150 K, using Mo-Ka radiation (λ = 0.71073 Å) from a fine-focus sealed tube with a curved graphite monochromator. Using Olex2[88], the structure was solved with the ShelXT [89] structure solution program using Intrinsic Phasing and refined with the ShelXL [90] refinement package using Least Squares minimization. The complete crystallographic data are presented in the **Appendix**.

5. Molecular docking method

Ligand-receptor docking calculations were run using the Schrodinger Suit 2021–2. Ligands and biomolecules were prepared using Maestro version 12.8.117. Coordination bonds were treated as zero-order bonds, and formal charges were adjusted accordingly. No post-docking minimization was used. Structures of TrpD (PDB ID 4OWV and 4OWN) were selected for the docking studies.

For 4OWV, the crystalized anthranilate substrate was used for the generation of the receptor grid in the active site. In the case of 4OWN, three different ligands were used for the grid generation.

Ligand sampling was set to flexible. Epik state penalties were added to the docking score. Receptor grids were prepared for each protein studied. Five poses returned per ligand and were inspected manually.

6. Antibacterial activity: minimum inhibitory concentration (MIC) assay

The minimum inhibitory concentration (MIC) assay of 4fa, 5fa, 6fa, Ag4fa, Ag5fa and Ag6fa solutions in DMSO were performed in accordance with the protocols from the Clinical and Laboratory Standards Institute [91]. Gram-positive (*Staphylococcus aureus* ATCC 25923 and *Bacillus cereus* ATCC 14579) and Gram-negative (*Escherichia coli* ATCC 25922 and *Pseudomonas aeruginosa* ATCC 27583) bacterial strains were inoculated in tubes containing 10.0 mL of BHI (Brain Heart Infusion KASVI) and incubated for 18 h at 35-37 °C. An inoculum of each bacterial suspension was added into new sterile BHI tubes until reaching the value of 1.0 of the nephelometric McFarland scale (~$3.0 \cdot 10^8$ CFU/mL). The samples were solubilized or suspended in sterile deionized H_2O (stock solution 10 mg/mL) and 30 μL of each sample were added to the second well of the 96-well plate. Serial dilutions were performed in the remaining 6 wells. Subsequently, 70 μL of sterile BHI medium and 100 μL of the suspensions containing the microorganisms in the 1.0 McFarland scale were added to each sequential dilution, until reaching 0.5 McFarland (~$1.5 \cdot 10^8$ CFU/mL) to a final volume of 200 μL per well, with concentrations varying from 1500 μg/mL to 23.44 μg/mL. The microplates were incubated for 18 h at 35-37 °C in a humidity chamber with stirring at 100 rpm. After incubation, 15 μL of resazurin at 0.02% in sterile aqueous solution were added to each well. The measurements were performed after 3 h of re-incubation time. The first well was used as growth control, containing 30 μL of sterile deionized water, 70 μL of sterile BHI medium and 100 μL of the suspensions containing the microorganisms in the 1.0 McFarland scale.

These assays were performed in collaboration with Prof. Dr. Wilton Rogério Lustri from Universidade de Araraquara, UNIARA.

7. Antimycobacterial activity assays

The MIC_{90} is the lowest concentration of compound able to inhibit 90% of cellular growth when compared to the positive control, calculated by linear regression. The MIC_{90} of the compounds tested were determined by the REMA method (*Resazurin Microtiter Plate Assay)*, using as experimental control the antibiotics rifampicin (RIF), moxifloxacin (MOX) and isoniazid (INZ), that are commercially available for tuberculosis therapy. This method consists in serial dilutions in 96-well microplates, using resazurin as a bacterial viability indicator[92].

Ligands, complexes, $AgNO_3$, RIF, MOX and INZ were solubilized in dimethylsulfoxide (DMSO) and the stock solutions were prepared at 10,000 µg/mL. The compounds were diluted in the microplate to obtain the concentration range between 25 and 0.098 µg/mL.

The MIC_{90} values were determined for the *M. tuberculosis* $H_{37}Rv$ (ATCC 27294) strain, that was cultivated in Middlebrook 7H9 medium, supplemented with OADC 10% (oleic acid, albumin, dextrose and catalase) at 37°C, under stirring. The concentration was adjusted to $5 \cdot 10^5$ CFU/mL. Then, 100 µL of this inoculum were added to the microplate wells containing the samples.

In each plate, some wells were used as positive control (containing only culture medium and the mycobacteria) and negative control (only culture medium). The microplates were incubated at 37°C for seven days and then 30 µL of resazurin solution (0,01% in Middlebrook 7H9 DIFCO® medium supplemented with 10% OADC) were added to indicate cellular viability. The fluorescence readings were performed after 24 hours at the emission/excitation wavelengths of 530/570nm using the Cytation 5 Cell Imaging Multi-Mode Reader (Biotek®). Two independent assays were performed.

These assays were performed in collaboration with Prof. Dr. Fernando Pavan from Universidade Estadual Paulista "Júlio de Mesquita Filho", UNESP -Araraquara.

8. Cell antiproliferative activity assay

In this assay, the cells were grown in 96-well plates with a cell density of $1.5 \cdot 10^4$ cells/well and incubated for 24 hours at 37°C. The compounds ($AgNO_3$, Ag4fa, Ag5fa and Ag6fa) were solubilized in DMEM (Dulbecco's Modification of Eagle's Medium), without fetal bovine serum (SFB – Gibco), at initial concentration of 10,000 µg/mL with 5% of DMSO and diluted in the complete culture medium. Concentrations of the compounds were chosen based on preliminary tests so the response curve could be observed.

Cells were treated with DMSO (0.5% - solvent control) and sodium azide (200 µg/mL – positive control). Wells containing cells without any treatment were used as negative control, apart from the sterility control and oxide-reduction false positive control that were also tested.

After 24 hours of incubation, the culture medium was removed and 50 µL of resazurin solution 0.001% were added to each well. The resazurin reduction assay (alamar Blue®) was performed according to the protocol described by Pagé et al.[93] that indicates the cellular metabolic profile. The microplates were incubated again for 2 to 4 hours and the results were registered using a microplate reader Cytation (Biotek®), where the excitation wavelength at 530 nm and the emission at 590 nm were filtered off.

The results were analyzed statistically using the GraphPad Prism 5 software, by the one-way analysis of variance (one-way ANOVA) to determine the statistical significances, followed by the Tukey test considering $p < 0.05$. The tests were performed in triplicate and the results were expressed as percentages of the negative control (complete culture medium).

The IC_{50} values were calculated as established by the U.S. Food and Drug Administration (FDA), meaning the concentration required to inhibit 50% of cellular growth through the GraphPad Prism 5 software. The selectivity index was determined by the ratio between IC_{50} values for the healthy cell lines and the tumor cell lines[94].

These assays were performed in collaboration with Prof. Dra. Flávia Aparecida Resende Nogueira from Universidade de Araraquara, UNIARA.

9. Mutagenicity assay method (Ames test)

The *Salmonella* mutagenicity assay was performed with the *Salmonella typhimurium* strains TA100, TA98, TA97a and TA102, preincubated for 20 min with the test substances, with and without metabolic activation[95]. Five different concentrations of complexes, diluted in DMSO and selected based on a preliminary toxicity test, were assayed.

The S9-mix prepared from livers of Sprague–Dawley rats, treated with the polychlorinated biphenyl mixture Aroclor 1254 (500 mg/kg), was purchased from Molecular Toxicology Inc. (Boone, NC, USA) and freshly prepared before each test. This S9 mixture reveals whether the substance is mutagenic in its original form or whether it needs to be metabolized or activated to become mutagenic [95].

The standard mutagens used as positive controls in experiments without S9 mix were 4 -nitro-*o*-phenylenediamine (10 μg/ plate) for TA98 and TA97a, sodium azide (1.25 μg/ plate) for TA100 and mitomycin (0.5 μg/ plate) for TA102. In experiments with S9 activation, 2-anthramine (1.25 μg /plate) was used with TA98, TA97a and TA100 and 2-aminofluorene (10 μg/ plate) with TA102. Dimethylsulfoxide served as the negative (solvent) control (100 μL/ plate). All experiments were performed in triplicate.

The statistical analysis was performed with the Salanal computer program, adopting the Bernstein model. The data (revertants/ plate) were assessed by analysis of variance (ANOVA), followed by linear regression. The mutagenic index (MI), defined as the average number of revertants per plate divided by the average number of revertants per plate in the negative control (solvent), was calculated for each dose. A sample was considered positive when the mutagenic index was equal to or greater than 2 for, at least, one of the tested doses and also if it had a reproducible dose-response curve[96].

The mutagenicity assay was performed in collaboration with Prof. Dra. Flávia Aparecida Resende Nogueira from Universidade de Araraquara, UNIARA.

IV. Results and discussion

1. Fluoroanthranilic acids and their Ag(I) complexes

1.1. Single crystal X-ray diffraction of 4fa, 6fa and Ag5fa

Compounds 4fa and 6fa crystallized in the monoclinic $P2_1/n$ and $P2_1/c$ space groups, respectively (Figure 4). The ligand 4fa has 3 molecules in the asymmetric unit (Z' = 3). The crystal structure of 5fa has been reported previously in the literature[97] and is brought in for comparison purposes. The main bond lengths agree with reported values in the CSD[98] for similar structures[97,99,100] and are reported in Table 1. Similar to the crystal structure of 5fa[97], 4fa and 6fa also present an intramolecular hydrogen bond involving N1-H···O2. In agreement to many carboxylic acid crystal structures[101,102], 4fa and 6fa form noncovalent dimers with the R2,2(8) ring motif (see Figure 5).

Table 1. Selected bond lengths and angles from 4fa and 6fa crystal structures.

4fa bonds	Length / Å	6fa bonds	Length / Å
C4—F1	1.364(2)	C6—F1	1.350(2)
C7—O1	1.323(2)	C7—O1	1.318(2)
C7—O2	1.237(2)	C7—O2	1.235(2)
C1—C7	1.461(2)	C1—C7	1.471(2)
C2—N1	1.362(2)	C2—N1	1.360(2)

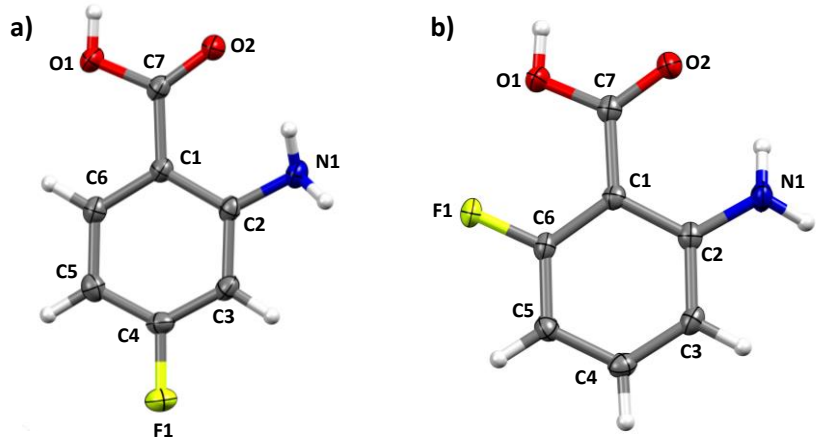

Figure 4. Molecular view of compounds (a) 4fa* and (b) 6fa. Displacement ellipsoids are drawn at the 50% probability level. H atoms were not labeled for clarity. *Only one of the three 4fa molecules present in the asymmetric unit is represented.

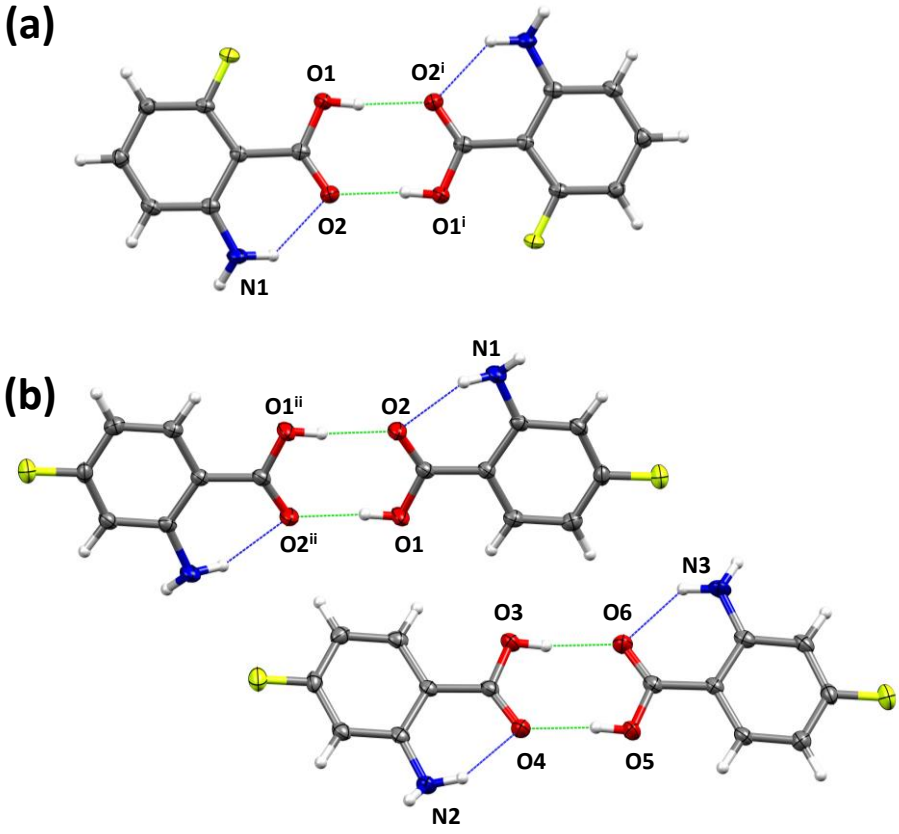

Figure 5. Intramolecular hydrogen bonding (dashed blue) and carboxylic acid R2,2(8) hydrogen bonding ring motif (dashed green) present in (a) 6fa and (b) 4fa. Symmetry codes: (i) 1-x, -y, 1-z; (ii): 1-x, 2-y, 1-z. Ellipsoids drawn at the 50 % probability level.

The supramolecular structure of 4fa is formed by offset π···π stacking[103] (distance between ring centroids of approximately 3.66 Å, see Figure 6 (a)) of symmetrically independent 4fa units along the crystallographic axis *a*. Lattice interactions along the other directions occur mainly by N-H···F and C-H···F hydrogen bonds (Figure 6 (b)).

In contrast to what was observed for 4fa, no offset π···π stacking interactions are observed in 6fa. However, C-H···π interactions[103] are present in the crystal structure of 6fa, forming a zigzag pattern along the *b* axis (Figure 7 (a)). Additionally, the different position of the fluorine in 6fa seems to lead to absence of N-H···F hydrogen bonds in 6fa (Figure 7 (b)).

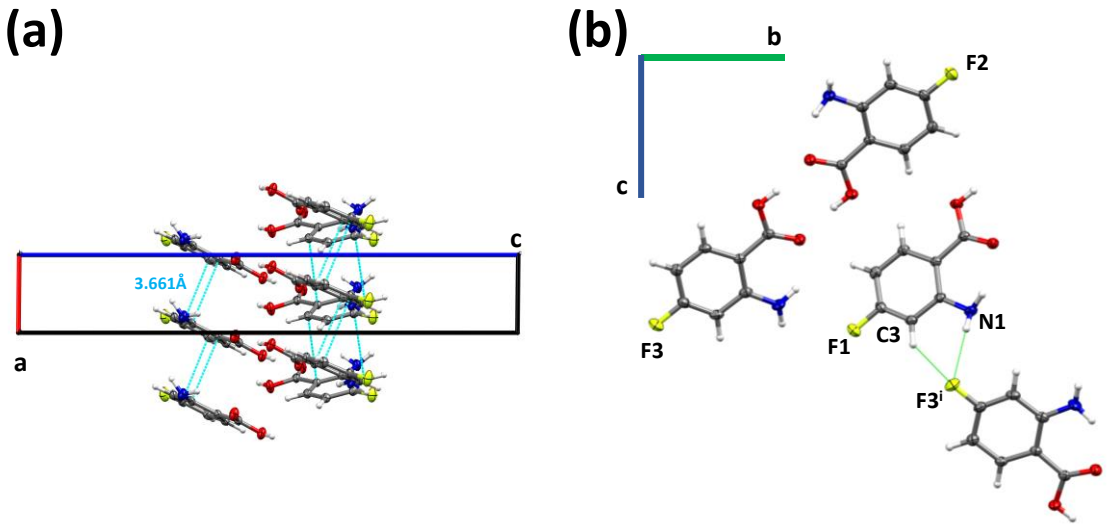

Figure 6. Intermolecular interactions present in 4fa. (a) Offset π···π stacking and (b) N1-H1B ···F3i and C3-H3···F3^{i} hydrogen bonds. Symmetry code: (i) -1/2-x, 1/2+y, 3/2-z.

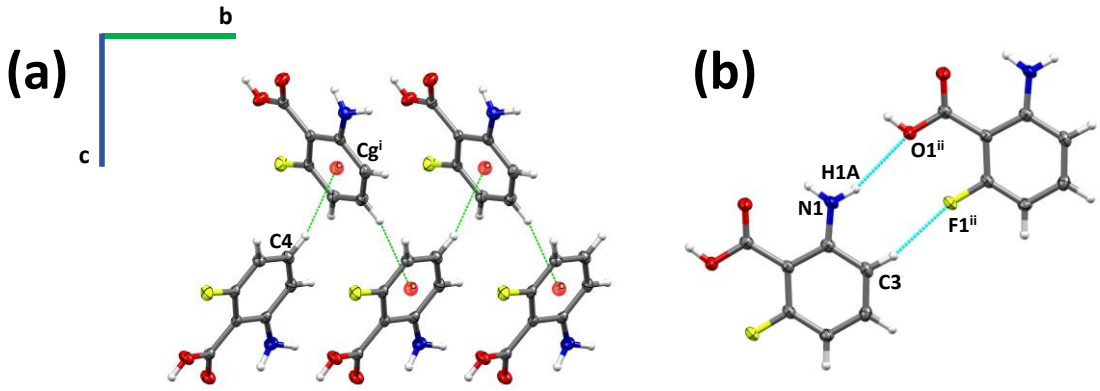

Figure 7. Intermolecular interactions present in 6fa. (a) C-H···π interactions and (b) hydrogen bonds. Symmetry codes: (i) 1-x, 1/2+y, 1/2-z; (ii) 1+x, 1+y, z.

Several attempts of crystallization were made for the silver(I) complexes. It was possible to obtain single crystals only for Ag5fa, accomplished by the slow evaporation of a diluted ethanolic solution. A summary of the crystal parameters is given in the **Appendix**. The asymmetric unit of this crystal contains one unit of the coordination compound with a 1:1 metal:ligand ratio ($AgC_7H_5FNO_2$). The coordination of the 5fa molecule to the metal occurs by the amino group and both oxygen atoms of the carboxylate moiety in a bridging manner, as it can be seen in the representation of the unit cell in Figure 8**.** The bond lengths and angles are summarized in Table 2.

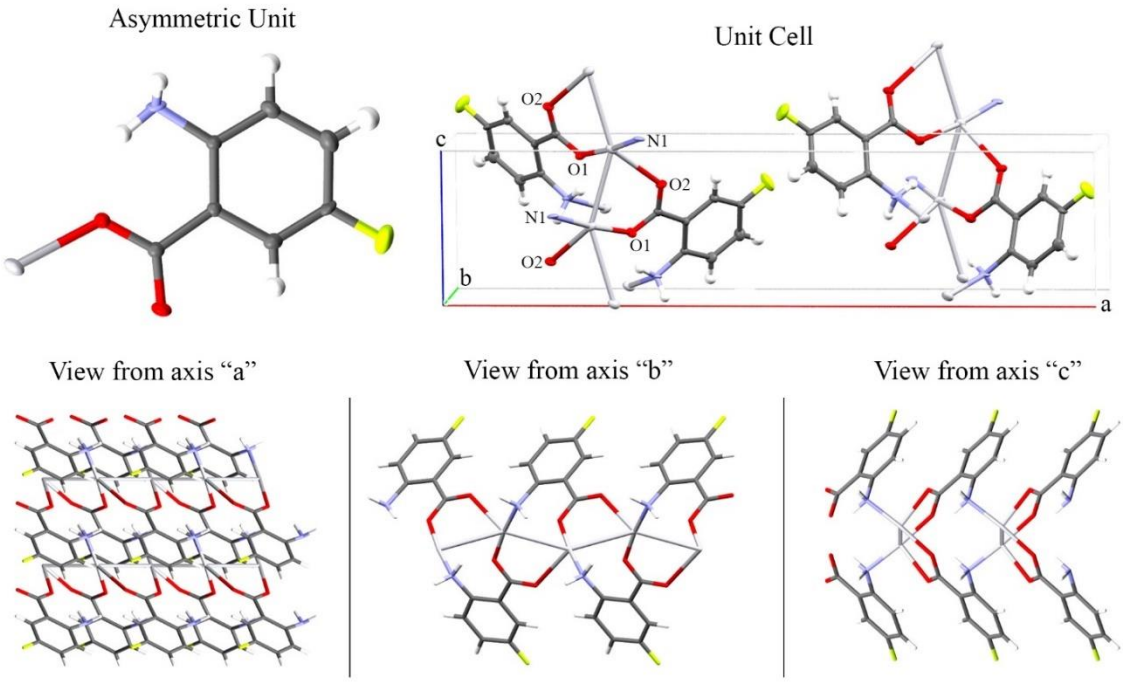

Figure 8. Asymmetric unit and unit cell of the crystal structure of Ag5fa and representation of the view of the crystal cell from the axis “a”, “b” and “c”. Color codes: carbon = dark grey, hydrogen = white, oxygen = red, nitrogen = blue, fluorine = light green, silver = light grey.

The two Ag-O bond lengths are considerably different, as presented in Table 2. The Ag-O1 distance is 2.121(5) Å and it is opposite to the Ag-N1^{ii} bond (angle O1-Ag1-N1^{ii} = 173.9(2)°, see symmetry codes), while the length of the Ag-O2^{i} bond is 2.677(5) Å (angle O2-Ag1-N1 = 101.23(18)°). As Ag(I) is coordinated to three atoms that are in the same plane, the geometry that best describes the coordination sphere is a distorted trigonal planar geometry, almost in a “T” shaped coordination. This geometry is true when argentophilic interactions are not considered to determine the geometry of the complex, which is commonly assumed [27]. The same “T” shaped geometry was observed in other silver coordination polymers where there are Ag-N and Ag-O bond lengths of approximately 2.1 Å and a longer third Ag-O bond close to 2.6 Å [104–106].

Table 2. Bond lengths and angles in the coordination sphere of Ag(I).

Bond	**Length (Å)**
Ag1-Ag1^{i}	3.0783(6)
Ag1-O1	2.121(5)
Ag1-O2^{i}	2.677(5)
Ag1-N1^{ii}	2.150(6)
Atoms	**Angle (°)**
Ag1^{i}-Ag1-Ag1^{iii}	148.10(3)
O1-Ag1-Ag1^{i}	91.56(13)
O1-Ag1-Ag1^{iii}	67.64(14)
O1-Ag1-N1^{ii}	173.9(2)
O2^{i}-Ag1-N1^{ii}	101.23(18)
N1^{ii}-Ag1-Ag1^{i}	83.34(14)
N1^{ii}-Ag1-Ag1^{iii}	115.50(14)

Symmetry codes: (i) -x + 1/2, y, z - 1/2; (ii) -x+1/2, y-1, z+1/2; (iii) -x + 1/2, y, z+1/2.

In Figure 8 it is also possible to observe the argentophilic interactions between the silver ions (Ag1-Ag1^{i} = 3.0783(6) Å) that form a chain of silver ions in the structure along the crystallographic c-axis (angle Ag1-Ag1-Ag1 = 148.10 (3)°). The chains are interconnected because the carboxylate group and the amino group of the same ligand coordinate to different silver atoms that belong to neighboring chains, forming a 2D structure which corresponds to a layer of silver ions in the direction of the (100) crystallographic plane. The ions are properly located in the middle of the structure and the fluorine atoms are distributed along both faces of the layer (see Figure 9).

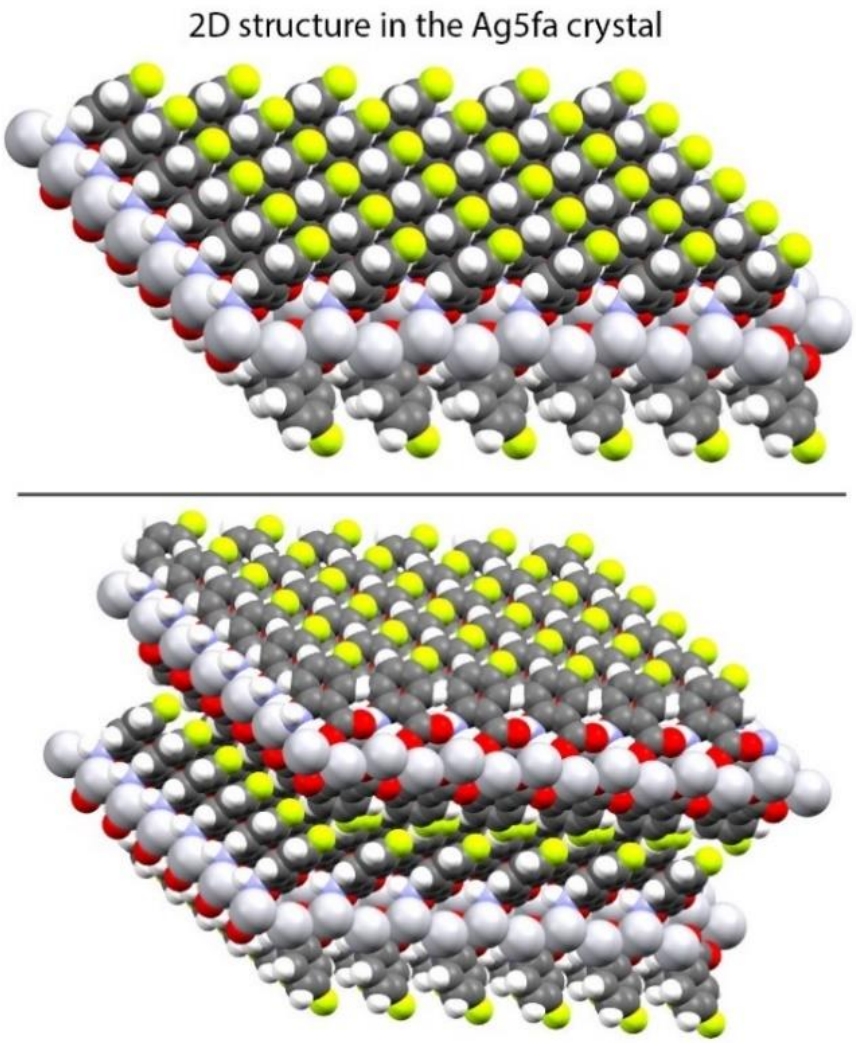

Figure 9. Representation of the 2D structure observed for the Ag5fa complex and the stacking of two of these layers. Color codes: carbon = dark grey, hydrogen = white, oxygen = red, nitrogen = blue, fluorine = light green, silver = light grey.

1.2. Infrared Spectroscopic characterization

The infrared spectra of 4fa, 5fa, 6fa and 4,5-fa were compared with their respective Ag(I) complexes. The Table 3 summarizes the most important band assignments for confirming the coordination of the ligands to the silver ions, while the respective spectra are shown in Figures 10, 11, 12 and 13.

Table 3. Assigment of selected infrared spectra bands of 4fa, 5fa, 6fa, 4,5-fa and their respective Ag(I) complexes.

	Wavenumber (cm^{-1})							
	4fa	**Ag4fa**	**5fa**	**Ag5fa**	**6fa**	**Ag6fa**	**4,5fa**	**Ag-4,5fa**
$\nu_{as}NH_3$ / $\nu_{as}NH_2$	3506 /	3167	3490 /	3175	3488 /	3230	3491 /	3175
$\nu_{s}NH_3$ / $\nu_{s}NH_2$	3383 /	3092	3350 /	3096	3376 /	3100	3370 /	3101
$\nu_{as}COO^-$ / $\nu_{as}COO^-$	1655 /	1583	1644 /	1597	1659 /	1579	1678 /	1599
$\nu_{s}COO^-$ / $\nu_{s}COO^-$	1422 /	1340	1364 /	1342	1426 /	1348	1422 /	1338
$\nu_{d}NH_3$ / $\nu_{d}NH_2$	1594 /	1515	1599 /	1527	1581 /	1510	1511 /	1508
$\nu_{s}NH_3$	1568		1491		1551		1571	

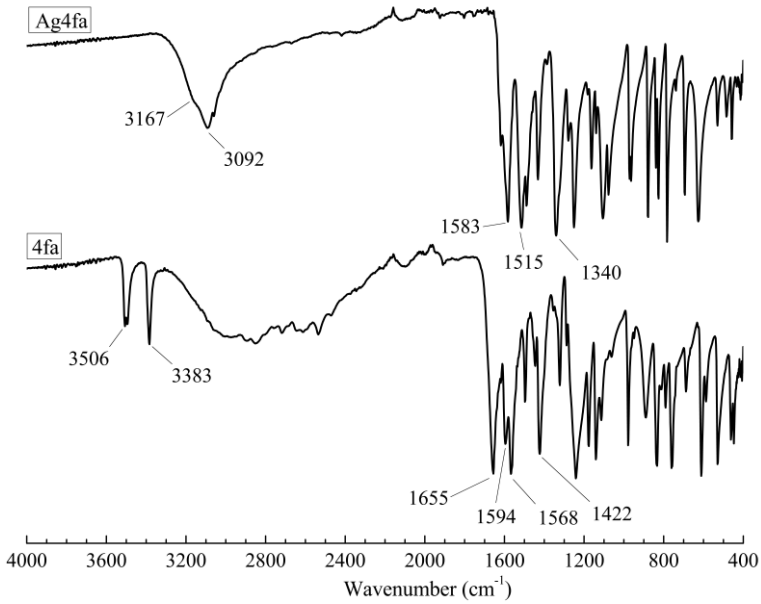

Figure 10. Infrared spectra of 4fa and Ag4fa from 4000 to 400 cm^{-1}.

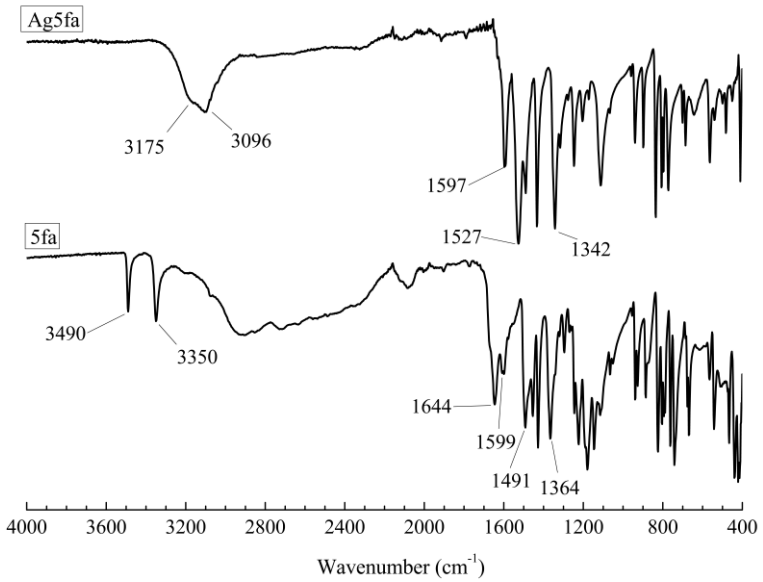

Figure 11. Infrared spectra of 5fa and Ag5fa from 4000 to 400 cm^{-1}.

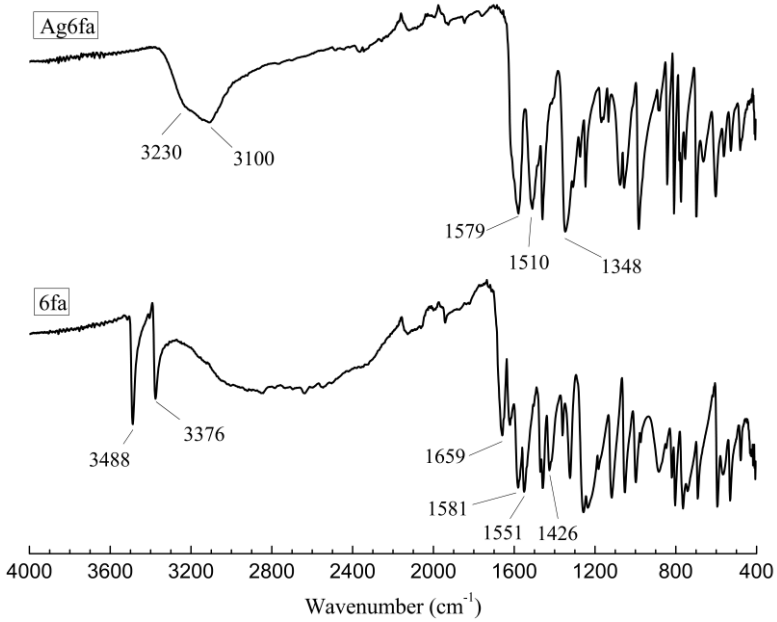

Figure 12. Infrared spectra of 6fa and Ag6fa from 4000 to 400 cm^{-1}.

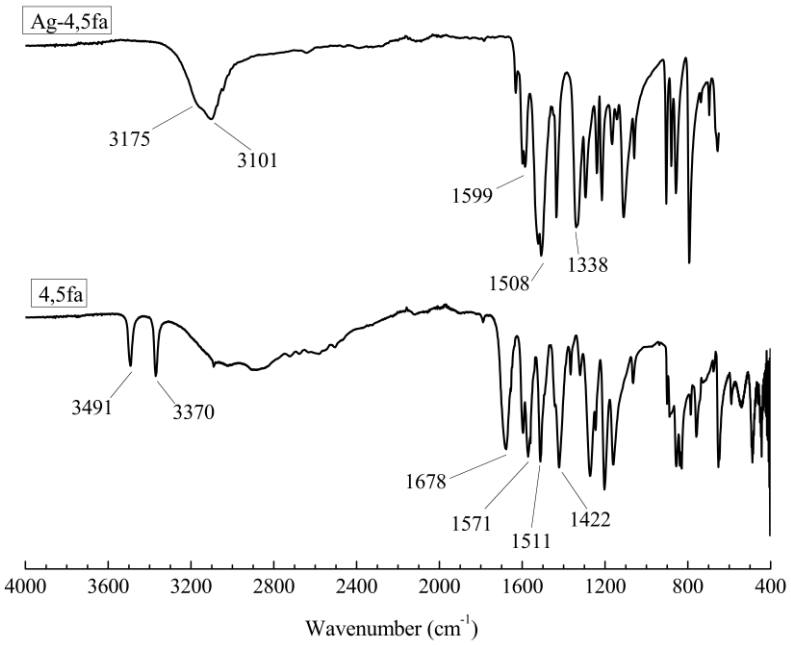

Figure 13. Infrared spectra of 4,5fa and Ag-4,5fa from 4000 to 400 cm^{-1}.

In the infrared spectra of the ligands, the carbonyl stretching νC=O bands corresponding to the protonated carboxylic acid moieties are not observed in the region between 1790 and 1690 cm^{-1}, suggesting that the ligands must be in the zwitterionic form, with charged NH_3^+ and COO^- groups [107]. Evidence for the coordination was found monitoring the bands of $\nu_d NH_3$ (degenerate NH_3 stretching) and $\nu_s NH_3$ (symmetric NH_3 stretching) in the region above 3350 cm^{-1} in the spectra of the ligands and comparing them with the $\nu_{as} NH_2$ (asymmetric NH_2 stretching) and $\nu_s NH_2$ (symmetric NH_2 stretching) for the complexes, which are observed in the spectral region between 3230 and 3092 cm^{-1}. Such change in the absorption energy of these bands suggests the coordination of the NH_2 moiety of the fluoroanthranilic acids to silver.

The coordination of the carboxylate group of the fluoroanthranilic acid isomers to silver was also evaluated. Shifts in the $\nu_{as} COO^-$ and $\nu_s COO^-$ bands are observed when the IR spectra of the complexes are compared to those of the respective ligands. Such results attest for coordination of the carboxylate group to the metal centers. It is also interesting to notice that the difference in energy between $\nu_{as} COO^-$ and $\nu_s COO^-$ (Δ) in the ligands 4fa, 5fa and 6fa does not change considerably after coordination (see Table 4), suggesting a bidentate bridging coordination of the carboxylate [107,108] as it is observed in the crystal structure of Ag5fa. Therefore, it also suggests that Ag4fa, Ag6fa and Ag-4,5fa might have the same bridged bidentate coordination, and probably a similar molecular structure to Ag5fa.

Table 4. Variation in the wavenumber of the symmetric and asymmetric vibrational modes of the carboxylate moiety for the fluoroanthranilic ligands and their silver complexes.

	Wavenumber (cm^{-1})							
	4fa	**Ag4fa**	**5fa**	**Ag5fa**	**6fa**	**Ag6fa**	**4,5fa**	**Ag-4,5fa**
Δ (ν_{as}COO-) - (ν_{s}COO-)	233	243	280	255	233	231	256	261
(Δ complex) - (Δ ligand)	10		-25		-2		5	

1.3. Thermogravimetry (TG) and differential thermal analysis (DTA) of silver complexes

Elemental analyses suggested a 1:1 metal:ligand ratio for all the four complexes as showed in the experimental section. The thermogravimetric analyses were performed to confirm the composition of the silver complexes and to ascertain its thermal stability under a controlled heating program.

The results of thermal degradation of the Ag(I) complexes with 4fa, 5fa, 6fa and 4,5fa can be found at the Figures 14, 15, 16 and 17. The TG curves represent the percentage of mass loss associated with a temperature gradient. For the Ag(I) complexes, the 1:1 metal:ligand composition suggested by the elemental analysis was confirmed. Starting at approximately 170°C, mass losses were observed of 58.0% for Ag4fa, 58.7% for Ag5fa, and 58.5% for Ag6fa, corresponding to one molecule of fluoroanthranilic acid (theoretical mass loss of the ligand: 58.8%). In the case of Ag-4,5fa, the percentage mass loss corresponding to the ligand was 60.3%, while the expected for the 1:1 composition was 61.8% The ligand oxidation is completed at 595°C for Ag4fa, 530°C for Ag5fa, 361°C for Ag6fa and 600°C for Ag-4,5fa.

The residual mass of the complexes were compatible with metallic silver as the experimental residual for Ag4fa, Ag5fa and Ag6fa are 41.6, 40.6 and 41.1%, respectively (theoretical residue 41.0%) and for Ag-4,5fa the residue was 39.4% which is close to the expected value of 38,5%. The DTA curves of these complexes show exothermic peaks corresponding to the oxidation of the organic moiety of the complexes leading to the formation of Ag° as it can be observed in the following figures.

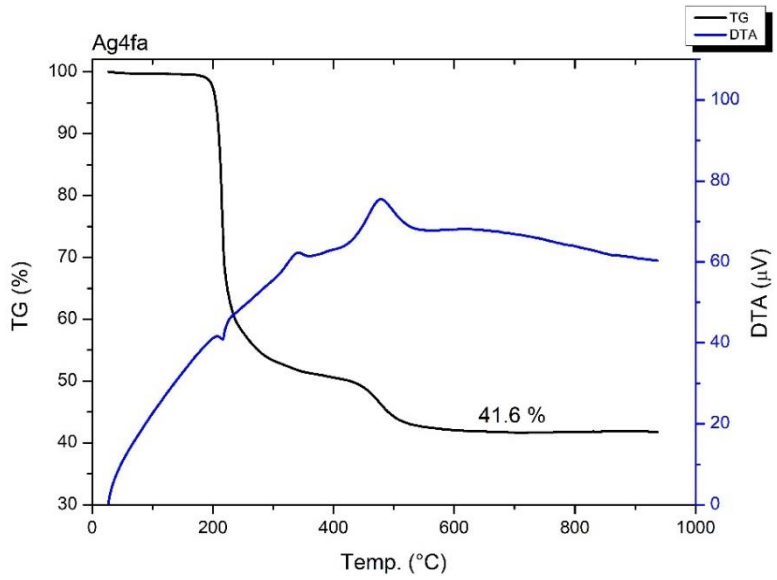

Figure 14. Thermogravimetric (TG) and differential thermal analysis (DTA) curves for Ag4fa.

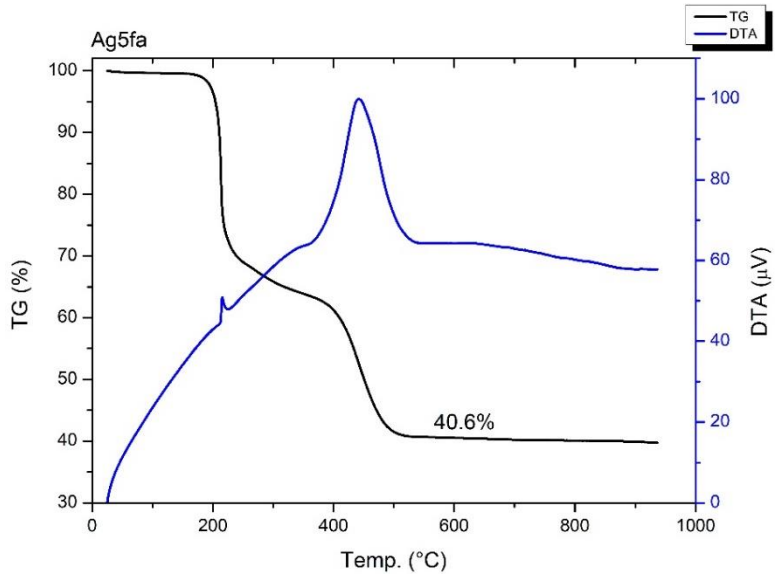

Figure 15. Thermogravimetric (TG) and differential thermal analysis (DTA) curves for Ag5fa.

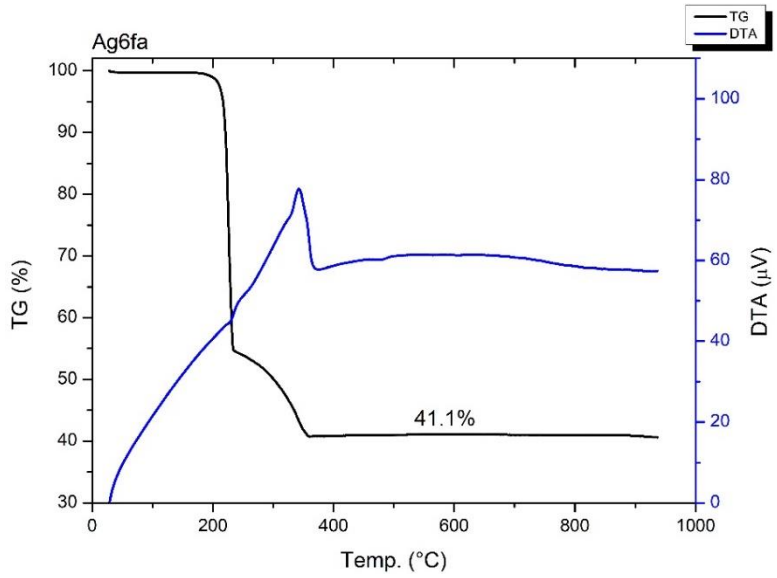

Figure 16. Thermogravimetric (TG) and differential thermal analysis (DTA) curves for Ag6fa.

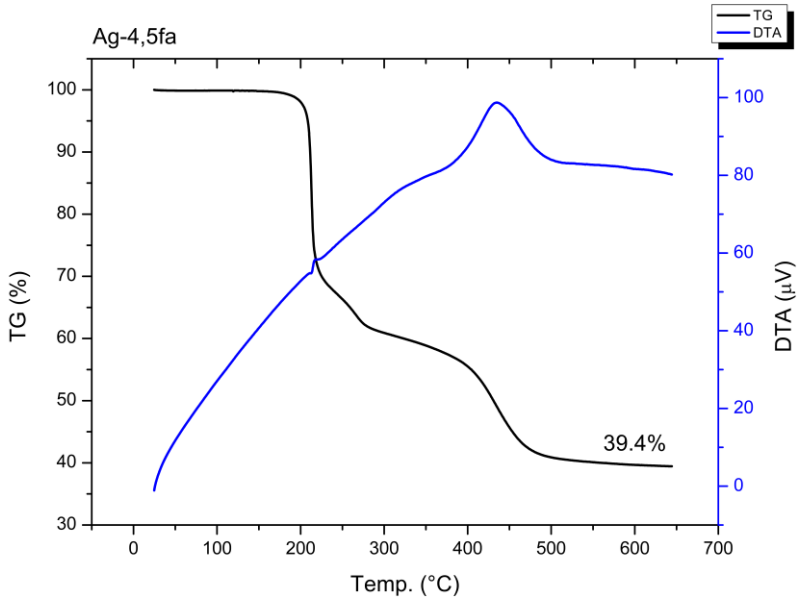

Figure 17. Thermogravimetric (TG) and differential thermal analysis (DTA) curves for Ag-4,5fa.

1.4. Mass spectrometry

Mass spectrometric measurements in the positive mode revealed species with peaks corresponding to the silver isotopic pattern of a silver complex with fluoroanthranilic acid. Figure 18 and Figure 19 show the comparison of the theoretical isotopic pattern of the species $[Ag(C_7H_6FNO_2)]^+$ and $[Ag(C_7H_6FNO_2)_2]^+$ (where $C_7H_6FNO_2$ corresponds to 4fa, 5fa or 6fa) with the experimental ones of the silver complexes at m/z 261.9453 and m/z 416.9816 for Ag4fa (relative errors 7.2 ppm and 1.9 ppm), m/z 261.9556 and m/z 416.9816 for Ag5fa (relative errors 46.5 ppm and 1.9 ppm) and m/z 261.9556 and m/z 416.9816 for Ag6fa (relative errors 46.5 ppm and 1.9 ppm). The full mass spectra of the complexes are presented in the **Appendix**.

The observation of the species containing one silver and one fluoroanthranilic acid molecule ($AgC_7H_6FNO_2$) agree with the composition suggested based on elemental and thermal analyses. On the other hand, species containing Ag(I) and two molecules of fluoroanthranilic acids were also observed. Such species may come from the extended structure of the complexes as seen in the crystal structure of Ag5fa.

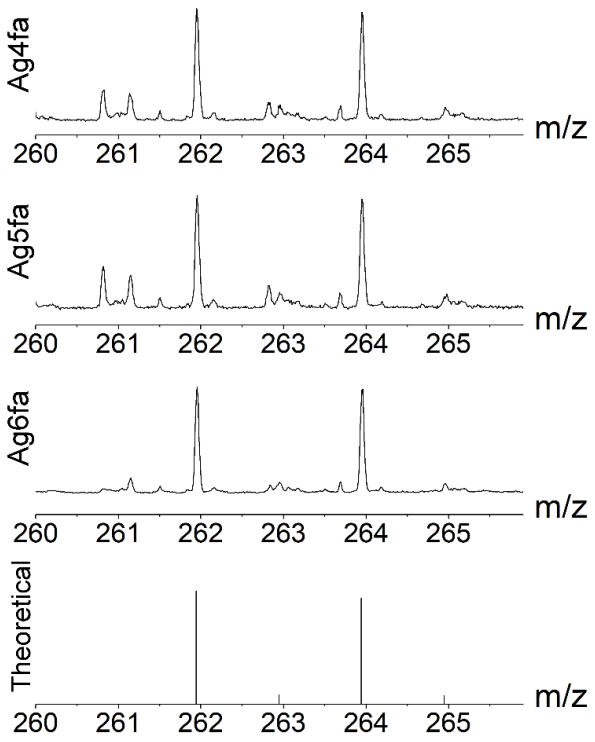

Figure 18. Mass spectra of Ag4fa, Ag5fa, Ag6fa (top to bottom) and theoretical isotopic pattern for $AgC_7H_6FNO_2$ from m/z 260 to 265.

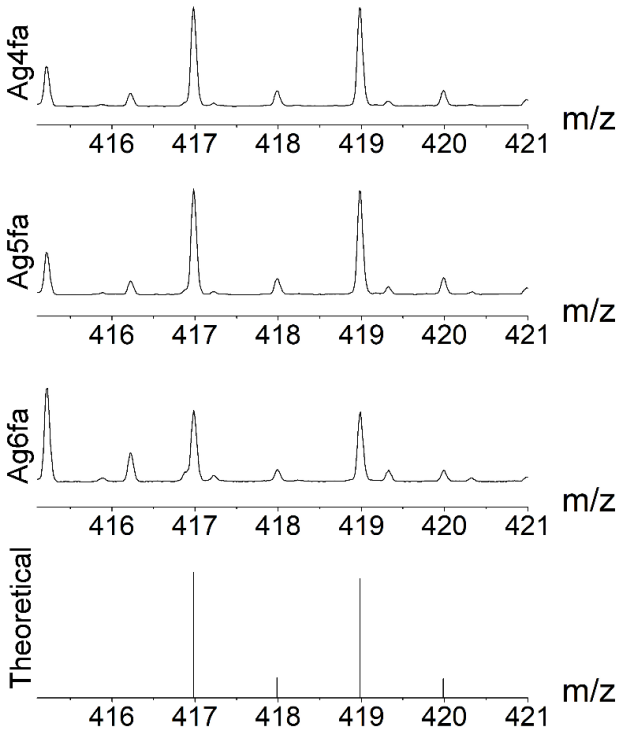

Figure 19. Mass spectra of Ag4fa, Ag5fa, Ag6fa (top to bottom) and theoretical isotopic pattern for $Ag(C_7H_6FNO_2)_2$ from m/z 416 to 421.

1.5. NMR spectroscopy

The Ag(I) complexes were characterized by NMR experiments in DMSO-d^6. The NMR spectra of the coordination compounds were compared with the free ligands and the attribution of ^1H and ^{13}C signals was confirmed by {^1H,^{13}C} HSQC (heteronuclear single quantum coherence) and {^1H,^{13}C} HMBC (heteronuclear multiple bond coherence) techniques, which give coherent signals from hydrogen and carbon atoms separated by a single bond or multiple bonds, respectively. While the ^1H and ^{13}C NMR spectra with attributions are presented in Figures 20-27 , the {^1H,^{13}C} HSQC and HMBC spectra obtained for all the silver complexes and their ligands are presented in the **Appendix**.

First, for 4fa and Ag4fa, only slightly changes in the shift of all the hydrogen signals are observed in the ^1H NMR spectra (Figure 20), apart from the signal of the amine hydrogen atoms that is present in the spectra of the complex but not of the ligand. The absence of this signal might be because of intermolecular hydrogen bonds (not present in the coordination compound) or because of high rotational liberty of the amine moiety in the ligand [109]. However, important shifts can be noticed in the ^{13}C spectra (Figure 21) for the signal of carbon atoms **2** and **7**. Carbon **2** is directly bonded to the nitrogen of the amine moiety and is shifted by 7.3 ppm after coordination, while atom **7** is the carbon of the carboxylic acid which is shifted by 2.7 ppm. These results confirm coordination of 4fa by the amine and carboxylic acid moieties.

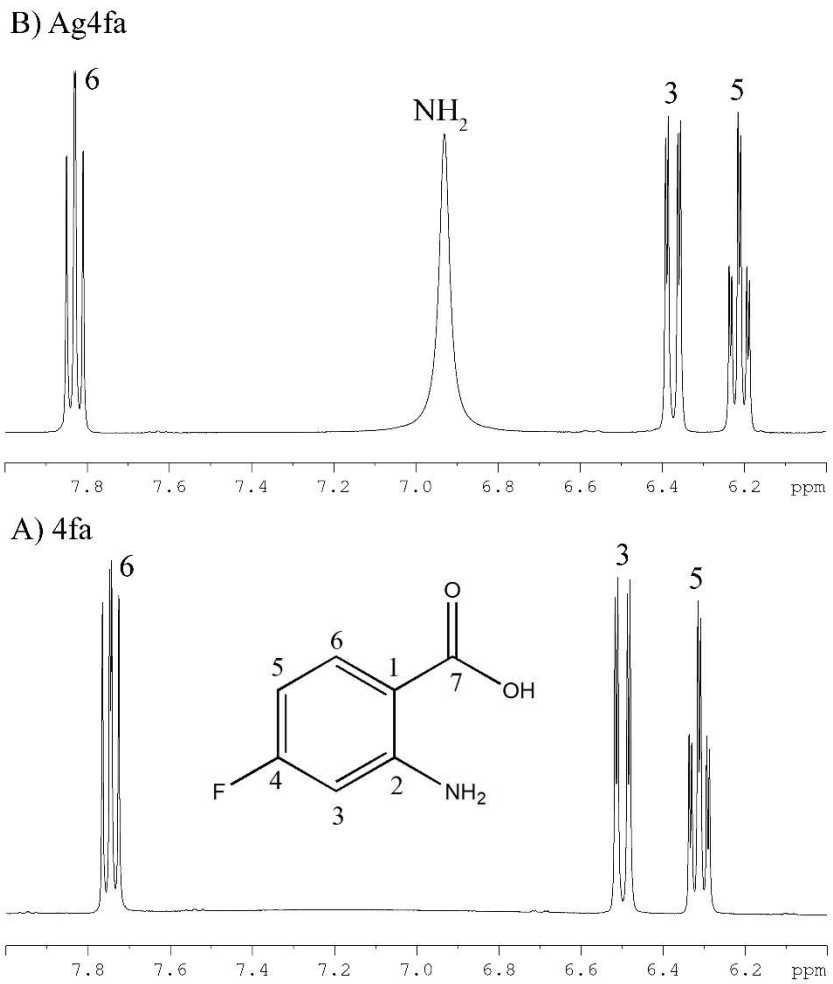

Figure 20. The ^{1}H NMR spectra of 4fa (A) and Ag4fa (B) in DMSO-d^{6}.

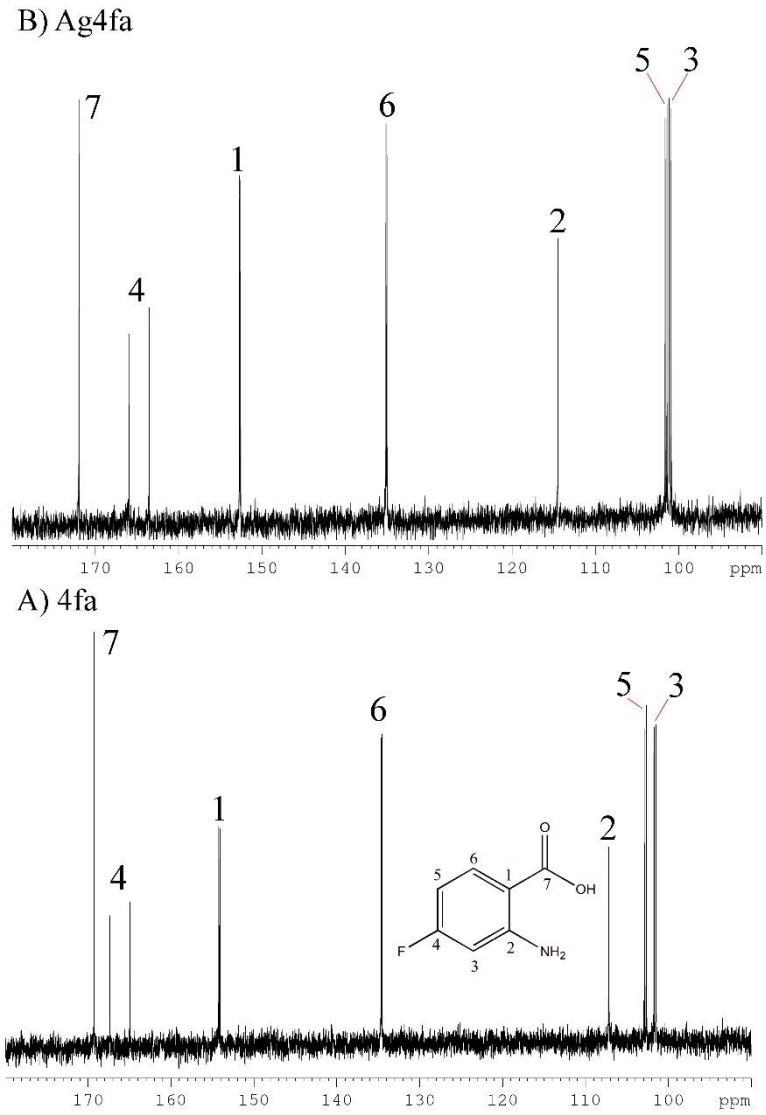

Figure 21. The ^{13}C NMR spectra of 4fa (A) and Ag4fa (B) in DMSO-d^6.

Similar results were observed for the ^{1}H NMR of 5fa and Ag5fa (Figure 22), but in this case the hydrogens from the amine in the spectra of the ligand and the complex are observable and in very different chemical shifts, in 8.61 ppm in the ligand and 6.56 ppm in the complex (Δ=2.05 ppm). It evidences that the electron density changes in the amine group of Ag5fa, probably due to coordination. The shape of this signal is also sharpened suggesting that the rotation of the amine group is restricted for the complex or that the hydrogen bonds are limited.

The ^{13}C NMR spectra of 5fa and Ag5fa (Figure 23) also suggests coordination by the amine group as the signal of carbon **2** shifts 8.1 ppm and coordination by the carboxylic acid as carbon **7** and **1** are shifted by 2.0 ppm and -2.1 ppm, respectively.

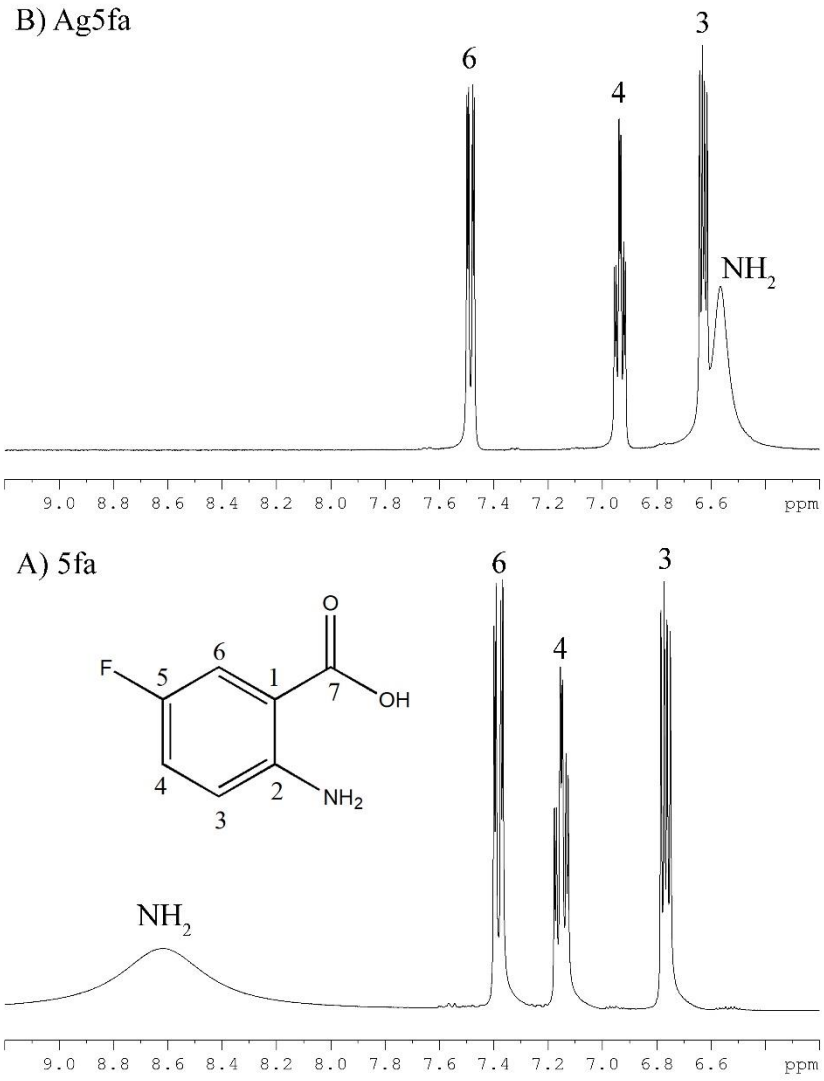

Figure 22. The ^{1}H NMR spectra of 5fa (A) and Ag5fa (B) in DMSO-d^{6}.

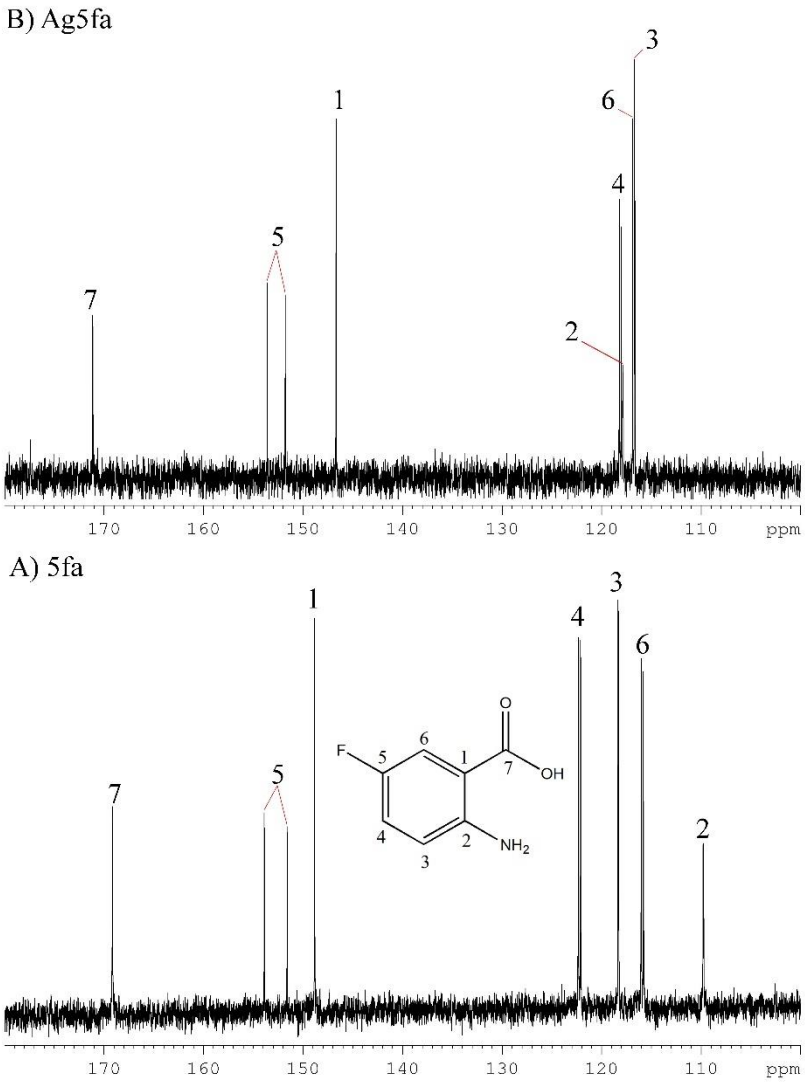

Figure 23. The ^{13}C NMR spectra of 5fa (A) and Ag5fa (B) in DMSO-d^6.

For 6fa and Ag6fa the ^{1}H NMR signal of the amine hydrogens is absent in the spectra of the ligand but in the spectra of Ag6fa (Figure 24) it appears merged with the signal of the hydrogen **4**. Once again, the ^{13}C NMR spectra (Figure 25) suggested coordination of the fluoroanthranilic by the amine group and carboxylic acid as carbon atoms **1**, **2** and **7** are shifted by -2.46, 9.24 and 1.23 ppm, respectively, after coordination.

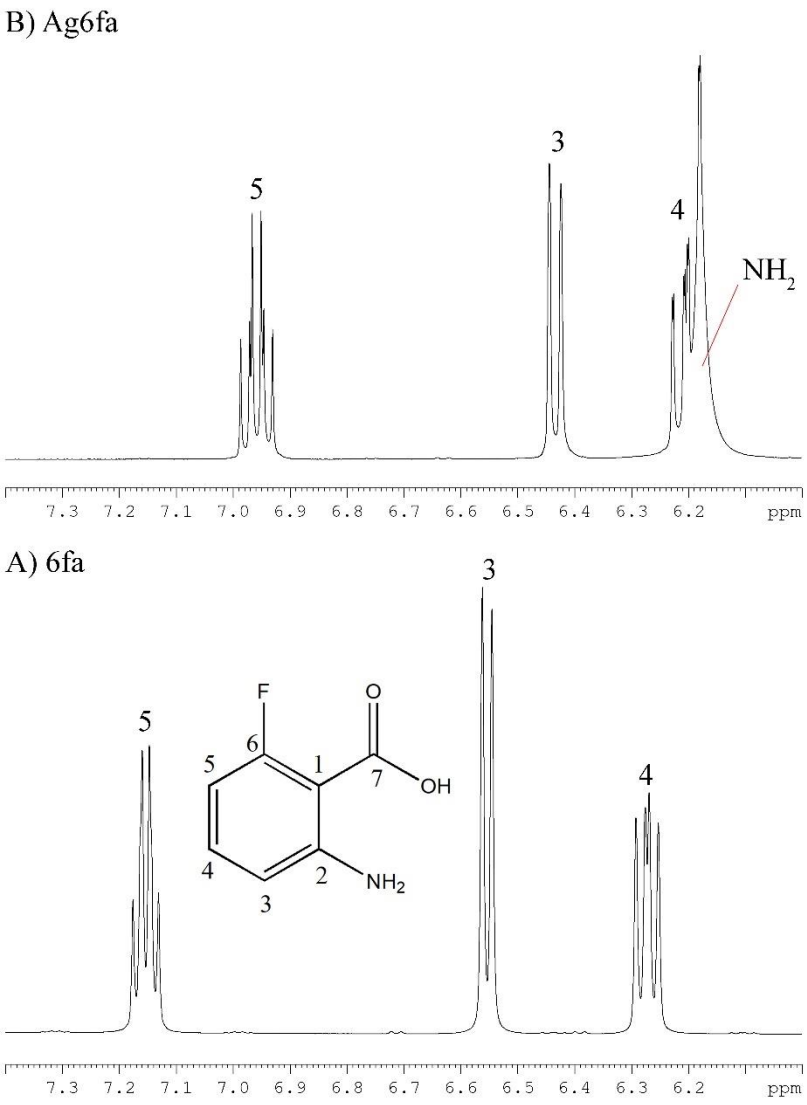

Figure 24. The ^{1}H NMR spectra of 6fa (A) and Ag6fa (B) in DMSO-d^{6}.

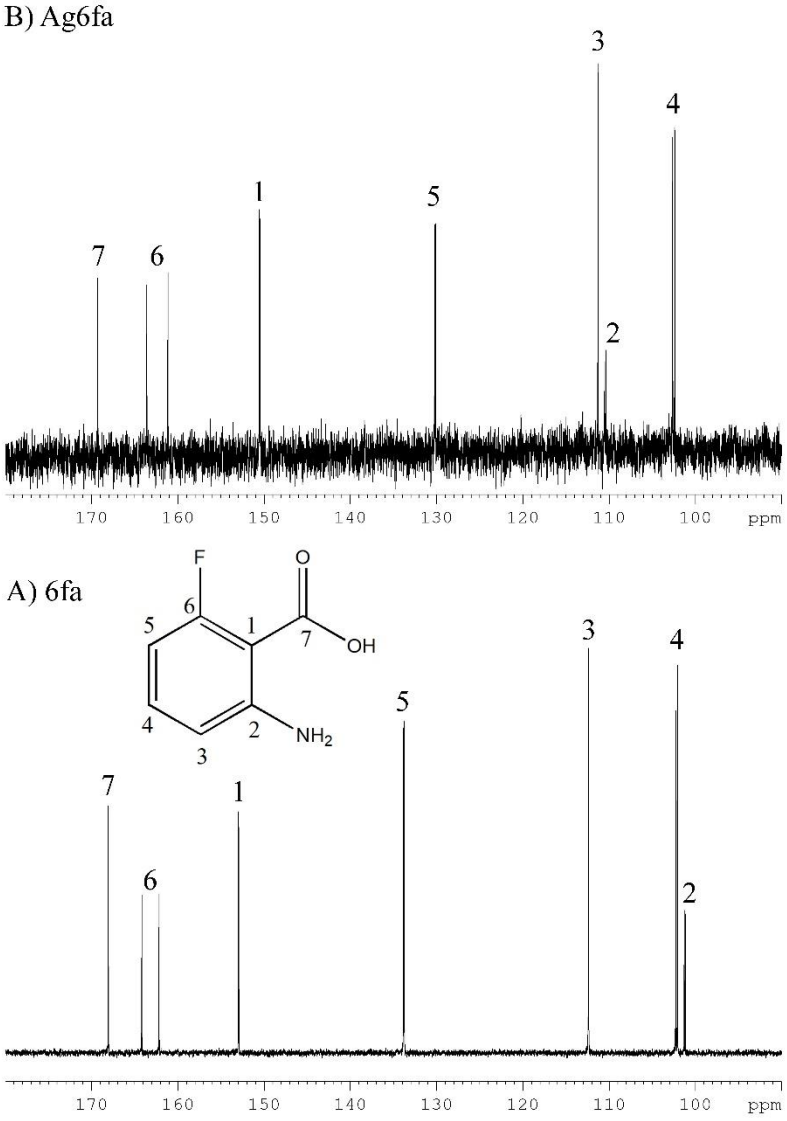

Figure 25. The ^{13}C NMR spectra of 6fa (A) and Ag6fa (B) in DMSO-d^6.

Finally, the ^{1}H NMR spectra of 4,5fa and Ag-4,5fa are shown in Figure 26. In this case, the only two hydrogen atoms bound to the aromatic ring are in the positions **3** and **6** and their signals are slightly shifted by 0.07 and -0.16 ppm, respectively, after coordination. The NH_2 signal is also observed at 6.79 ppm only in the spectra of the complex. More evident suggestions that coordination happens by the carboxylate and amino groups of 4,5fa are observed in the ^{13}C spectra (Figure 27), where carbon atoms **1**, **2** and **7** are the ones with the highest shifts after coordination.

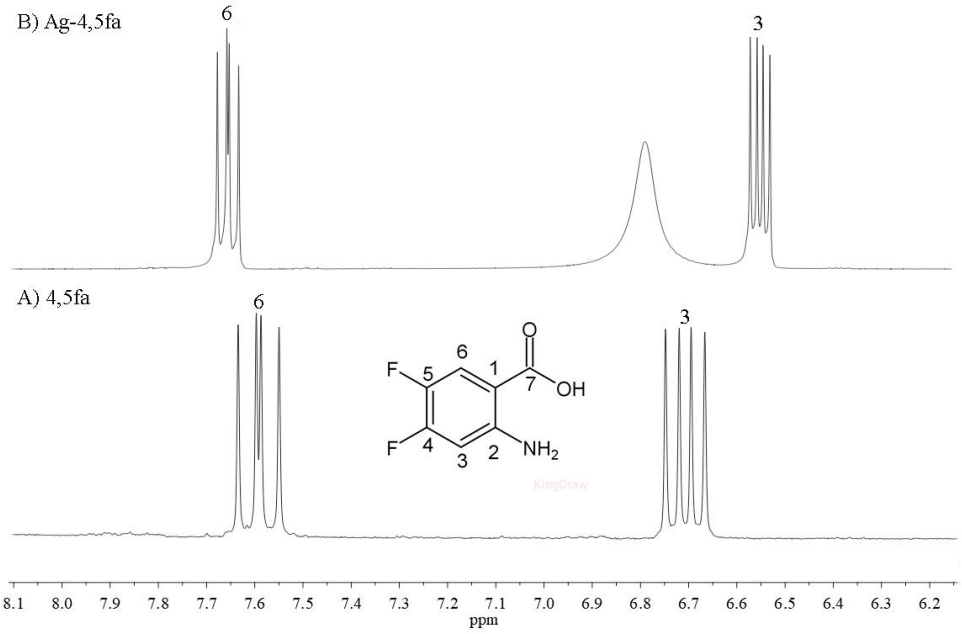

Figure 26. The ^{1}H NMR spectra of 4,5fa (A) and Ag-4,5fa (B) in DMSO-d^{6}.

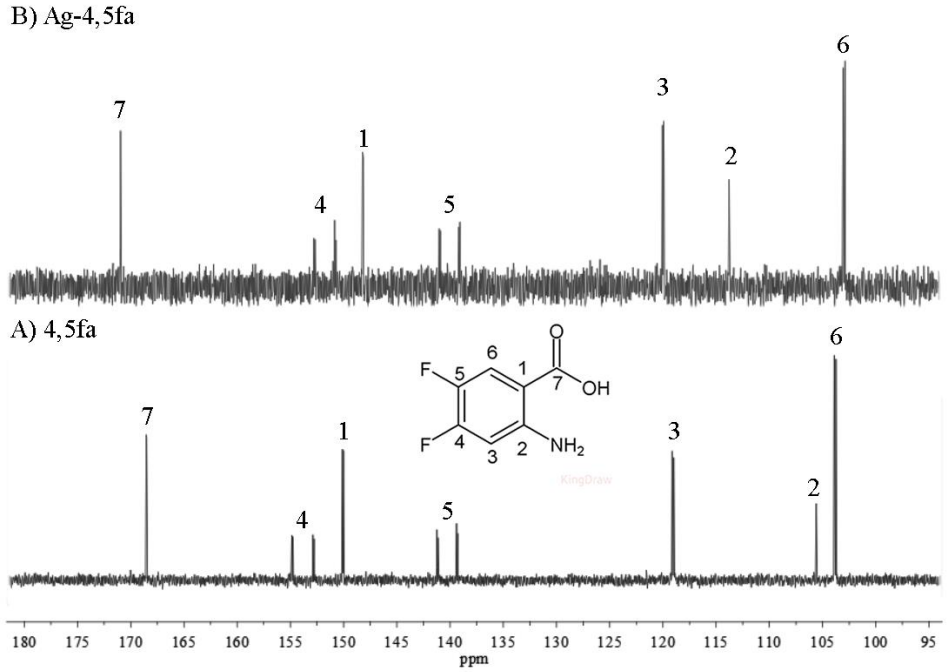

Figure 27. The ^{13}C NMR spectra of 4,5fa (A) and Ag-4,5fa (B) in DMSO-d^{6}.

The chemical shifts of ^{13}C were summarized in Table 5, where it is evident that, for all these examples, the most significant variation in chemical shift after coordination occurs in carbon **2** which is directly bound to the amino group. With the coordination of Ag^{+} to the amino group, the electron density in the neighbor carbon atom is lowered (the atom is deshielded) and it experiences a stronger magnetic field, therefore the chemical shift is moved downfield, at higher frequencies. In the case of the fluoroanthranilic ligands, this mentioned difference in chemical shift after coordination (Δ) for carbon **2** is between 6.9 and 9.2 ppm, as seen in Table 5. Similar consequence is observed for carbon atom **7** from the carboxylic acid moiety that is also involved in coordination.to the Ag ion.

Table 5. The ^{13}C NMR chemical shifts for 4fa, 5fa, 6fa, 4,5fa, Ag4fa, Ag5fa, Ag6fa and Ag-4,5fa and the difference (Δ) between the signal of the respective ligands and complexes.

	^{13}C NMR shifts (ppm)						
Carbon atoms	1	2	3	4	5	6	7
4fa	154.2	107.2	101.6	166.1	102.8	134.6	169.3
Ag4fa	152.6	114.5	101	164.8	101.5	135.1	172
Δ	-1.6	**7.3**	-0.6	-1.3	-1.3	0.5	2.7
5fa	148.8	109.8	118.3	122.2	152.7	115.9	169.1
Ag5fa	146.7	116.7	117.9	118.1	152.7	116.8	171.1
Δ	-2.1	**6.9**	-0.4	-4.1	0.0	0.9	2.0
6fa	153.0	101.2	112.4	102.2	133.8	163.2	168.1
Ag6fa	150.5	110.4	111.3	102.5	130.2	162.4	169.3
Δ	-2.5	**9.2**	-1.1	0.3	-3.6	-0.8	1.2
4,5fa	150.0	105.6	119.0	153.8	140.3	108.8	168.5
Ag-4,5fa	148.2	113.8	120.0	151.7	140.0	102.9	170.9
Δ	-1.8	**8.2**	1.0	-2.1	-0.3	-5.9	2.4

It is observed in all the ^{13}C NMR spectra of each of these fluorinated compounds that the signals of carbon atoms bound to fluor have high $^{1}J_{CF}$ coupling constants (between 230 and 252 Hz) and therefore the signals appear duplicated in the spectra. Furthermore, smaller coupling constants between C and F are also observed due to $^{2}J_{CF,}$ $^{3}J_{CF}$ and $^{4}J_{CF}$, that are couplings with two, three or four chemical bonds between carbon and fluorine atoms, as shown in Table 6. These values are mostly in agreement with the literature, with

($^{1}J_{CF} \approx 250$ Hz) >> ($^{2}J_{CF} \approx 20$ Hz) > ($^{3}J_{CF} \approx 8$ Hz) > ($^{4}J_{CF} \approx 3$ Hz). (Ref: Hans Reich's Collection, available at: https://organicchemistrydata.org/)

To confirm coordination of 4fa, 5fa, 6fa and 4,5fa to Ag(I) by the amine group, {^{1}H,^{15}N} HSQC and HMBC NMR experiments were performed. Figure 28 shows the HMBC NMR spectra of 4fa, Ag4fa, 5fa, Ag5fa, 6fa and the HSQC NMR spectrum of Ag6fa. The ^{15}N signals were shifted upfield by -2.6 ppm for Ag4fa, -3.7 ppm for Ag5fa and -4.9 ppm for Ag6fa. This data, combined with the observed shifts in ^{13}C NMR signals of carbon **2**, confirm the coordination by the amine group. Separately, Figure 29 presents the HSQC and HMBC of the Ag-4,5fa complex. The signal of the nitrogen atom of the 4,5fa ligand was not observed in neither HSQC nor HMCB {^{1}H, ^{15}N} spectra and therefore it was not possible to calculate the change in chemical shift after coordination.

Table 6. Carbon-Fluor NMR coupling constants (J_{CF}) for the fluoroanthranilic acids and their Ag complexes. Coupling constants are expressed as $^{x}J_{CF}$ where "x" corresponds to 1, 2, 3 or 4 bonds between C and F atoms.

	$^{x}J_{CF}$	C1	C2	C3	C4	C5	C6	C7
4fa	1				247.41			
	2			24.28		22.81		
	3		-				11.7	
	4	13.27						
Ag4fa	1				243.49			
	2			23.92		21.41		
	3		-				10.85	
	4	12.47						

	$^{x}J_{CF}$	C1	C2	C3	C4	C5	C6	C7
5fa	1					230.68		
	2				23.07		22.38	
	3	-		7.09				
	4		6.42					-
Ag5fa	1					229.19		
	2				22.68		~18.7	
	3	-		~3.64				
	4		5.56					-

	$^{x}J_{CF}$	C1	C2	C3	C4	C5	C6	C7
6fa	1						252.75	
	2	4.9				12.15		
	3		14.21		23.68			2.21
	4			2.59				
Ag6fa	1						246.5	
	2	6.11				11.49		
	3		15.58		23.76			-
	4			2.35				

	$^{x}J_{CF}$	C1	C2	C3	C4	C5	C6	C7
4,5fa	1				249.57	233.09		
	2			17.64	14.25	13.78	19.95	
	3	11.17	3.91	2.54				
	4	-	1.36					2.11
Ag-4,5fa	1				245.08	230.92		
	2			16.53	13.85	13.26	19.55	
	3	10.31	-	-				
	4	-	-					-

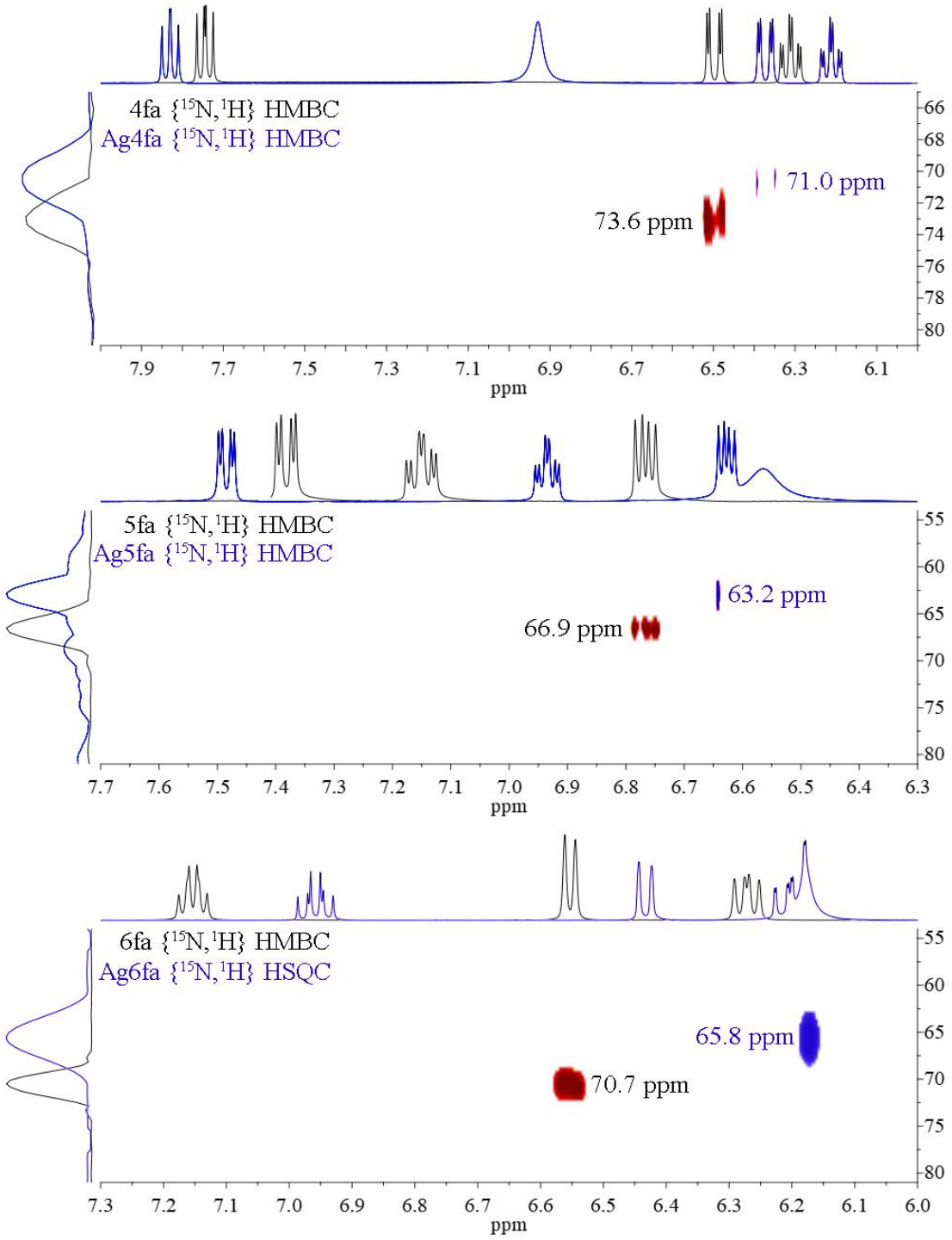

Figure 28. The {^{15}N, ^{1}H} NMR spectra of the ligands (black) and Ag(I) complexes (blue) in DMSO-d^{6}.

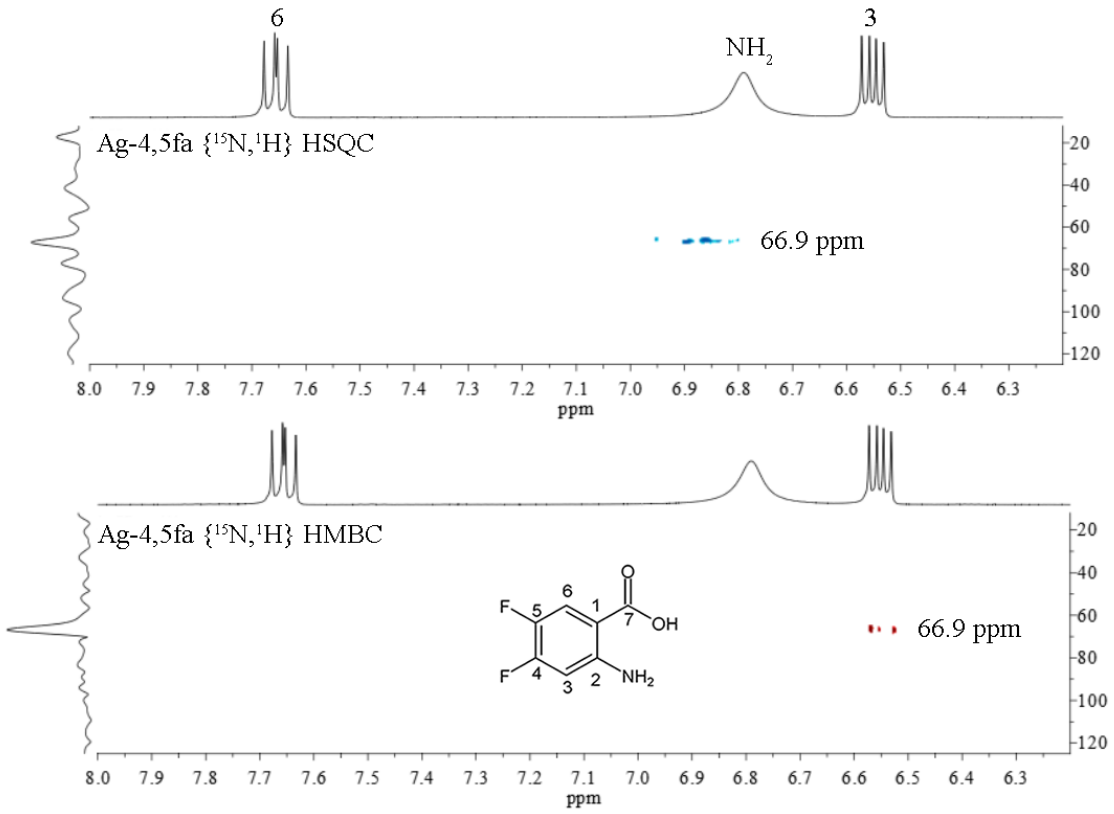

Figure 29. The {^{15}N, ^{1}H} HSQC (top) and HMBC (bottom) NMR spectra of Ag-4,5fa in DMSO-d^{6}.

Although, sufficient evidences of coordination were observed by NMR spectroscopy, some ^{19}F NMR experiments were also performed to further characterize these compounds in DMSO solution. The ^{19}F atoms are highly sensitive to electronic density changes and exhibit a large chemical shift range (~300 ppm) [110]. Therefore, similar changes in the chemical shifts were observed upon coordination in all four complexes with fluoroanthranilic acids, as shown in Figure 30.

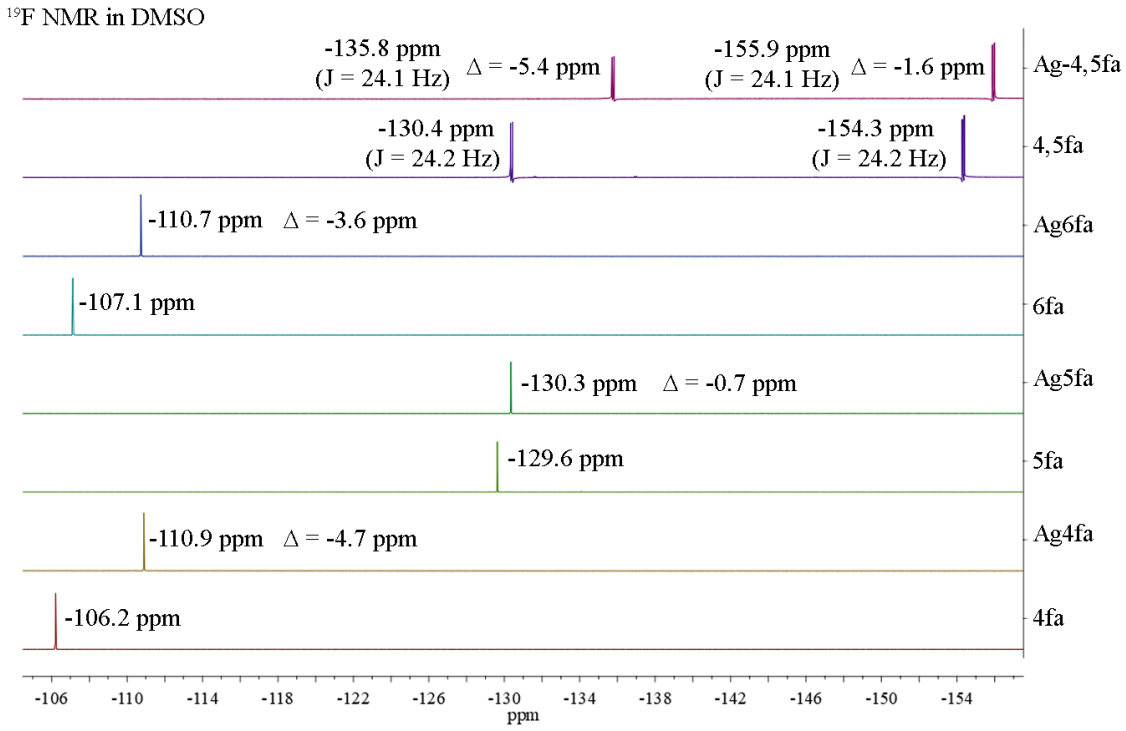

Figure 30. The ^{19}F NMR spectra of fluoroanthranilic ligands and their respective silver complexes in DMSO.

1.6. Fluorescence spectroscopy of the fluoroanthranilic ligands and their complexes.

The fluorescence of the fluoroanthranilic ligands was first observed visually under UV light as shown in Figure 31 (3.0 µmol/L in acetonitrile) and later the spectra were recorded in acetonitrile solution (0.1 µmol/L) using the optimal excitation wavelength (λ_{exc}) for the maximum fluorescent emission intensity. The spectra are presented in Figure 32 and the fluorescence data with the wavelength of maximum fluorescent emission (λ_{max}), excitation wavelength (λ_{exc}) and fluorescence intensity are in Table 7.

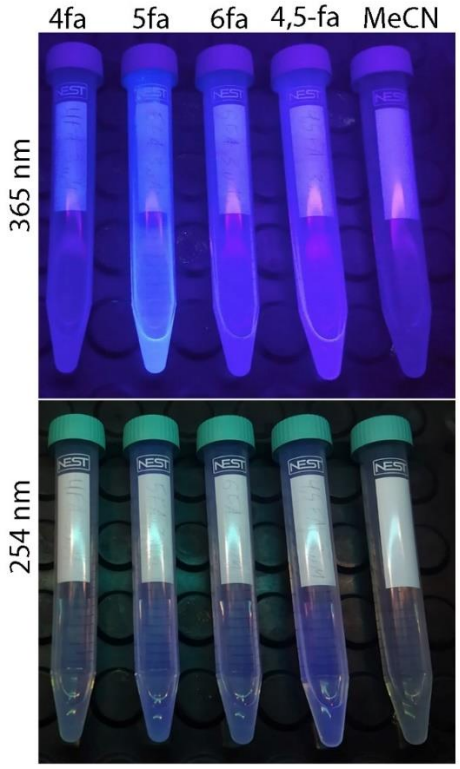

Figure 31. Fluorescence of 4fa, 5fa, 6fa and 4,5-fa solutions (3.0 µmol/L) in acetonitrile under UV light of 365 and 254 nm. A sample containing only acetonitrile is also shown for comparison.

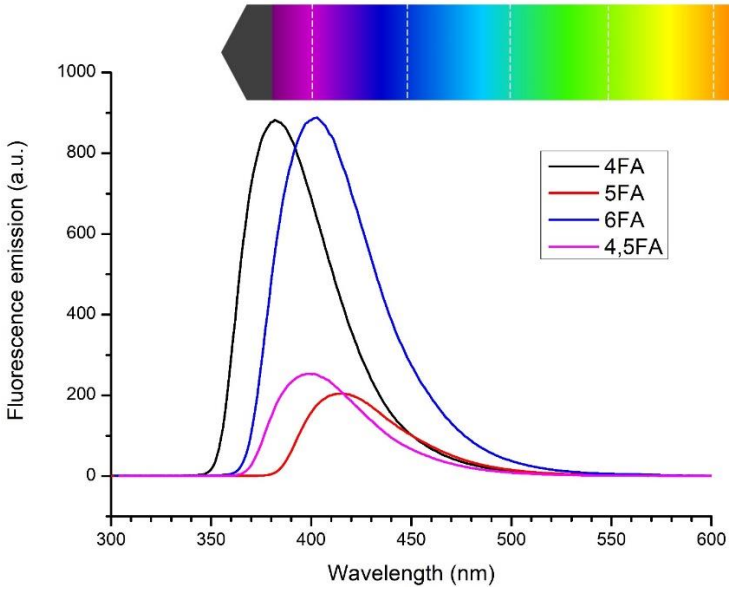

Figure 32. Emission fluorescence spectra of 4fa, 5fa, 6fa and 4,5-fa from 300 to 600 nm in acetonitrile solution (0.1 µmol/L).

Table 7. Fluorescence data for fluoroanthranilic acids: excitation wavelengths, fluorescent emission wavelengths and relative intensity of emitted signal.

Molecules	**λ_{ex} (nm)**	**λ_{max} (nm)**	**Intensity (a.u.)**
4fa	274.0	381.8	882.1
5fa	294.0	413.0	203.7
6fa	282.0	403.1	887.8
4,5-fa	284.3	399.4	253.0

Moreover, the fluorescence emission of 4fa, 5fa, 6fa and their respective silver complexes (Ag4fa, Ag5fa and Ag6fa) were also recorder from 300 to 550 nm. In this case DMSO was used as solvent due to the lower solubility of the complexes in other solvents and the spectra of these solutions at 0.1 µmol/L were recorded using the same excitation wavelength of 280 nm for all species. (Figure 33).

The maximum fluorescent emissions were observed at 382 nm for 4fa and Ag4fa, 398 nm for 6fa and Ag6fa and 412 nm for 5fa and Ag5fa, following the same order of energy gaps proposed by theoretical studies that are shown in the next section. It is noticed that the fluoresce emission is still present in the complexes although in lower intensity for Ag4fa and Ag5fa in comparison to their respective free ligands (see Figure 33, black and blue lines). The fluorescence emission in the solution of the complexes was not

attributed to degradation of the coordination compound (and presence of free ligands), as the stability of these solutions was confirmed by NMR spectroscopy.

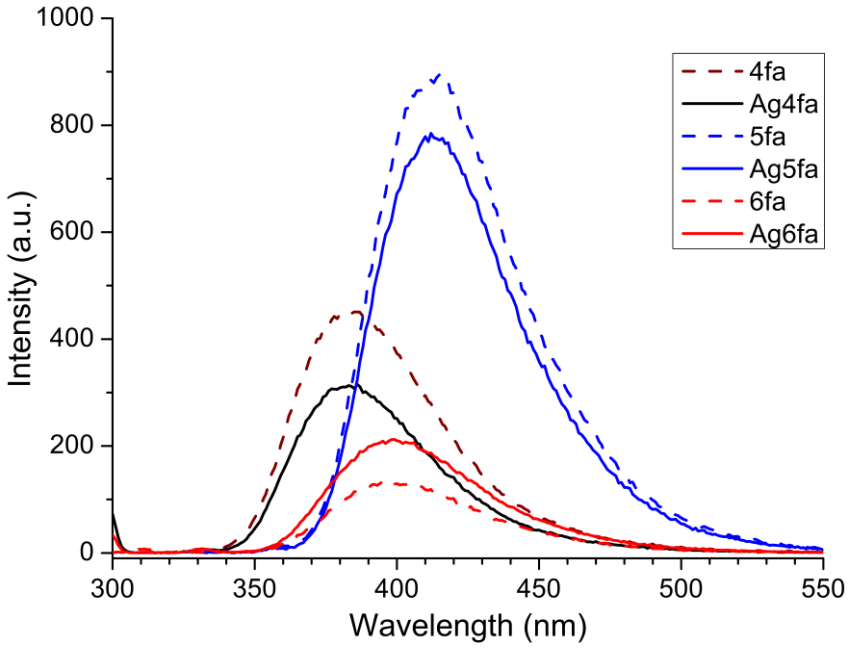

Figure 33. Emission fluorescence spectra of 4fa, 5fa, 6fa and their respective silver complexes from 300 to 550 nm, in DMSO, using the same excitation λ (280nm).

1.7. Theoretical calculations and UV-Vis spectroscopy of the fluoroanthranilic acid ligands.

The theoretical studies of the electronic properties of 4-fluoroanthranilic acid (4fa), 5-fluoroanthranilic acid (5fa) and 6-fluoroanthranilic acid (6fa) were performed by the analyses of their molecular orbitals (MO) and their excited states. These calculations were performed in collaboration with professor Douglas Henrique Pereira from UFT (Universidade Federal do Tocantins). Figure 34 shows the calculated energies for the highest occupied molecular orbital (HOMO) and the lowest unoccupied molecular orbital (LUMO) and the energy gap (ΔE) between them for the ligands 4fa, 5fa and 6fa.

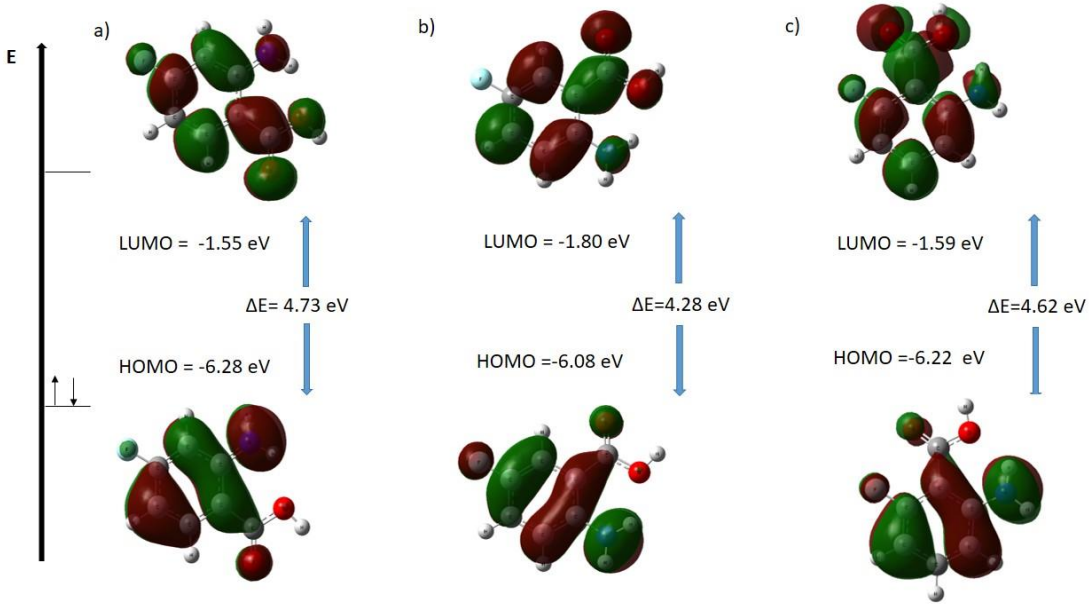

Figure 34. HOMO, LUMO and gap for: a) 4-fluoroanthranilic acid (4fa), b) 5-fluoroanthranilic acid (5fa) and c) 6-fluoroanthranilic acid (6fa).

Distinguished characteristics of π orbitals for HOMO and LUMO are observed in the aromatic rings of the compounds. The energy gap value is the highest for 4fa (4.73 kcal mol^{-1}), followed by the gap energy in 6fa (4.62 kcal mol^{-1}) and 5fa (4.28 kcal mol^{-1}), suggesting that the position of the fluorine atom in the structures indeed alters the energies of the orbitals, and consequently other properties such as the fluorescence emission.

The UV-Vis spectra of these ligands (including 4,5fa) were recorded and can be seen in Figure 35. These data were than compared with the theoretical maximum absorption wavelength considering the calculated excited states.as shown in Table 8.

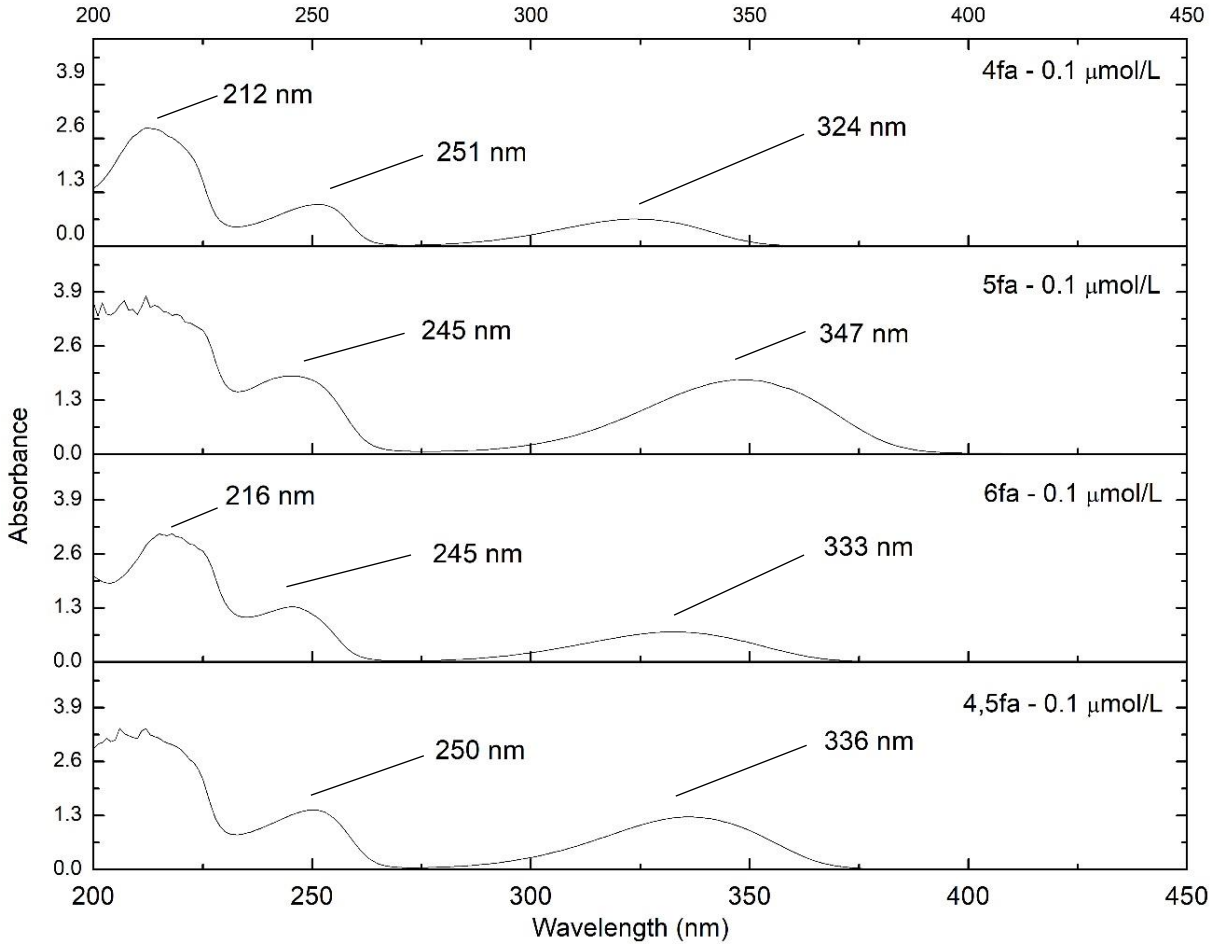

Figure 35. UV-Vis spectra for the fluoroanthranilic acid ligands 4fa, 5fa, 6fa and 4,5fa from 200 to 450nm, recorded in acetonitrile 0.1 μmol/L.

Table 8. Maximum absorption wavelength (λmax) for 4fa, 5fa and 6fa obtained by the calculations in comparison to the experimental results. The UV-Vis spectra were obtained from solutions in the concentration of 0.1 μmol/L in MeCN.

	4fa	5fa	6fa
Theoretical λmax (nm)	374.17	424.19	380.63
Experimental λmax (nm)	324	347	333

According to the calculations, the maximum absorption wavelengths for these ligands are 374.17 nm for 4fa, 380.63 nm for 6fa and 424.19 nm for 5fa, considering the theoretical situation where the molecules would be in the vacuum. Although these values are higher than the experimental λmax obtained by UV-Vis spectroscopy, the increasing order of λmax is the same: 4fa < 6fa < 5fa. Therefore, the experimental results for UV-Vis and fluorescence spectroscopy agree with the theoretical calculation indicating that 5fa has the lower gap energy.

1.8. Molecular docking studies

To further investigate the antimycobacterial activity of the fluoroanthranilic acid isomers and specifically the difference between them, theoretical molecular docking studies were performed to evaluate the affinity of these isomers with the active site of the anthranilate phosphoribosyltransferase (TrpD) from *Mycobacterium tuberculosis*. For this study, two crystal structures of TrpD, named 4OWN and 4OWV were retrieved from the Protein Data Bank (PDB) and used as targets for the molecular docking.

The docking studies were performed not only with the fluoroanthranilic acids 4fa, 5fa, 6fa and 4,5fa, but also with other structurally similar molecules such as 2-amino-3-hydroxybenzoic acid (2A3H-BA) and 2-hydroxy-4-aminobenzoic acid (2H4A-BA), to evaluate the intensity of their interaction and determine if one of them would be more easily incorporated in the synthesis of tryptophan, or if they are able to somehow inhibit that pathway. We are also interested to kwon if different isomers of fluorotryptophan (that would be the product of incorporation of fluoroanthranilic acids in the pathway) could inhibit the allosteric regulatory site in the anthranilate synthase (TrpE - 5CWA).

AnPRT (TrpD) catalyzes the Mg^{2+}-dependent transfer of a phosphoribosyl group from PRPP (5′-phosphoribosyl-1′-pyrophosphate) to anthranilate to form 5′-phosphoribosyl anthranilate. In the TrpD structure there are two distinct binding sites for anthranilate (see Figure 36). One site is located over 8 Å (1 Å=0.1 nm) from PRPP at the entrance to a tunnel (position 1) leading to the active site, whereas in the inner site (position 2) anthranilate is adjacent to PRPP, in a catalytically relevant position for the transfer of the phosphoribosyl group. It is proposed that anthranilate first binds to the outer site, providing an unusual mechanism for substrate capture and efficient transfer to the catalytic site following the binding of PRPP. [79]

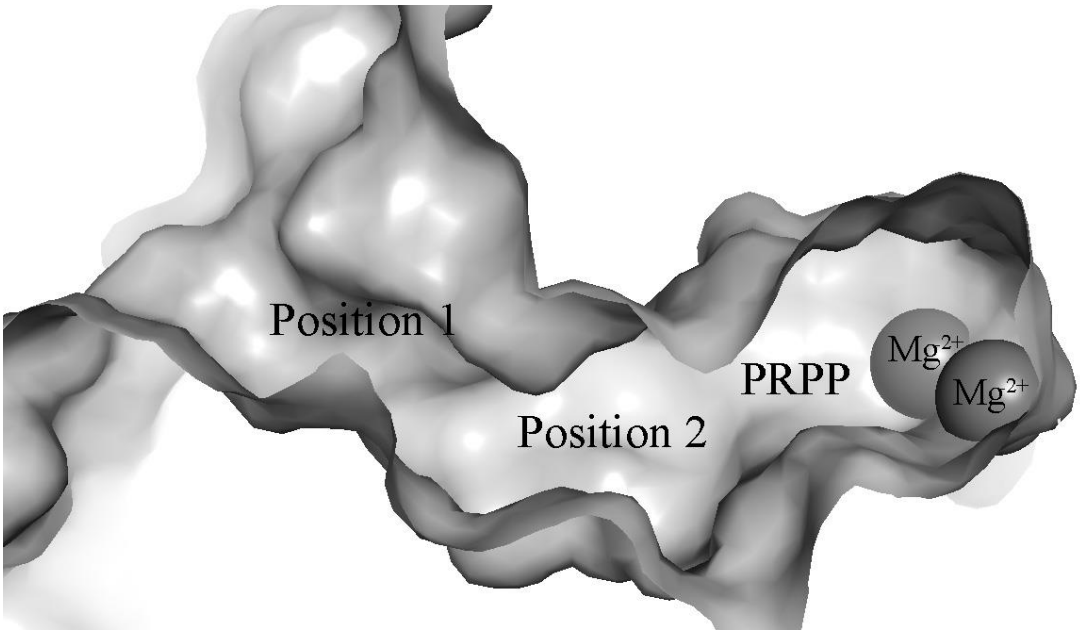

Figure 36. Representation of the catalytic pocket of TrpD with binding sites in Positions 1 and 2.

Docking in Position 1 showed that specially 5-fluoroanthranilic acid (5fa), but also 4,5-fluoroanthranilate (4,5-fa^{-1}) and 4-fluoroanthranilate ($4fa^{-1}$) have docking scores more negative than anthranilic acid, the original subtract of this enzyme, as presented in Table 9. The docking scores are correlated to the theoretical ΔG of this system, meaning that the more negative these values are, the stronger are the interactions observed, lowering the overall energy.

Table 9. Docking scores for the ligands evaluated on Position 1 of TrpD (4OWN).

Ligand	**Docking Scores for Position 1**
5fa	-5.735
4,5fa-1	-5.496
4fa-1	-5.44
2H4A-BA-1	-5.344
Anthranilic acid	*-5.235*
4,5-fa	-5.148
2H4A-BA	-5.135
5fa-1	-5.106
4fa	-5.045
6fa-1	-5.032

Hydrogen bonds were identified in the simulations between the amino and carboxylate groups of 4,5fa^{-1} and the residues His 183 and Arg 194, respectively (Figure 37). These interactions are very similar to the ones that involve the anthranilic acid substrate (Figure 38). Additionally, an hydrogen bond could be identified between the fluorine in the position 4 of the 4,5-fa^{-1} ligand and Ala 179 (F-H = 2.3 Å), which can also be observed for 4fa^{-1} with the same distance of 2.3 Å (not shown). Perhaps the explanation for the slightly more negative docking score for 4,5-fa^{-1} in comparison to 4fa^{-1} is the additional hydrogen bonds involving the fluorine in position 5 and Asn 138 (F-H1 = 2.3 Å and F-H2 = 2.5 Å). As might be expected, ligand 5fa and 5fa^{-1} also feature this hydrogen bond with Asn 138. The hydrogen bonds with similar intensity involving the fluorine atom in position 6 for 6fa and 6fa^{-1} was not found in that region.

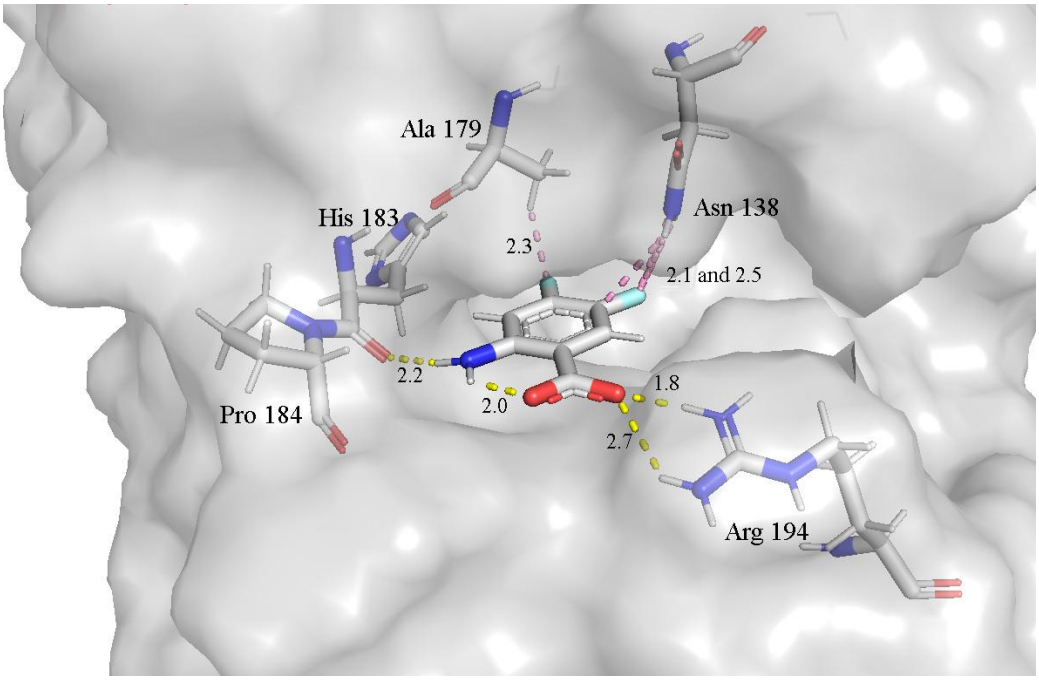

Figure 37. Ligand 4,5-fa^{-1} in Position 1 of TrpD. Light grey; hydrogen, grey: carbon, blue: nitrogen, red: oxygen, light blue: fluorine. Dashed lines: interaction distances in Angstrom (Å).

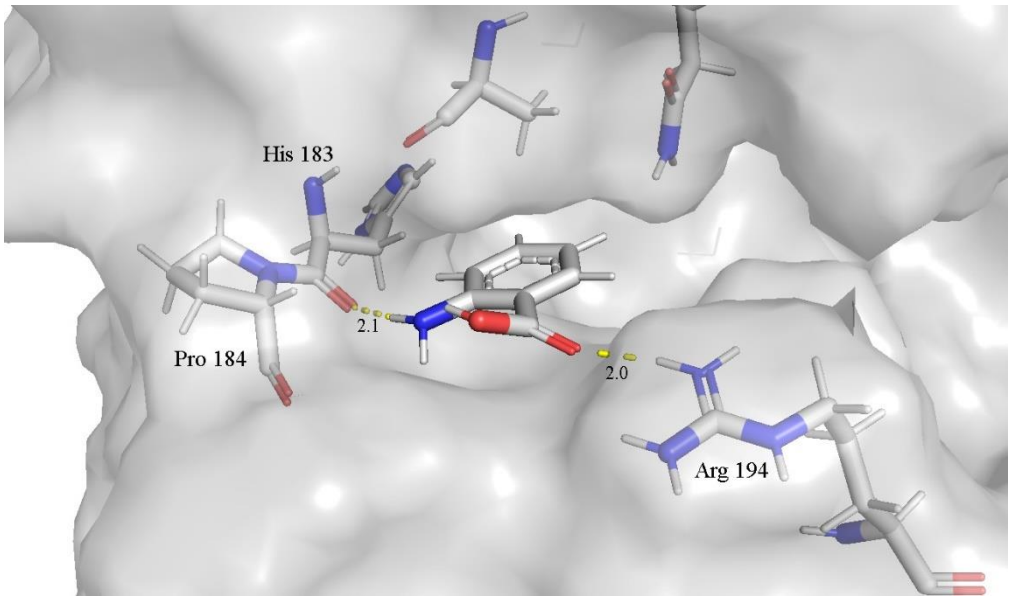

Figure 38. Anthranilic acid substrate in Position 1 of TrpD, obtained from docking calculations. Light grey; hydrogen, grey: carbon, blue: nitrogen, red: oxygen, light blue: fluorine. Dashed lines: interaction distances in Angstrom (Å).

One possible explanation for the more negative docking score of 5fa is that, besides the polar interactions with His 183 and Arg 194 and hydrogen bond with Asn 138, the position of this ligand is optimal when considering solvent exposure. In this case, the highly electronegative fluorine atom in position 5 creates a dipole moment that is directed towards the region of the enzyme that is exposed to water. The 2D scheme in Figure 39 shows the interactions of 5fa in the position 1 of TrpD, including the region of solvent exposure.

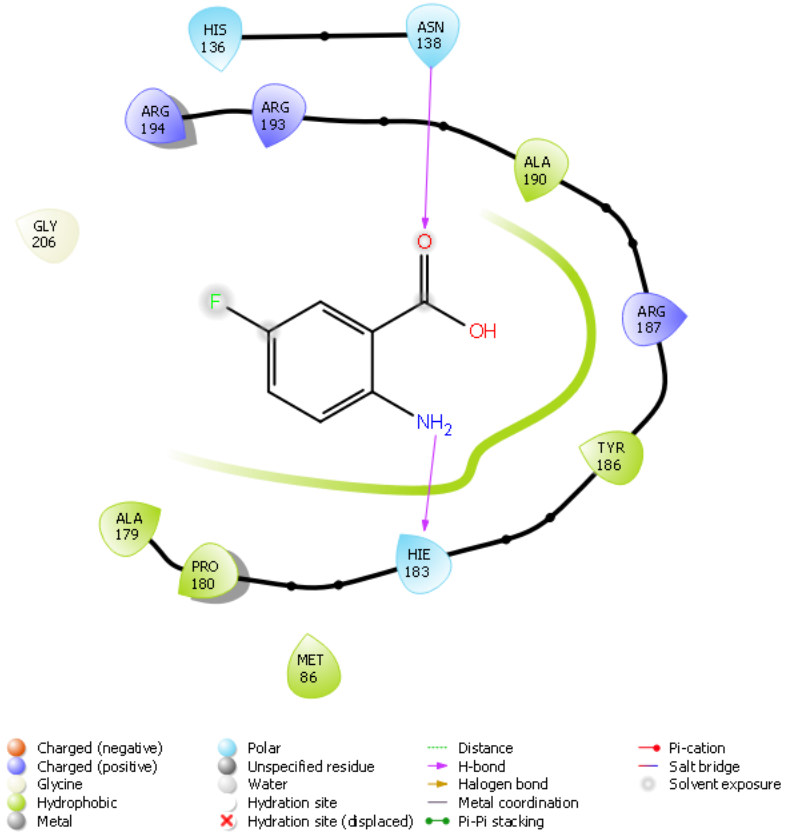

Figure 39. Scheme of interaction observed in the molecular docking of 5fa molecule in the Position 1 of the catalytic pocket of TrpD (4OWN).

In the case of the catalytic relevant Position 2 of TrpD, the molecules 2A3H-BA and 2H4A-BA showed more favorable interactions, followed by 4fa and 45-fa (see Table 10). The Position 2 is a mostly hydrophobic pocket adjacent to the PRPP site, where the substrate is positioned for the catalytic transfer of the phosphoribosyl group. For the Position 2 it was not possible to identify major interactions that would justify higher docking score for these ligands. A scheme with the key interactions observed between 5-fluoroanthranilate molecule and the crystal structure of of TrpD Position 2 is shown in Figure 40.

Table 10. Docking scores for the ligands evaluated on Position 2 of TrpD (4OWN).

Ligand	**Docking Scores for Position 2**
2A3H-BA-1	-4.841
2H4A-BA	-4.711
4fa-1	-4.477
2A3H-BA	-4.423
4,5-fa	-4.389
2H4A-BA-1	-4.363
5fa-1	-4.190
6fa-1	-4.094
Anthranilate	-3.996
Anthranilic acid	-3.995
4fa	-3.960
4,5-fa-1	-3.959
5fa	-3.738
INH	-3.674
6fa	-3.178

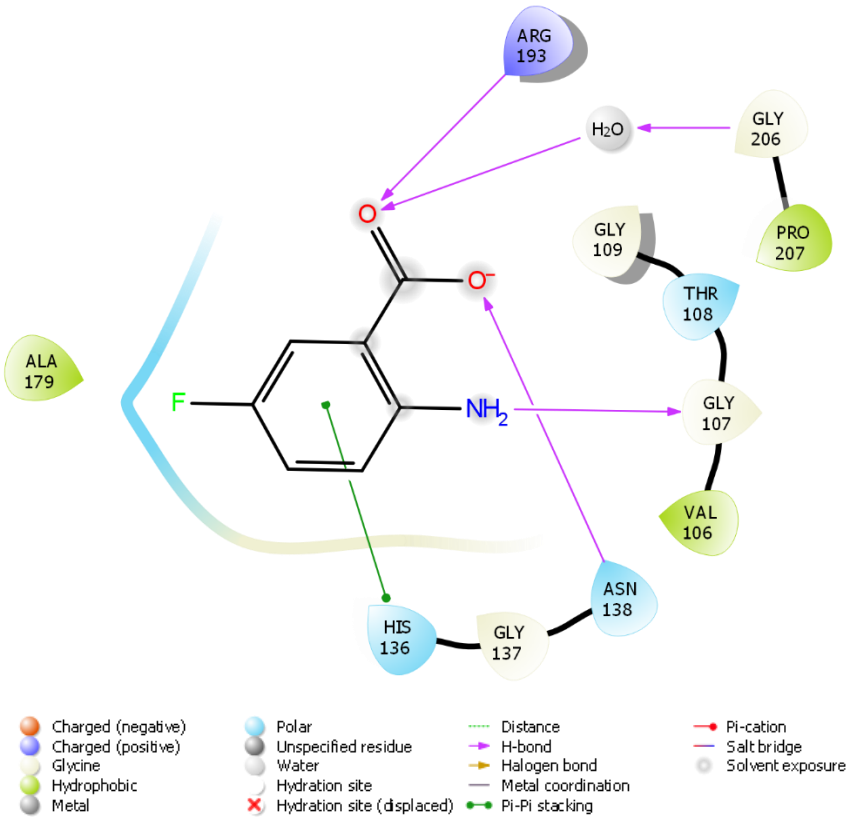

Figure 40. Scheme of interaction observed in the molecular docking of 5fa molecule in the Position 2 of the catalytic pocket of TrpD (4OWN).

2. Biological assays

The biological activity evaluation was performed for the complexes Ag4fa, Ag5fa and Ag6fa and their respective ligands in most cases. The biological activity of 4,5fa and Ag-4,5fa was not yet tested.

2.1. Antibacterial assays

The biological *in vitro* activity of the silver complexes was first evaluated over Gram-positive *S. aureus* and *B. cereus* and Gram-negative *E. coli* and *P. aeruginosa* bacterial strains. The results are presented in Table 11.

Table 11. Minimum inhibitory concentration (in μg/mL) of fluoroanthranilic acids and their Ag(I) complexes against *S. aureus*, *B. cereus*, *E. coli* and *P. aeruginosa*.

	MIC (μg/mL)			
	S. aureus	***B. cereus***	***E. coli***	***P. aeruginosa***
4fa	*	*	*	*
5fa	*	*	*	*
6fa	*	*	*	*
Ag4fa	62.25	62.25	62.25	62.25
Ag5fa	62.25	62.25	62.25	62.25
Ag6fa	62.25	62.25	62.25	62.25
$AgNO_3$	≤ 31.25	≤ 31.25	≤ 31.25	≤ 31.25

* Non active

The fluoroanthranilic acids were not able to inhibit the growth of any of the selected bacterial strains even at the highest concentration tested (1500 μg/mL). On the other hand, the silver complexes inhibited the bacterial strains in MIC of 62.25 μg/mL (237.6 μmol/L). Since the ligands were inactive over the considered bacterial strains, the activity of the complexes were attributed to the presence of the silver ion [111]. The antibacterial activity of this metal ion is well established in the literature [112]. The Ag(I) ions may inhibit bacterial growth in different ways, such as binding to DNA, interfering with the cell electron transport system, interacting with cell membranes or by inhibiting thiol-containing proteins/enzymes [20,113]. The antibacterial activity of Ag(I) is evidenced by the MIC of $AgNO_3$ observed in this experiment (≤ 31.25 μg/mL or ≤ 183.9 μmol/L). Even though the activity of the complexes is slightly lower than the activity of $AgNO_3$, the latter is known to be toxic to human tissues even at low concentrations, limiting its applicability [23,114,115].

2.2. Antimycobacterial assay

The activity of the Ag(I) complexes were evaluated over *M. tuberculosis* by the parameter of MIC_{90} (minimum inhibitory concentration of 90% of bacterial growth). Table 12 shows the values of MIC_{90} obtained by this assay for the complexes, free ligands, $AgNO_3$ and the commercial antituberculosis drugs rifampicin (RIF), moxifloxacin (MOX) and isoniazid (INZ). In the same Table are presented data from the literature on the previously reported activity of the ligands 4fa, 5fa and 6fa.

Table 12. Left: MIC_{90} against *M. tuberculosis* for the ligands, silver complexes, $AgNO_3$, rifampicin (RIF), moxifloxacin (MOX) and isoniazid (INZ), expressed in µg/mL and µmol/L with the standard deviation values. Right: Data of inhibitory concentration of ligands 4fa, 5fa and 6fa previously reported in the literature against *M. tuberculosis*.

	Data from this work		Data from literature		
	MIC_{90} (µg/mL) [116]	**MIC_{90} (mmol/L)** [116]	**GIC_{50} (mmol/L)** [77]*	**MIC/MBC (mmol/L)** [117]**	**MIC (mmol/L)** [76]
4fa	3.9 ± 1.9	25.0 ± 12.5	12 ± 8.0	-	
5fa	2.8 ± 0.2	17.9 ± 1.5	17 ± 11	62.5/ 125.1	5
6fa	4.7 ± 0.4	30.6 ± 2.7	250 ± 200	62.5/ 125.1	5
$AgNO_3$	4.3 ± 2.0	25.2 ± 12.0			
Ag4fa	2.6 ± 0.1	9.8 ± 0.5			
Ag5fa	4.2 ± 2.2	15.9 ± 8.6			
Ag6fa	2.6 ± 3.1	9.8 ± 11.9			
INZ	0.19 ± 0.01	1.36 ± 0.06			
MOX	< 0.098	< 0.24			
RIF	< 0.098	< 0.12			

* *M. tuberculosis* mc^2 6230 cells in Sauton's media (resazurin microtiter assay - REMA) [77]
** *M. tuberculosis* BSG001, stable bioluminescent derivative of H37Rv
MIC_{90}: Minimum Inhibitory Concentration to inhibit 90% of cell growth.
GIC_{50}: Inhibitory Concentration to inhibit 50% of cell growth
MIC: Minimum Inhibitory Concentration.
MBC: Minimum Bactericidal Concentration

The work of Islam et at.[77] points out that the MIC for fluoroanthranilates might vary with the incubation time due to the mechanism of action of these molecules, once there is a time-dependent buildup of toxic fluorotryptophan which can take more than 24 h to reach the inhibitory concentration needed. At that point the highest inhibition is observed as the fluorotryptophan is incorporated. After this period (24 to 48h) the fluorotryptophan levels in the medium decrease again, allowing increased tryptophan synthesis and thus reducing the apparent inhibitory concentration at longer time points.

Moreover, the activities of the silver complexes against *M. tuberculosis* were comparable or higher than other silver complexes reported in the literature, which are also in the micromolar range [27,118–123]. The complexes include ligands such as thiazole, thiourea, bipyridine, phosphanes and others.

The overall *in vitro* antibacterial activity of the Ag4fa, Ag5fa and Ag6fa complexes suggest that the nature of the fluoroanthranilic ligand is determinant for their ability to

inhibit specifically the growth of *M. tuberculosis*, as the same complexes and ligands had a much higher inhibiting concentration for other bacteria species such as *S. aureus*, *B. cereus*, *E. coli* and *P. aeruginosa*.

This observation is also supported by the literature due to the mechanism of action of the fluoroanthranilic acids against *M. Tuberculosis*. Their mechanism involves the tryptophan biosynthetic pathway, which is particularly important for *M. Tuberculosis* that has limited access to amino acids (such as tryptophan) inside macrophages.[124]

2.3. Antiproliferative assays of cancer cells

The Ag4fa, Ag5fa and Ag6fa complexes were also evaluated regarding their cytotoxicity over different human cell lines using the resazurin cell viability assay. Three normal cell lines were chosen to evaluate cytotoxicity in healthy cells: a cell line of human fibroblasts (GM07492), normal lung tissue cells (MRC-5) and human umbilical vein endothelial cells (HUVEC). Likewise, five cancer cell lines were evaluated: liver cancer cells (Hep G2), adenocarcinoma human alveolar basal epithelial cells (A-549), epithelial colorectal adenocarcinoma cells (Caco-2), immortal cervical cancer cells (HeLa) and breast cancer cells (MCF-7).

The results are presented as IC_{50} (concentration able to inhibit 50% of cellular growth) in Table 13. The average viability of each cell line treated with the compounds are presented in Figures 41, 42 and 43. The selectivity index (SI), which is the ratio between the IC_{50} for healthy and cancer cell lines, was also calculated for each compound (Figure 44). High selectivity index values indicate high selectivity for cancer cells in this experiment.

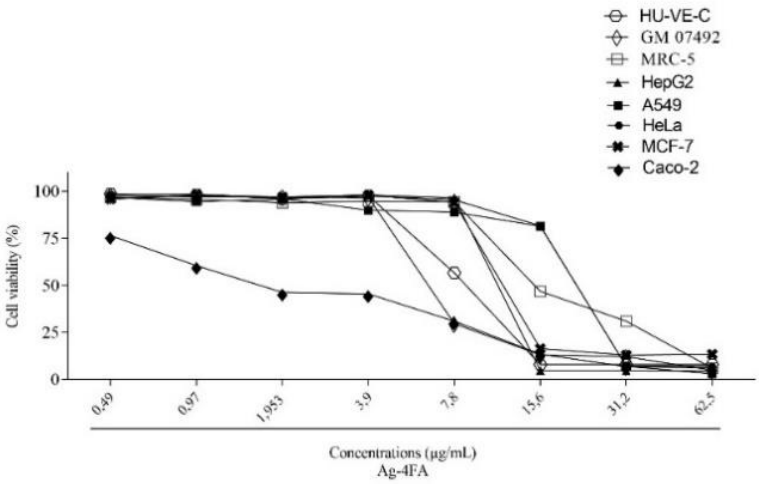

Figure 41. Cell viability of three human normal cell lines (GM07492, MRC-5 and HU-VE-C) and five human cancer cell lines (HepG2, A-549, Caco-2, HeLa and MCF-7) treated with Ag4fa (0.49 to 62.5 µg/mL)

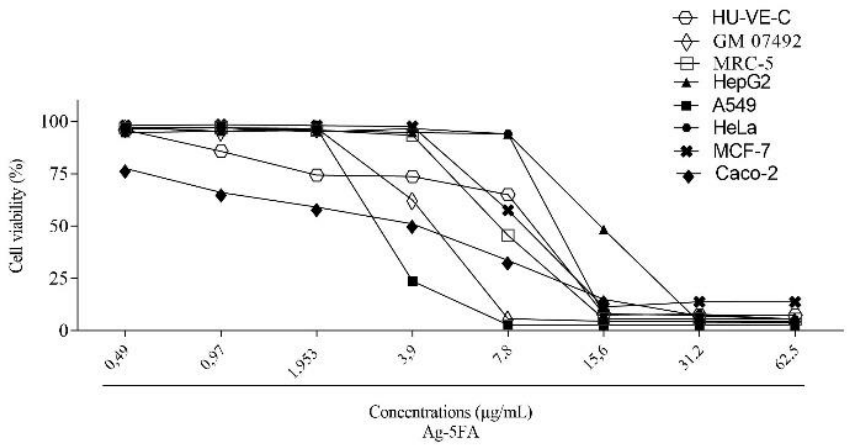

Figure 42. Cell viability of three human normal cell lines (GM07492, MRC-5 and HU-VE-C) and five human cancer cell lines (HepG2, A-549, Caco-2, HeLa and MCF-7) treated with Ag5fa (0.49 to 62.5 µg/mL)

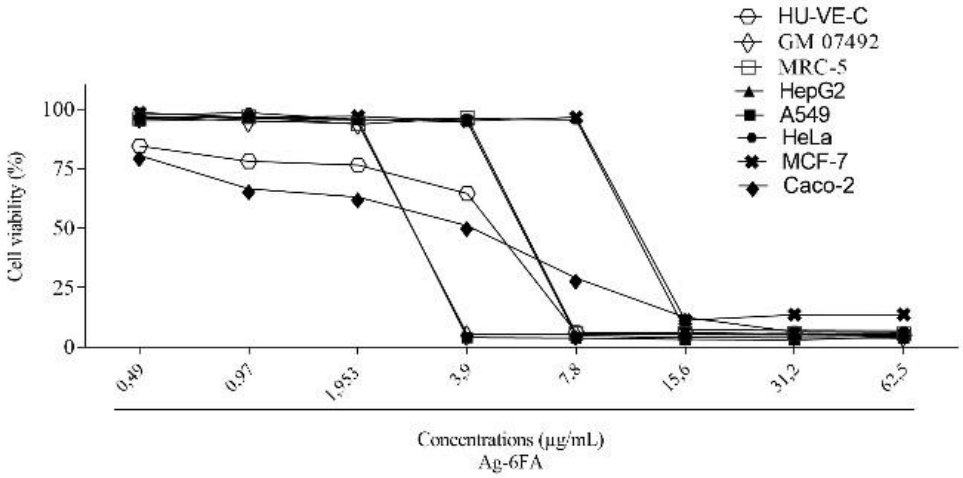

Figure 43. Cell viability of three human normal cell lines (GM07492, MRC-5 and HU-VE-C) and five human cancer cell lines (HepG2, A-549, Caco-2, HeLa and MCF-7) treated with Ag6fa (0.49 to 62.5 µg/mL).

Table 13. Values of IC_{50} (in µg/mL and µmol/L) of Ag4fa, Ag5fa, Ag6fa and $AgNO_3$ against three human normal cell lines (GM07492, MRC-5 and HUVEC) and five human cancer cell lines (HepG2, A-549, Caco-2, HeLa and MCF-7).

	IC_{50} (µg/mL)							
	GM07492	**MRC-5**	**HUVEC**	**HepG2**	**A-549**	**Caco-2**	**HeLa**	**MCF-7**
$AgNO_3$	3.2 ± 0.2	6.7 ± 0.2	2.19 ± 0.09	12.1 ± 0.9	3.37 ± 0.01	17.3 ± 0.6	6.6 ± 0.2	5.97 ± 0.07
Ag4fa	6.68 ± 0.09	18 ± 1	8.4 ± 0.2	11.3 ± 0.2	20.1 ± 0.3	2.1 ± 0.2	20.2 ± 0.6	12.0 ± 0.8
Ag5fa	4.3 ± 0.1	7.5 ± 0.4	7.2 ± 0.6	15.4 ± 0.9	3.3 ± 0.1	2.8 ± 0.4	11.2 ± 0.1	8.70 ± 0.09
Ag6fa	2.7 ± 0.2	5.7 ± 0.3	3.2 ± 0.1	5.6 ± 0.2	2.74 ± 0.03	2.9 ± 0.1	11.5 ± 0.6	12.0 ± 0.3
	IC_{50} (µmol/L)							
	GM07492	**MRC-5**	**HUVEC**	**HepG2**	**A-549**	**Caco-2**	**HeLa**	**MCF-7**
$AgNO_3$	19 ± 1	39 ± 1	12.9 ± 0.5	71 ± 6	19.84 ± 0.06	102 ± 4	39 ± 1	35.1 ± 0.4
Ag4fa	25.5 ± 0.3	68 ± 4	32.2 ± 0.6	43.1 ± 0.8	77 ± 1	7.8 ± 0.7	77 ± 2	46 ± 3
Ag5fa	16.6 ± 0.5	29 ± 1	28 ± 2	59 ± 4	12.4 ± 0.5	11 ± 1	42.9 ± 0.4	33.2 ± 0.3
Ag6fa	10.4 ± 0.8	22 ± 1	12.1 ± 0.5	21.2 ± 0.9	10.5 ± 0.1	11.1 ± 0.4	44 ± 2	46 ± 1

Cell lines: Human fibroblasts (GM07492), normal lung tissue cells (MRC-5), human umbilical vein endothelial cells (HUVEC), liver cancer cells (Hep G2), adenocarcinomic human alveolar basal epithelial cells (A-549), epithelial colorectal adenocarcinoma cells (Caco-2), immortal cervical cancer cells (HeLa) and breast cancer cells (MCF-7).

The results show dissimilar cytotoxic profiles for each complex. For Ag4fa, the most susceptible cells were the epithelial colorectal adenocarcinoma ones (Caco-2) with an IC_{50} of 2.05 ± 0.18 µg/mL. The selectivity of Ag4fa towards Caco-2 was also noteworthy, as the SI is 8.07 considering the MRC-5 cell line. Conversely, the Ag5fa and Ag6fa complexes were active but not selective for the cancer cells. The lowest IC_{50} values for Ag5fa were observed against Caco-2 (2.82 ± 0.39 µg/mL) and A-549 (3.25 ± 0.14 µg/mL), while for Ag6fa the IC_{50} values are lower than 4.0 µg/mL for GM 07492, HUVEC, A-549 and Caco-2. This result led us to believe that the ligand structure is essential for the selectivity of the Ag4fa complex over tumoral cells.

Silver nitrate was evaluated for comparison and it was also cytotoxic to all cell lines, but without selectivity to cancer cells. Also, $AgNO_3$ was especially cytotoxic for the healthy cell line HUVEC (IC_{50} = 2.19 ± 0.09 µg/mL).

The cytotoxicity of the silver complexes observed *in vitro* against Caco-2 cells corroborates other studies in the literature showing especial sensibilization of these cells by silver nanoparticles and silver ions [125–128]. However, the results presented here show that $AgNO_3$ (which can be considered a source of free Ag(I) ions) was less cytotoxic to Caco-2 cells (IC_{50} = 17.26 ± 0.62 µg/mL) than the three complexes (IC_{50} ≈ 2 µg/mL). Therefore, the coordination of silver ions by biologically relevant ligands may potentialize the inhibition of epithelial colorectal adenocarcinoma cells.

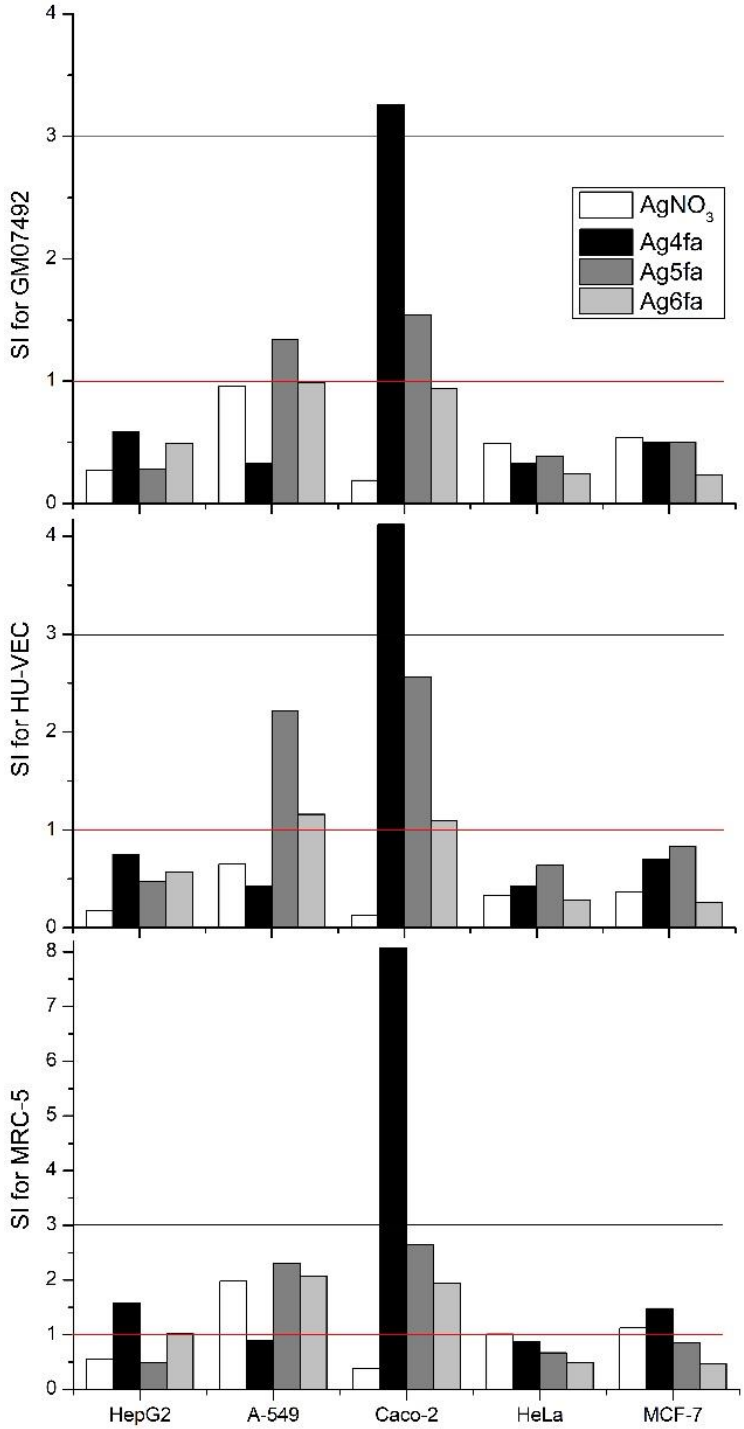

Figure 44. Selectivity index (SI) of the compounds tested against the cancer cell lines in reference to the healthy cells MRC-5, HUVEC and GM07492. Values of SI < 1 (under the red line) are for compounds more cytotoxic to the normal cell than to the cancer cell and values of SI > 3 (above the black line) were considered selective to cancer cells.

2.4. Mutagenicity assay and DNA interaction

The potential mutagenicity of the silver(I) complexes was also evaluated and the assays showed that none of the strains of *S. typhimurium* induced two-fold or greater increase in the mean number of revertants when exposed to different concentrations of complexes, as compared to the negative control group, indicating the absence of any mutagenic activity under the conditions used in this study. The mean number of revertants/plate (M), the standard deviation (SD) and the mutagenic index (MI) after the treatments with Ag4fa, Ag5fa and Ag6fa, observed in *S. typhimurium* strains TA98, TA100, TA102 and TA97a, in the presence (+S9) and absence (-S9) of metabolic activation can be found at Table 14.

Table 14. Mean number of revertants/plate (M), standard deviation (SD) and mutagenic index (MI) after the treatments with Ag4fa, Ag5fa and Ag6fa, observed in *S. typhimurium* strains TA98, TA100, TA102 and TA97a, in the presence (+S9) and absence (-S9) of metabolic activation.

Ag-4FA	**Number of revertants (M ± SD)/ plate and MI**							
Treatments	**TA 98**		**TA 100**		**TA 102**		**TA 97a**	
µg/plate	**-S9**	**+S9**	**-S9**	**+S9**	**-S9**	**+S9**	**-S9**	**+S9**
DMSO	28 ± 2	23 ± 3	140 ± 24	143 ± 12	266 ± 28	346 ± 29	189 ± 14	139 ±18
0.31	30 ± 8 (1.07)	27 ± 2 (1.18)	153 ± 13 (1.09)	175 ± 7 (1.23)	269 ± 26 (1.01)	390 ± 18 (1.13)	184 ± 12 (0.97)	168 ± 11 (1.21)
0.62	31 ± 6 (1.13)	24 ± 3 (1.07)	165 ± 27 (1.18)	196 ± 15 (1.37)	323 ± 13 (1.21)	389 ± 11 (1.12)	176 ± 11 (0.93)	142 ± 15 (1.02)
1.25	31 ± 2 (1.13)	28 ± 1 (1.24)	171 ± 15 (1.22)	160 ± 11 (1.12)	313 ± 33 (1.18)	448 ± 29 (1.29)	175 ± 10 (0.92)	160 ± 19 (1.16)
1.8	29 ± 1 (1.04)	25 ± 3 (1.11)	169 ± 10 (1.21)	178 ± 13 (1.25)	290 ± 15 (1.09)	451 ± 25 (1.30)	162 ± 12 (0.86)	151 ± 7 (1.09)
2.5	28 ± 1 (1.00)	24 ± 2 (1.07)	134 ± 11 (0.96)	165 ± 6 (1.16)	210 ± 28 (0.79)	435 ± 22 (1.26)	144 ± 14 (0.76)	132 ± 10 (0.95)
C+	624 ± 83[a]	803 ± 56[d]	1665± 62[b]	1790 ± 92[d]	1960 ± 79[c]	1465 ± 81[e]	1102 ± 78[a]	1470 ± 74[d]
Ag-5FA	**Number of revertants (M ± SD)/ plate and MI**							
Treatments	**TA 98**		**TA 100**		**TA 102**		**TA 97a**	
µg/plate	**-S9**	**+S9**	**-S9**	**+S9**	**-S9**	**+S9**	**-S9**	**+S9**
DMSO	28 ± 2	23 ± 3	140 ± 24	143 ± 12	266 ± 28	346 ± 29	189 ± 14	139 ±18
0.31	31 ± 8 (1.13)	26 ± 1 (1.16)	170 ± 7 (1.21)	160 ± 14 (1.12)	273 ± 32 (1.02)	398 ± 30 (1.15)	199 ± 5(1.05)	152 ± 5 (1.10)
0.62	28 ± 1 (1.02)	25 ± 2 (1.09)	159 ± 11 (1.14)	157 ± 9 (1.10)	256 ± 19 (0.96)	361 ± 18 (1.04)	174 ± 15 (0.92)	146 ± 11 (1.05)
1.25	28 ± 3 (1.02)	23 ± 0 (1.02)	146 ± 17 (1.04)	141 ± 13 (0.99)	260 ± 11 (0.98)	389 ± 23 (1.12)	171 ± 15 (0.90)	150 ± 13 (1.08)
1.8	22 ± 0 (0.80)	25 ± 1 (1.09)	143 ± 4 (1.02)	158 ± 11 (1.11)	241 ± 37 (0.90)	320 ± 21 (0.92)	177 ± 18 (0.93)	150 ± 17 (1.08)
2.5	23 ± 3 (0.84)	26 ± 3 (1.13)	152 ± 12 (1.08)	132 ± 7 (0.92)	232 ± 14 (0.87)	335 ± 19 (0.97)	131 ± 8 (0.69)	133 ± 6 (0.96)
C+	624 ± 83[a]	803 ± 56[d]	1665± 62[b]	1790 ± 92[d]	1960 ± 79[c]	1465 ± 81[e]	1102 ± 78[a]	1470 ± 74[d]
Ag-6FA	**Number of revertants (M ± SD)/ plate and MI**							
Treatments	**TA 98**		**TA 100**		**TA 102**		**TA 97a**	
µg/plate	**-S9**	**+S9**	**-S9**	**+S9**	**-S9**	**+S9**	**-S9**	**+S9**
DMSO	28 ± 2	23 ± 3	140 ± 24	143 ± 12	266 ± 28	346 ± 29	189 ± 14	139 ±18
0.31	27 ± 1 (0.98)	26 ± 6 (1.13)	153 ± 15 (1.09)	153 ± 4 (1.07)	299 ± 16 (1.12)	366 ± 26 (1.06)	193 ± 11 (1.02)	162 ± 9 (1.17)
0.62	32 ± 5 (1.15)	27 ± 1 (1.20)	179 ± 12 (1.28)	181 ± 23 (1.27)	277 ± 23 (1.04)	410 ± 13 (1.18)	222 ± 11 (1.17)	156 ± 16 (1.12)
1.25	29 ± 1 (1.05)	24 ± 6 (1.07)	145 ± 8 (1.04)	140 ± 14 (0.98)	292 ± 20 (1.10)	381 ± 17 (1.10)	179 ± 14 (0.94)	174 ± 22 (1.25)
1.8	23 ± 2 (0.84)	22 ± 3 (0.98)	186 ± 13 (1.33)	130 ± 7 (0.91)	277 ± 26 (1.04)	332 ± 15 (0.96)	174 ± 21 (0.92)	171 ± 7 (1.23)
2.5	24 ± 2 (0.87)	21 ± 1 (0.91)	144 ± 5 (1.03)	109 ± 12 (0.76)	222 ± 14 (0.83)	317 ± 11 (0.92)	177 ± 13 (0.94)	142 ± 10 (1.03)
C+	624 ± 83[a]	803 ± 56[d]	1665± 62[b]	1790 ± 92[d]	1960 ± 79[c]	1465 ± 81[e]	1102 ± 78[a]	14704[d]

Complementarily to the mutagenicity test, the interaction of the complexes and ligands with DNA was preliminary evaluated by agarose gel electrophoresis. In this experiment, plasmid DNA pGEX-4T1 was selected as a model, which has mainly three different forms that can be separated by electrophoresis in distinct bands: open circular (OC), linear (LF) and super coiled (SC) forms, as shown in Figure 45.

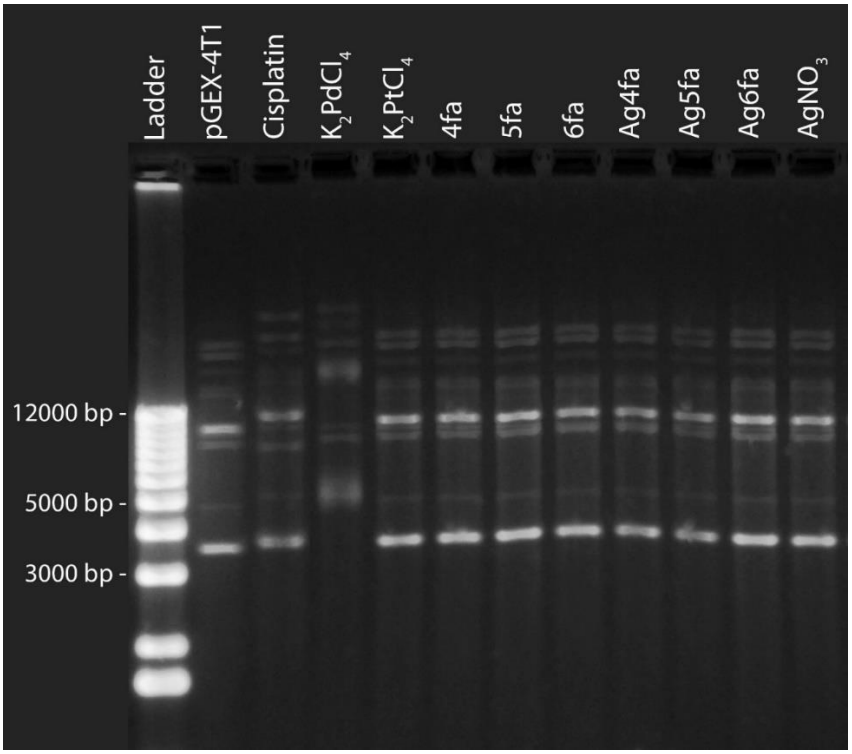

Figure 45. Agarose gel electrophoresis assay of the pGEX-4T1 plasmid DNA in the presence of 5fa, Ag5fa and $AgNO_3$.

As can be seen in Figure 45 the first column is a weight marker (DNA ladder), the second column is the plasmid DNA reference, and the remaining columns are the DNA samples in the presence of the compounds. Comparing the samples with the reference it can be seen that 4fa, 5fa, 6fa, their respective silver complexes and $AgNO_3$ did not induce any major changes in the bands, thus do not interact with the plasmid DNA in the concentrations tested (35 and 70 µmol L^{-1}). Examples of positive results for plasmid DNA interaction can be noticed for K_2PdCl_4 and Cisplatin (CisPt), which are known for binding DNA [39,40,129,130]. The antimicrobial properties of Ag(I) complexes can often be attributed to DNA interaction [31,131].

3. Cu(II) complexes

A series of copper complexes with 6fa and three different auxiliary ligands was synthesized. The auxiliary ligands chosen for this series were 2,2′-bipyridine (bipy), 4,4'-dimethyl-2,2'-bipyridine (4,4'-Mebipy) and phenanthroline (phen) and their Cu(II) complexes were named Cu1, Cu2 and Cu3 respectively. There are examples of similar Cu(II) complexes in the literature bearing phenanthroline and Schiff bases derived from 4fa and 4,5-fa [48,85], that motivated the synthesis of the similar complexes but with the 6fa ligand.

The elemental analyses of the complexes are consistent with the ratio of one Cu(II) for each auxiliary ligand and two deprotonated 6fa molecules, which would also suggest that the complexes are neutral and have no counterions (NO_3^- anions were not compatible with the elemental analysis). So far, the Cu(II) complexes were characterized by elemental analysis, infrared spectroscopy and mass spectrometry, which led us to suggest a molecular composition and possible coordination sites, but not to determine structures.

3.1. Infrared spectroscopy of the Cu(II) complexes with 6fa

The infrared spectra of the complexes were compared to 6fa and the most noticeable stretching differences between their vibrational modes that would justify coordination are presented in Table 15 and indicated in Figure 46.

Table 15. Main vibrational modes from 6fa ligands shifted upon coordination in the complexes Cu1, Cu2 and Cu3.

	Wavenumber (cm^{-1})			
	6fa	**Cu1**	**Cu2**	**Cu3**
$\nu_{as}NH_2$	3488	3432	3445	3447
$\nu_{s}NH_2$	3376	3324	3326	3327
$\nu_{as}COO^-$	1659	1622	1620	1620
$\nu_{s}COO^-$	1426	1379	1377	1377

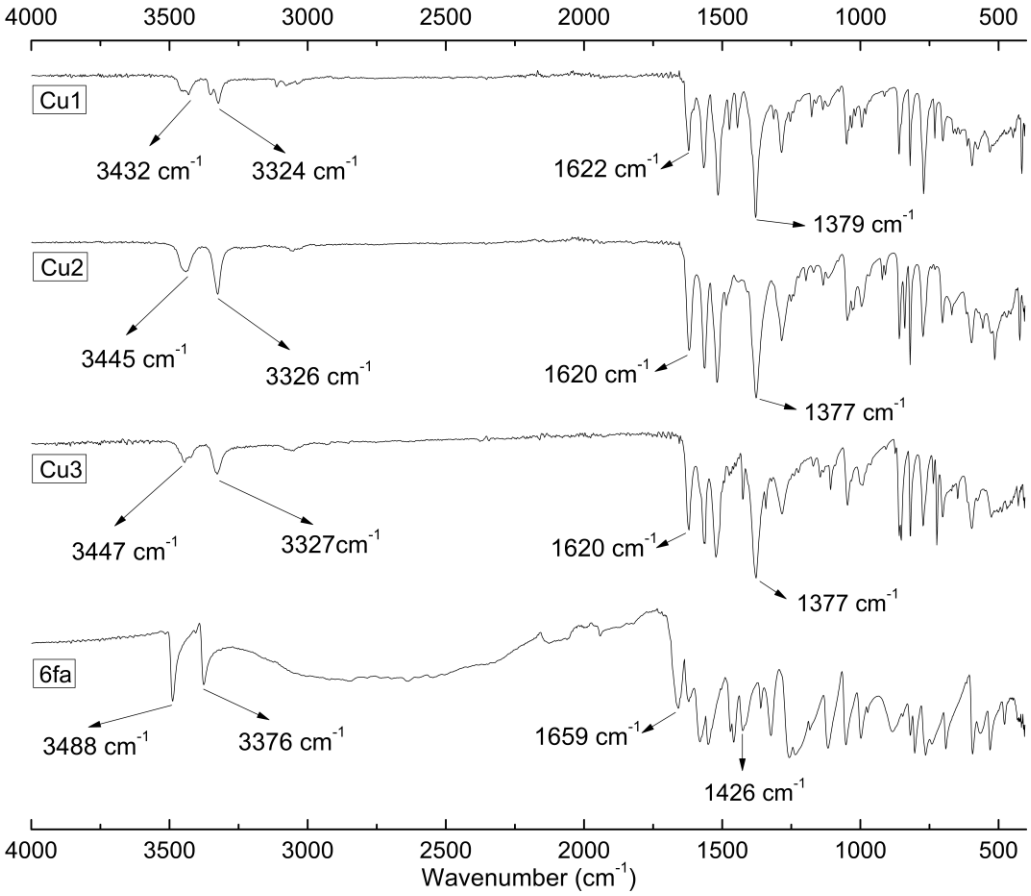

Figure 46. Infrared spectra of 6fa and the copper complexes Cu1, Cu2 and Cu3 from 4000 to 400 cm^{-1}.

The vibrational modes of the amine from the 6fa ligand ($\nu_{as}NH_2$ and ν_sNH_2) are shifted to lower energies in the spectra of the complexes for at least 41 and 49 cm^{-1}, respectively. Likewise, the $\nu_{as}COO^-$ and ν_sCOO^- vibrational modes were also shifted upon coordination in approximately 37 and 47 cm^{-1} for all three coordination compounds. The difference between the asymmetric and symmetric modes of ν_aCOO^- ($\Delta = [\nu_{as}(COO^-) - \nu_s(COO^-)]$) is higher for the Cu complexes (Δ = 243 cm^{-1}) than for the free ligand (Δ = 233 cm^{-1}), indicating a coordination of only one oxygen atom of the carboxylate anion to the metal center.[132]

3.2. Mass spectrometric analysis of Cu(II) complexes.

The experiments of mass spectrometry were performed in the positive mode to identify cations derived from the copper complexes. Peaks corresponding to the Cu(I) species $[Cu(bipy)]^+$, $[Cu(4,4'\text{-}Mebipy)]^+$ and $[Cu(phen)]^+$ were present at m/z 219.0525

(calc. 218.9984), 247.0009 (calc. 247.0296) and 243.0639 (calc. 242.9984), respectively, and are observed due to the experimental conditions of ionization.

Isotopic patterns of Cu(II) were also identified being consistent with chemical species containing Cu(II), one auxiliary ligand and one molecule of 6fa, with a positive charge: $[Cu(bipy)6fa]^+$ (m/z 373.1454), $[Cu(4,4'\text{-Me bipy})6fa]^+$ (m/z 401.0144) and $[Cu(phen)6fa]^+$ (m/z 997.1467). These peaks are presented in Figure 47, where they are compared with the calculated isotopic patterns.

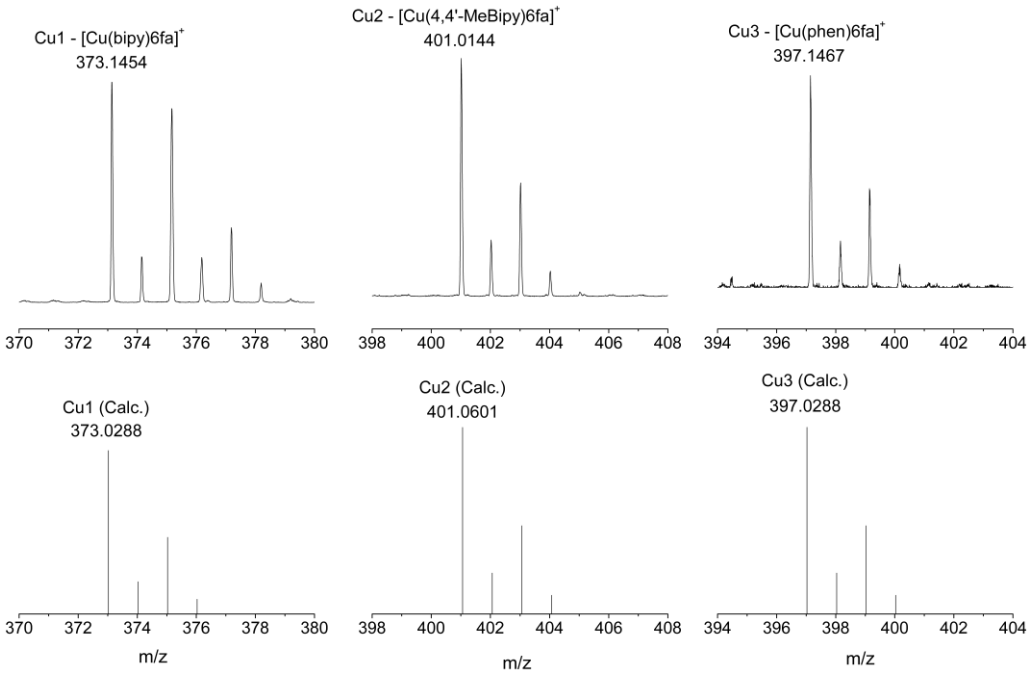

Figure 47. Mass spectra of the $[Cu(bipy)6fa]^+$, $[Cu(4,4'\text{-Me bipy})6fa]^+$ and $[Cu(phen)6fa]^+$ ions (top) and their respective theoretical isotopic patterns (bottom).

The mass spectrometric results are in accordance with the elemental analyses as the molecular ions observed are products of the loss of one 6fa ligand from the original coordination compounds, conferring them a positive charge.

3.3. Single crystal X-ray diffraction of Cu(II) complexes

Crystals of the three Cu(II) complexes, obtained by the slow evaporation of the filtrated aqueous solution, were collected and analyzed by X-ray diffraction

For the complex Cu3 a refinement of the crystal structure was performed in collaboration with Prof. Dr. Marcos Antonio Ribeiro from the Universidade Federal do Espírito Santo (UFES). However, the crystal data quality was not good enough to completely refine the structure with the necessary precision to publish these results. Nonetheless, it is clearly possible to identify the Cu(II) complex with two phenanthroline

ligands and one 6fa molecule coordinated by the carboxylate group (Cu-O = 1.993Å), as shown in the pre-refinement results in Figure 48. The asymmetric unit also contains two molecules of water and a molecule of methanol from the solvent and also a nitrate counterion in a special symmetry position.

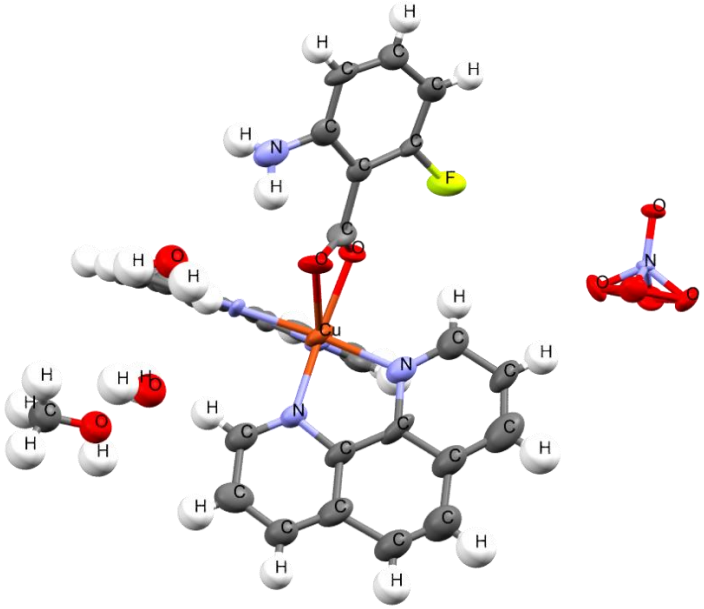

Figure 48. Pre-refinement results for the crystal structure of complex Cu3.

A similar problem was observed in the crystal structures of Cu1 and Cu2 as it is shown in the unrefined structures in Figure 49.

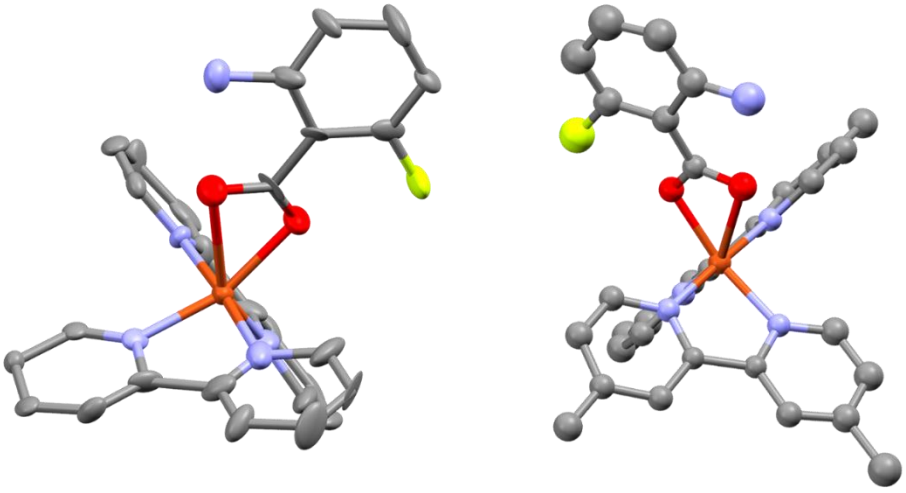

Figure 49. Unrefined crystal structures of Cu1 and Cu2.

These preliminary data indicates that the soluble species isolated by crystallization (Figure 50) are different than the ones isolated by precipitation (powder samples) and that were analyzed by IR-ATR, elemental analysis, thermal analysis and mass spectrometry.

While the powder samples seem to have in their composition one Cu(II) ion, one auxiliary ligand and two 6fa ligands, the crystal samples are composed by the Cu(II) center, two auxiliary ligands and one 6fa ligand.

New data collection will be necessary to advance in the crystallographic studies, but the pre-refinement results are encouraging nonetheless. Given the relative ease to obtain crystals of these Cu(II) complexes, we expect that in time it will be possible to elucidate these structures.

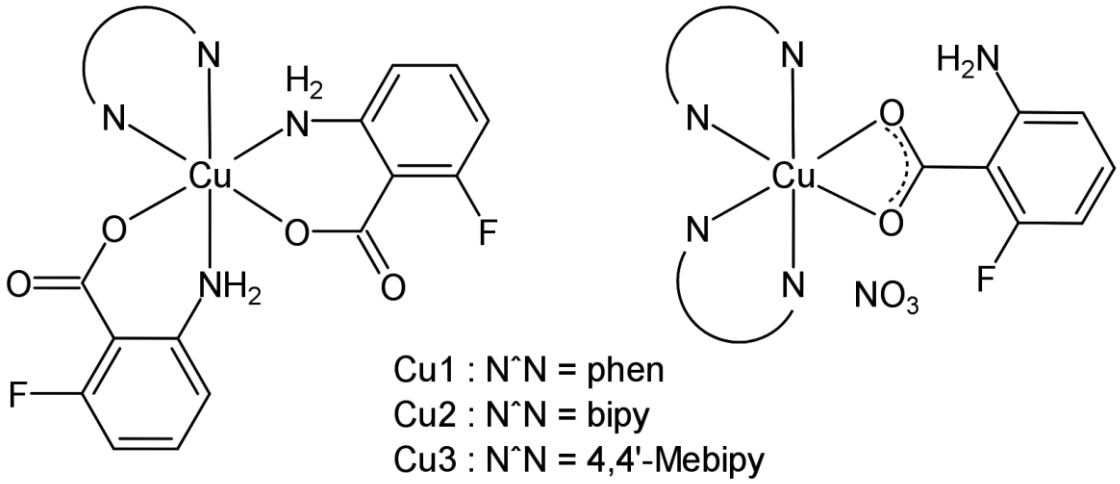

Figure 50. Proposed structures for the powder samples (left) and crystal samples (right) of Cu1, Cu2 and Cu3.

4. Pd(II) complex with D-cycloserine

D-Cycloserine (D-4-amino-3-isoxazolidone, dcs) is an antibiotic that is biosynthesized by *Streptomyces* bacteria and it is used as second line treatment of TB by the name of Seromycin® [133]. This drug interferes in the synthesis of the bacterial cell wall competitively inhibiting the enzymes D-alanine racemase (Alr) and D-alanine-D-alanine ligase (Ddl), which are essential for the synthesis of peptidoglycans that ensure the cell wall integrity and rigidity [134–137]. This mechanism of action is of great interest when searching for a synergic activity between multiple drugs or of a drug and metal ion since the damage in the cell wall not only harms the bacteria but also increases its susceptibility to other antibacterial agents that acts inside the cell[138]. This is one of the reasons that dcs is administered in cases of MDR-TB and XDR-TB in association with other antituberculosis drugs [134,138].

The dcs is also an interesting coordinating molecule as it contains nitrogen and oxygen donor atoms. The structure of dcs, presented in Figure 51, allows chelation of metal ions, such as Zn(II), Ni(II), Hg(II), Co(II), Cd(II) [139], Cu(II) [140–143], Fe(II) [144], Cr(III), Mn(II) [145], Pd(II), Pt(II) [146] and Ag(I) [27]. The structures of dcs in different pH values are also represented in Figure 51, which suggests how versatile its coordination chemistry can be. The molecule of dcs is a small heterocyclic zwitterion in which the donor atoms might be more or less available to coordination depending on pH values.

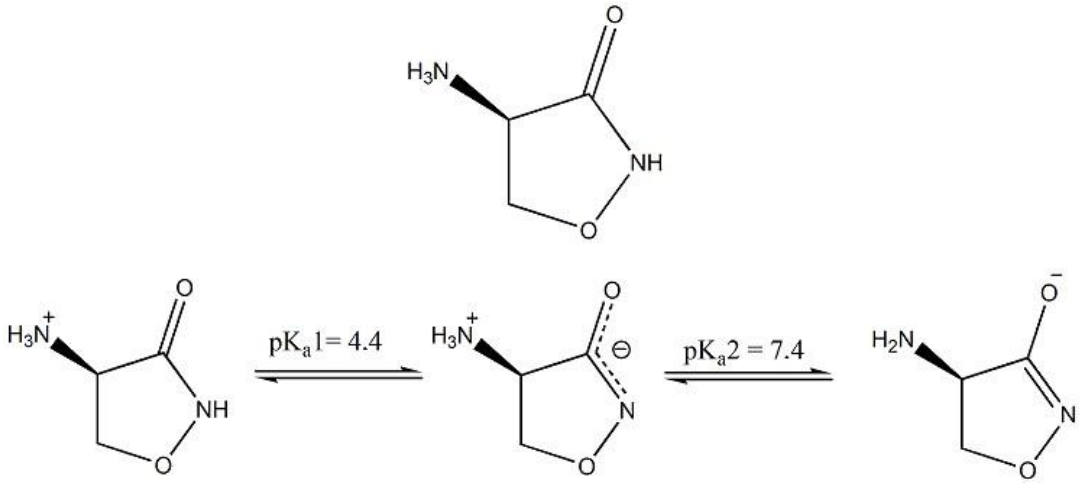

Figure 51. Structure of D-cycloserine

A good example of the versatility of coordination of dcs is the Ag(I) complex with this ligand, which was previously synthesized by our research group [27]. This complex has a polymeric structure with a distorted trigonal pyramidal geometry around the metal ion, involving the oxygen of carbonyl group and nitrogen atoms of the amino group and of the heterocyclic ring. Regarding its biological activity, the *in vitro* assays showed the activity of this complex against not only *M. tuberculosis*, but also *S. aureus*, *E. coli* and *P. aeruginosa* bacteria strains. In addition, the Ag(I) complex also showed a remarkable *in vitro* activity against breast cancer and leukemia cells.

In the attempt of synthesize a Pd(II) complex with dcs, the 2,2'-bipyridine was chosen as a chelating and auxiliary ligand to restrict the coordination possibilities of dcs to the metal ion and increase stability. Also, the synthesis of Pt(II) and Pd(II) complexes with planar ligands such as 2,2'-bipyridine (bipy) and 1,10-phenanthroline (phen) has been explored more in-depth in the last few years due to the various possibilities of these complexes to intercalate and bind to the DNA structure[147].

In order to properly isolate the complex, the salt NH_4PF_6 was used to selectively precipitate the cationic complex. Therefore, the Pd(II) coordination compound precipitates with PF_6^- as a counterion. The cationic complex isolated with PF_6^- was insoluble in dimethyl sulfoxide, ethanol, methanol, CH_2Cl_2, $CHCl_3$, acetonitrile, acetone, alkaline aqueous solution and acidic aqueous solution.

4.1. Infrared Spectroscopy of Pdbdcs.

The coordination of dcs to the Pd(II) was first evaluated by infrared spectroscopy comparing the complex with the ligand. Figure 52 shows both infrared spectra of Pdbdcs and dcs.

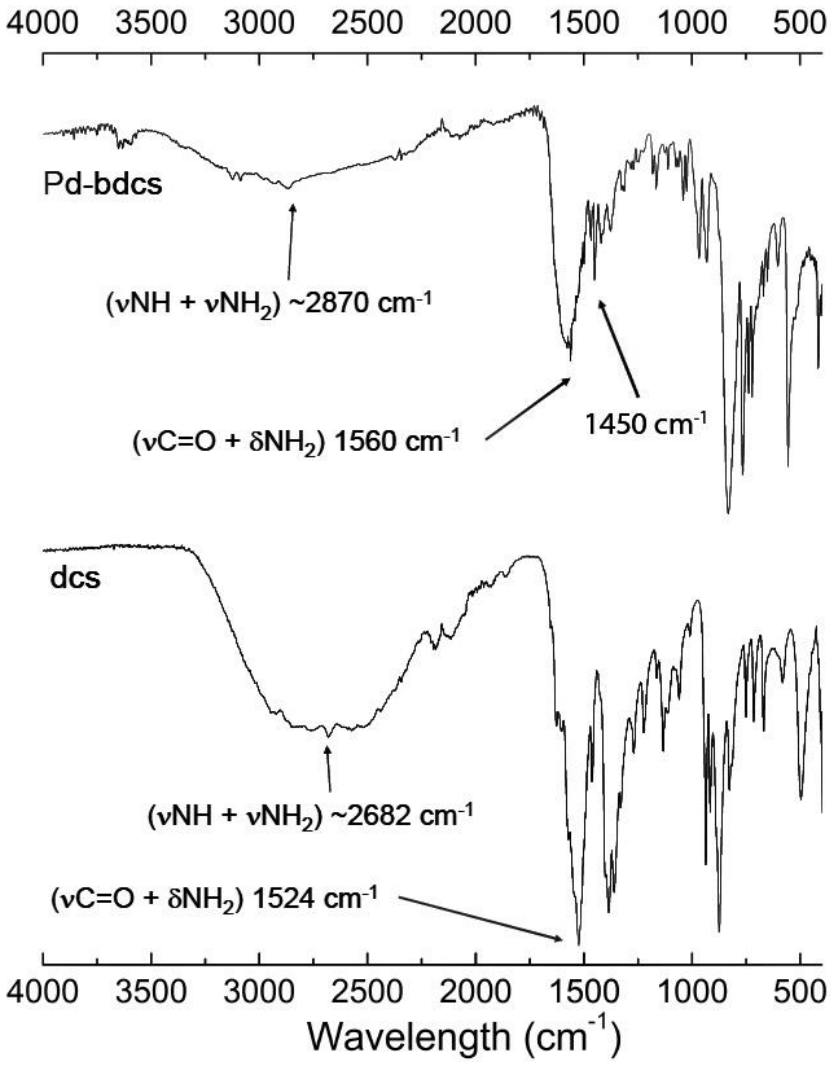

Figure 52. Infrared spectra of dcs (bottom) and Pdbdcs (top) from 4000 to 500 cm^{-1}.

The dcs infrared spectrum shows a broad band (~3400-2200 cm^{-1}) centered around 2682 cm^{-1} which can be attributed to the stretching frequencies νNH and νNH_2. The enlargement of this band is expected due to intermolecular hydrogen bonds between the cycloserine molecules. Noticeably, in the spectra of Pdbdcs the center of this band is shifted to around 2870 cm^{-1} suggesting the involvement of the nitrogen atoms in the coordination. Although the intensity of this mentioned band is lower in the spectra of the

complex, it is still a broad band, which can be a signal that the intermolecular hydrogen bonds are present in Pdbdcs as well.

The shift of the band attributed to the combination of νC=O and δNH_2 at 1524 cm^{-1} in the spectrum of dcs to 1560 cm^{-1} in the spectrum of Pdbdcs is also evidence of coordination, now suggesting coordination involving the carbonyl oxygen and/or the nitrogen from the amine.

Regarding the bipyridine moiety, the bands in the high energy region are nonmetal-sensitive since they originate in the heterocyclic aromatic ring of the ligand[132]. So, the band corresponding to the υ(C=N) is present at 1450 cm^{-1} in the spectrum of the complex and in the spectrum of free 2,2'-bipyridine (data not shown).

4.2. High resolution mass spectrometric analysis of Pdbdcs.

The mass spectrum of Pdbdcs (Figure 53 A) shows two main strong signals, the first at m/z 363.0077 matches the mass of $[Pd(bipy)(dcs)]^+$ with an relative error of -2.5 ppm to the theoretical isotopic pattern as it can be seen in Figure 53 B. The second is at m/z 465.0564 and corresponds to the ion $[Pd(bipy)(dcs)_2]^+$ with relative error of 11.8 ppm.

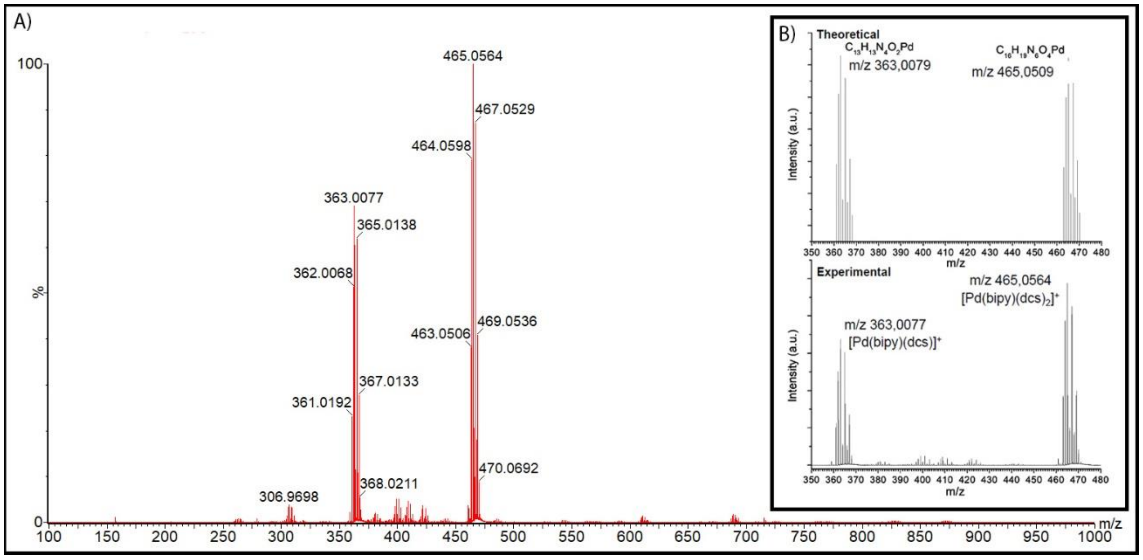

Figure 53. Complete high resolution mass spectrum of Pdbdcs from 100 to 1000 m/z (A) and comparison between experimental and theoretical mass spectra from 350 to 480 m/z (B).

The isotope patterns observed in Figure 53 are from ions with a +1 charge, given that the separation between the peaks of the pattern is a single unit of m/z. As the Pd(II) is an ion with +2 charge, a deprotonated cycloserine molecule bearing a negative charge must be present in both molecular ions observed in the spectrum, thus partially neutralizing the positive charge.

These results give some information about the composition of the complex. The elemental analysis of Pdbdcs suggests the composition $[Pd(bipy)(dcs)_2]PF_6$, with two molecules of dcs for each Pd(II) ion. Therefore, the ion $[Pd(bipy)(dcs)]^+$ with m/z 363.0077 should be a product of the dissociation of one dcs molecule from the complex in solution and the ion $[Pd(bipy)(dcs)_2]^+$ is the complex without the PF_6^- counterion.

Moreover, once the signal gain in the mass spectrometer was equally set for all the m/z values, the intensity of the signal is proportional to the concentration of the corresponding ions in solution. This shows that $[Pd(bipy)(dcs)]^+$ and $[Pd(bipy)(dcs)_2]^+$ are quite abundant in solution and are the major cationic species present.

4.3. Solid state NMR of Pdbdcs.

Due to the low solubility of Pdbdcs in common solvents, NMR experiments were performed in the solid state. In this case the coordination was investigated by ^{15}N NMR in comparison to the ligand as shows Figure 54, as this technique has shown to be an adequate tool to confirm nitrogen coordination of ligands to metal ions[148].

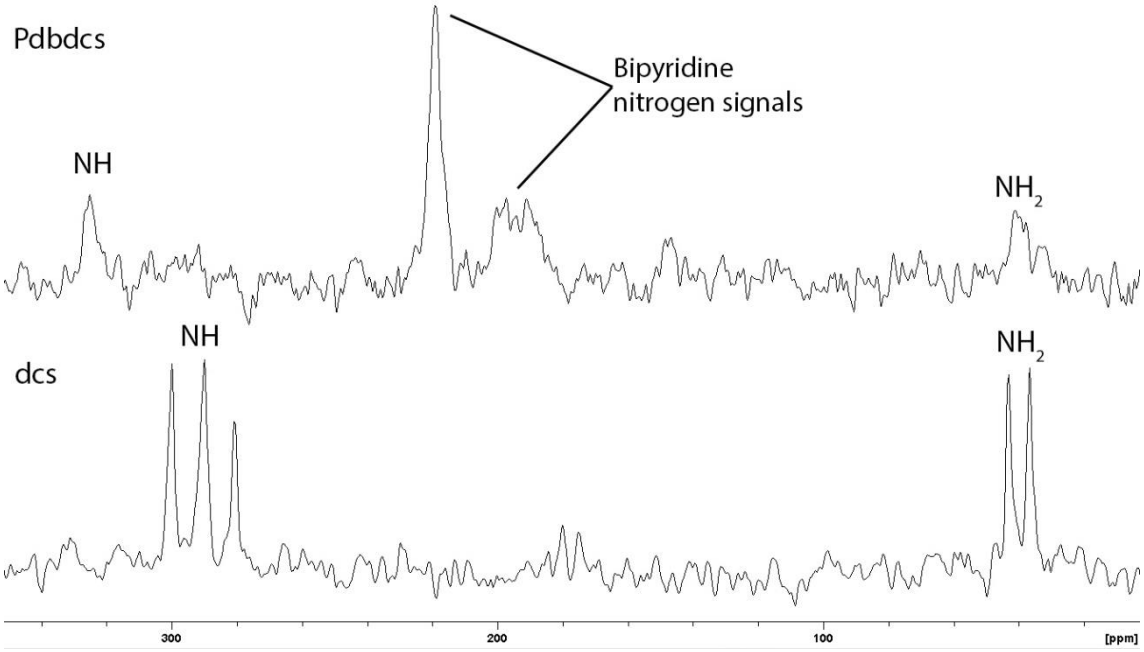

Figure 54. Solid state ^{15}N NMR spectra of dcs (bottom) and Pdbdcs (top).

Evidence of coordination of dcs to the metal ion is observed due to the significant shift of the NH signal from 290 ppm in the ligand to 325 ppm in the complex (Δ = 35ppm). However, no significant shift was observed for the NH_2 signal. In the NMR spectrum of Pdbdcs the signal of the nitrogen atoms of the coordinated bipyridine moiety are also present in the region between 180 and 240 ppm.

The signals of the nitrogen atoms in the NMR spectrum of dcs appear multiplied due to the zwitterionic nature of the molecule that allows different charge distributions in its structure, even in the solid state[149] (see Figure 54).

4.4. Antibacterial assays with Pdbdcs.

The antibacterial *in vitro* experiments were performed against two strains of Gram-positive (*S. aureus* and *B. cereus*) and two strains of Gram-negative bacteria (*E. coli* and *P. aeruginosa*) as shown in Table 16. The results are expressed in terms of minimum inhibitory concentration (MIC), that is the lowest concentration necessary to stop bacterial growth, therefore, the lower is the MIC the higher is the antibacterial activity.

Table 16. Values of MIC (in µg/mL and mmol/L) for dcs, Pdbdcs and K_2PdCl_4 against the four bacteria strains tested.

MIC (µg/mL)	***S. aureus***	***B. cereus***	***E. coli***	***P. aeruginosa***
dcs	46.87	93.75	93.75	93.75
Pdbdcs	375	375	375	375
K_2PdCl_4	1500	1500	750	750
MIC (mmol/L)	***S. aureus***	***B. cereus***	***E. coli***	***P. aeruginosa***
dcs	0.46	0.92	0.92	0.92
Pdbdcs	0.61	0.61	0.61	0.61
K_2PdCl_4	4.60	4.60	2.30	2.30

The complex was able to inhibit the growth of all the bacterial strains tested, both Gram-positive and Gram-negative, with the same MIC (375 µg/mL or 0.61 mmol/L), but there are different ways to interpret such results of MIC. If the value in µg/mL is used the antibacterial activity is based on the total mass of compound and, in this case, the activity of the complex is higher than the Pd(II) salt and significantly lower than the dcs. However, if the molar masses of the compounds are considered and MIC is expressed as mmol/L, the antibacterial activity of the complex and the ligand are very similar (in the same magnitude). This is because the molar mass of dcs (102.9 g/mol) is much lower than that of Pdbdcs (610.7 g/mol).

Regardless of the unit used to express the MIC, is it clear that the complex is more active than K_2PdCl_4 against all the bacteria tested and the presence of the ligands increases its activity, even if MIC values obtained for Pdbdcs are not considered high.

5. Crystal structure of Pt(II) complex with 6fa

Single crystals of the complex Pt6fa were obtained by the slow evaporation of an ethanolic solution. Table 17 summarizes the crystallographic data.

Table 17. Crystallographic data for the Pt6fa complex.

Name	**Pt6fa**
Empirical formula	$C_{14}H_{10}F_2N_2O_4Pt \cdot H_2O$
Formula weight (g mol^{-1})	521.35
Temperature (K)	150.15
Radiation - Mo Kα (Å)	0.71073
Crystal system	monoclinic
Space group	Cc
a, b, c (Å)	18.0965 (13), 8.4448 (6), 11.4611 (8)
β(°)	124.128 (1)
Volume ($Å^3$)	1449.87 (18)
Z	4
μ (mm^{-1})	9.73
F(000)	984
Crystal size (mm^3)	0.29 × 0.08 × 0.05
Index ranges	$-24 \leq h \leq 25$, $-12 \leq k \leq 12$, $-16 \leq l \leq 16$
Reflections collected	16743
Data/restraints/parameters	4313/2/220
R[F2 > 2s(F2)]; wR(F2); S	0.012, 0.026, 0.82
Δρmax, Δρmin (e Å−3)	0.99, −0.42

The crystal structure of Pt(II) complex (Figure 55) reveals a square-planar geometry with a cis coordination mode of the 6fa ligands with very little distortion. The distances in the coordination sphere are very similar to each other and the angles are typical of square geometry, close to 90°, as presented in Table 18, where the bond lengths of Pt6fa crystal are compared with the crystal of 6fa. After coordination, the O1-C7 bond is shortened in comparison to the ligand, as in Pt6fa the O1 is coordinated to Pt(II). Moreover, the C1-C7 bond in the complex is longer (weaker) than in the ligand.

Table 18. Selected bond lengths and angles from Pt6fa and 6fa crystal structures.

Pt6fa bonds	Length / Å Angles / °	6fa bonds	Length / Å
F1—C6	1.347 (5)	F1—C6	1.3491 (15)
O1—C7	1.290 (4)	O1—C7	1.3192 (16)
O3—C14	1.293 (4)		
O2—C7	1.242 (4)	O2—C7	1.2356 (15)
O4—C14	1.228 (4)		
C1—C7	1.493 (4)	C1—C7	1.4704 (18)
C8—C14	1.511 (5)		
Pt1—O3	2.025 (3)		
Pt1—O1	2.027 (2)		
Pt1—N2	2.027 (3)		
Pt1—N1	2.025 (3)		
O3—Pt1—O1	90.09 (11)		
O3—Pt1—N2	87.67 (11)		
O3—Pt1—N1	177.17 (15)		
N2—Pt1—O1	177.76 (10)		
N1—Pt1—O1	87.20 (11)		
N1—Pt1—N2	95.04 (12)		

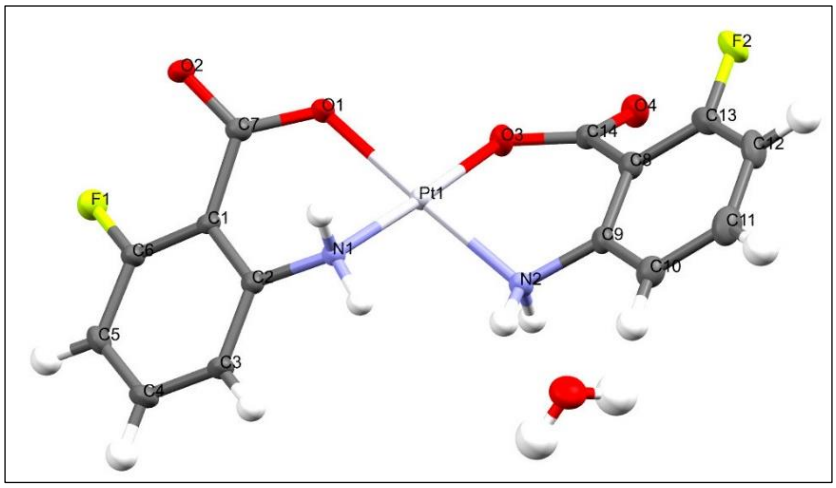

Figure 55. Crystal structure of Pt6fa.

One can notice in Figure 56 that the unit cell of the Pt6fa complex is composed of 4 asymmetric units (Z = 4) and that the plane that contains the metal center and the coordinated nitrogen and oxygen atoms is not the same plane of the benzyl rings. In fact they are at an angle of approximately 55° to each other. A water molecule is

present in the structure, forming a hydrogen bond with a hydrogen atom from N2 (hydrogen bond length 1.87 Å).

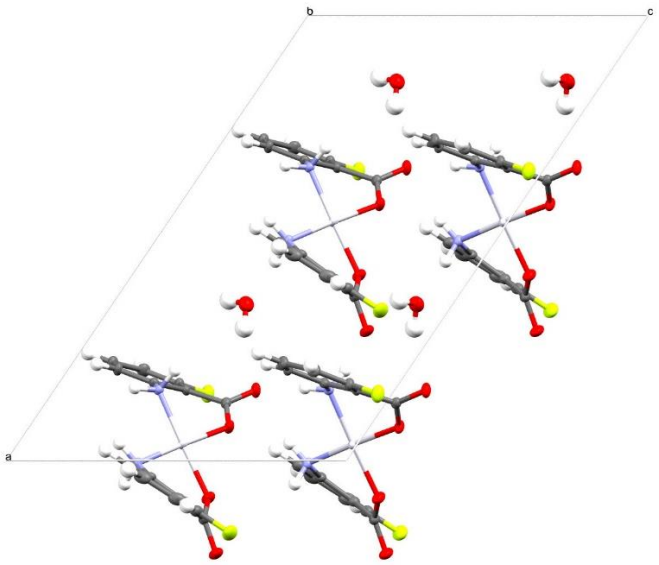

Figure 56. Unit cell representation of Pt6fa crystal along the “b” axis.

So far, the characterization of the Pt6fa complex was limited to the determination of its crystal structure. Attempts for the optimization of the synthesis procedure and a complete characterization of the complex by thermal and elemental analyses, infrared, UV-Vis and NMR spectroscopic techniques are envisaged.

V. Conclusions

Four silver(I) complexes were obtained with isomers of fluoroanthranilic acids: Ag4fa, Ag5fa, Ag6fa and Ag-4,5fa. These complexes have a 1:1 metal:ligand ratio with the molecular formula $AgC_7H_5FNO_2$ for the complexes with monofluorinated ligands (4fa, 5fa and 6fa) and $AgC_7H_4F_2NO_2$ for the complex with 4,5-fa.

Infrared and NMR spectroscopic analyses show that coordination of the ligands to silver(I) occurs by the nitrogen and oxygen atoms of the amine and carboxylate groups. The crystal structure of the silver(I) complex of 5-fluoroanthranilic acid was solved by single crystal X-ray diffraction analysis, and the results revealed a bidentate bridging coordination of the carboxylate groups and also coordination of the amino group to the silver ions in a distorted trigonal planar geometry. An extended 2D polymeric structure containing silver chains (bonded by argentophilic interactions) connected by the coordination with the 5fa ligands was observed.

The Ag(I) complexes Ag4fa, Ag5fa and Ag6fa showed an *in vitro* antibacterial activity with MIC = 62.25 µg/mL against Gram-positive and Gram-negative bacterial strains (*S. aureus*, *B. cereus*, *E. coli* and *P. aeruginosa*) and also against *M. tuberculosis* with MIC_{90} between 2.6 and 4.2 µg/mL. The free fluoroanthranilic acid isomers significantly inhibited *M. tuberculosis* growth in a similar concentration range of the complexes (MIC_{90} between 2.8 and 4.7 µg/mL), which suggests that the structure of the ligand is essential for the antituberculosis activity. The complexes are non-mutagenic, which encourages further studies about their antituberculosis properties against resistant and/or biofilm producing strains.

The cytotoxic activity assays revealed that the Ag4fa complex was particularly selective against epithelial colorectal adenocarcinoma cells (Caco-2, IC_{50} = 2.1 µg/mL) when compared to the normal human cell lines GM07492 (IC_{50} = 6.68 µg/mL), MRC-5 (IC_{50} = 18 µg/mL) and HUVEC (IC_{50} = 8.4 µg/mL), which are promising results considering the search of new bioactive silver compounds for cancer treatment.[116]

New Cu(II) complexes with 6fa and auxiliary ligands (phen, bipy or 4,4'-Mebipy) were also synthesized and partially characterized. In the case of this series of compounds, insoluble solid samples were isolated and characterization revealed an 1:2:1 ratio of Cu(II):6fa:ancillary ligand. Besides that, crystals were also obtained by the slow evaporation of an aqueous solution of each complex. Although it was not possible to refine the crystal structures obtained by X-ray crystallography, the composition of the complexes isolated as crystals seems to have a 1:1:2 ratio of Cu(II):6fa:ancillary ligand

and are also soluble in water, ethanol and methanol. Such coordination compounds may be further investigated using EPR spectroscopy and X-ray diffraction analysis.

A Pd(II) complex with dcs and bipyridine (Pdbdcs) was synthesized and characterized. The composition found for the complex is $[Pd(C_{16}H_{19}N_6O_4)]PF_6$. For this complex, the infrared spectroscopy suggests coordination by the nitrogen atoms of the amine and oxazolidinone groups, while the NMR experiments in the solid state confirms coordination by the nitrogen atom of the oxazolidinone moiety. Therefore, the possibility of coordination by both nitrogen atoms needs to be considered. The Figure 57 shows the proposed structure for this complex, even though further investigation must be done to determine its exact structure and coordination mode. As for this moment, the possibility of a polymeric structure, cannot be discarded. The first results about the synthesis and characterization of this complex were presented in the XIX BMIC / VI LaBIC / VIII Brazilian Meeting on Rare Earths Conference 2018, held in Fortaleza-CE, Brazil.

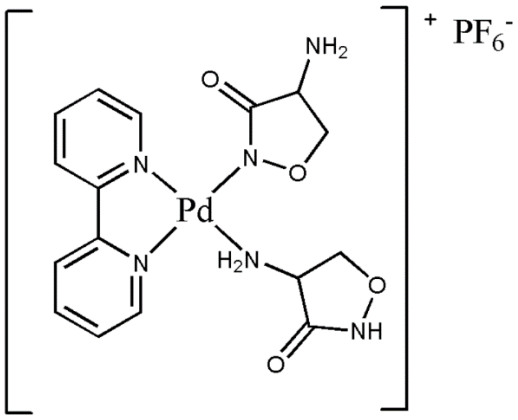

Figure 57. Proposed structure for Pdbdcs.

VI. Perspectives

For the silver(I) complexes with fluoroanthranilic acids, a possible next step could be the evaluation their activity against different strains of resistant *M. tuberculosis* as the fluoroanthranilic acids have great potential against strains that are resistant to the first line of TB treatment. Also, studies of cell internalization of these complexes could also be important to evaluate if they can reach their molecular target and if they can accumulate in any of the cell's organelles. Besides that, the fluorescence of the silver complexes with anthranilic acids could also be further explored as a way of identifying these species inside the cell.

The Pd(II) complex with dcs, as well as the series of Cu(II) complexes could have their structural characterizations completed, and their activities against *M. tuberculosis* could be explored. Particularly, for the Cu(II) complex there is a potential to study their redox properties and use it to affect biological targets like the DNA. The influence of the different auxiliary ligands on the coordination bond strength between Cu(II) and 6fa (and possible ligand exchange) should also be evaluated and further be correlated to biological activity.

The Pt(II) complex had its structure solved by X-ray diffraction, but no other characterizations could be performed until now. An optimization of the synthesis condition may be performed in the future. In this way, the complex could be fully characterized and evaluated concerning its biological activities.

VII. Financial Support

This study was supported by São Paulo State Research Foundation - FAPESP (Grants 2017/25995-6 and 2018/12062-4) This study was also financed in part by the Coordenação de Aperfeiçoamento de Pessoal de Nível Superior - Brasil (CAPES) - Finance Code 001 and CNPq (Conselho Nacional de Desenvolvimento Científico e Tecnológico, Grant 407012/2018–4).

VIII. Appendix

Appendix Table 1. Crystallographic data for the complex Ag5fa

Empirical formula	$AgC_7H_5FNO_2$
Formula weight (g mol^{-1})	261.99
Temperature (K)	150.15
Radiation - Mo Kα (Å)	0.71073
Crystal system	orthorhombic
Space group	$Pca2_1$
a, b, c (Å)	24.842 (5), 4.9310 (9), 5.9195 (12)
α, β, γ (°)	90
Volume ($Å^3$)	725.1(2)
Z	4
ρ_{calc} (g/cm^3)	2.400
μ (mm^{-1})	2.747
F(000)	504.0
Crystal size (mm^3)	0.276 × 0.12 × 0.087
2θ range for data collection (°)	3.278 to 61.058
Index ranges	$-35 \leq h \leq 35$, $-6 \leq k \leq 7$, $-8 \leq l \leq 8$
Reflections collected	23914
Independent reflections	2198 [R_{int} = 0.0338, R_{sigma} = 0.0166]
Data/restraints/parameters	2198/13/110
Goodness-of-fit on F^2	1.232
Final R indexes [I>=2σ (I)]	R_1 = 0.0334, wR_2 = 0.0671
Final R indexes [all data]	R_1 = 0.0368, wR_2 = 0.0682
Largest diff. peak/hole (e $Å^{-3}$)	2.21/-1.31
Flack parameter	0.04(8)

Appendix Table 2. Fractional Atomic Coordinates ($\times 10^4$) and Equivalent Isotropic Displacement Parameters ($Å^2 \times 10^3$) for Ag5fa.

Atom	***x***	***y***	***z***	**U(eq)**
Ag1	2329.7(2)	-2361.3(8)	5392(2)	16.67(10)
O1	2878.4(19)	806(11)	4632(8)	17.2(10)
N1	3166(2)	4285(11)	1424(9)	13.6(10)
C2	3592(3)	4935(14)	2972(11)	12.0(11)
O2	3356(2)	433(10)	7793(8)	16.6(9)
C7	3276(2)	1445(13)	5902(9)	12.9(12)
C1	3646(2)	3629(12)	5040(10)	11.2(11)
C5	4419(3)	6384(15)	5808(9)	16.3(14)
C6	4074(3)	4374(15)	6456(11)	16.5(13)
C4	4375(3)	7705(16)	3742(13)	22.4(14)
F1	4827(2)	7108(11)	7189(10)	38.1(13)
C3	3956(3)	6922(14)	2331(12)	17.8(13)

Appendix Table 3. Anisotropic Displacement Parameters ($Å^2 \times 10^3$) for Ag5fa.

Atom	**U_{11}**	**U_{22}**	**U_{33}**	**U_{23}**	**U_{13}**	**U_{12}**
Ag1	22.32(18)	12.59(17)	15.11(16)	1.5(4)	4.3(3)	-3.76(16)
O1	18(2)	20(2)	14(2)	4.6(18)	-3.0(17)	-7.2(19)
N1	22(3)	15(3)	4(2)	-1(2)	-2(2)	1(2)
C2	12(2)	13(3)	10(3)	0(2)	0(2)	0(2)
O2	20(2)	18(2)	11(2)	3.4(19)	2.2(18)	-2(2)
C7	13.9(15)	13.3(16)	11.6(17)	-0.5(12)	0.2(11)	0.0(12)
C1	11.2(11)	11.2(11)	11.2(11)	0.00(14)	0.00(14)	0.00(14)
C5	16(3)	26(3)	8(3)	-1(2)	-4(2)	-4(2)
C6	17(3)	20(3)	13(3)	1(3)	-1(2)	0(3)
C4	21(3)	18(3)	29(4)	3(3)	1(3)	-4(3)
F1	31(3)	36(3)	47(3)	4(3)	-20(2)	-14(2)
C3	21(3)	13(3)	19(3)	4(3)	2(3)	-1(2)

Appendix Table 4. Bond Lengths for Ag5fa.

Atom	Atom	Length/Å	Atom	Atom	Length/Å
Ag1	Ag1^{i}	3.0783(6)	O2	C7	1.242(7)
Ag1	Ag1^{ii}	3.0783(6)	C7	C1	1.505(8)
Ag1	O1	2.121(5)	C1	C6	1.405(9)
Ag1	N1^{iii}	2.150(6)	C5	C6	1.364(9)
O1	C7	1.280(7)	C5	C4	1.390(10)
N1	C2	1.436(8)	C5	F1	1.350(7)
C2	C1	1.389(8)	C4	C3	1.389(10)
C2	C3	1.386(9)			

^{i}1/2-X,+Y,-1/2+Z; ^{ii}1/2-X,+Y,1/2+Z; ^{iii}1/2-X,-1+Y,1/2+Z

Appendix Table 5. Bond Angles for Ag5fa.

Atom	Atom	Atom	Angle/°	Atom	Atom	Atom	Angle/°
Ag1^{i}	Ag1	Ag1^{ii}	148.10(3)	O1	C7	C1	116.6(5)
O1	Ag1	Ag1^{i}	91.56(13)	O2	C7	O1	123.7(6)
O1	Ag1	Ag1^{ii}	67.64(14)	O2	C7	C1	119.7(6)
O1	Ag1	N1^{iii}	173.9(2)	C2	C1	C7	124.9(5)
N1^{iii}	Ag1	Ag1^{i}	83.34(14)	C2	C1	C6	118.5(6)
N1^{iii}	Ag1	Ag1^{ii}	115.50(14)	C6	C1	C7	116.6(5)
C7	O1	Ag1	123.5(4)	C6	C5	C4	122.6(6)
C2	N1	Ag1^{iv}	115.6(4)	F1	C5	C6	119.5(6)
C1	C2	N1	122.0(6)	F1	C5	C4	117.9(6)
C3	C2	N1	117.6(6)	C5	C6	C1	119.9(6)
C3	C2	C1	120.4(6)	C3	C4	C5	117.2(6)
C7	O2	Ag1^{i}	128.5(4)	C2	C3	C4	121.4(6)

^{i}1/2-X,+Y,1/2+Z; ^{ii}1/2-X,+Y,-1/2+Z; ^{iii}1/2-X,-1+Y,1/2+Z; ^{iv}1/2-X,1+Y,-1/2+Z

Appendix Table 6. Torsion Angles for Ag5fa.

A	B	C	D	Angle/°	A	B	C	D	Angle/°
Ag1	O1	C7	O2	-6.2(9)	O2	C7	C1	C2	-179.0(6)
Ag1	O1	C7	C1	176.3(4)	O2	C7	C1	C6	0.9(9)
Ag1[i]	N1	C2	C1	124.5(6)	C7	C1	C6	C5	-178.5(6)
Ag1[i]	N1	C2	C3	-55.9(7)	C1	C2	C3	C4	-1.4(10)
Ag1[ii]	O2	C7	O1	-16.3(9)	C5	C4	C3	C2	0.9(11)
Ag1[ii]	O2	C7	C1	161.2(4)	C6	C5	C4	C3	0.8(11)
O1	C7	C1	C2	-1.4(9)	C4	C5	C6	C1	-2.0(11)
O1	C7	C1	C6	178.6(6)	F1	C5	C6	C1	179.3(6)
N1	C2	C1	C7	-0.3(10)	F1	C5	C4	C3	179.5(7)
N1	C2	C1	C6	179.8(6)	C3	C2	C1	C7	-179.9(6)
N1	C2	C3	C4	179.0(6)	C3	C2	C1	C6	0.2(9)
C2	C1	C6	C5	1.5(10)					

[i]1/2-X,1+Y,-1/2+Z; [ii]1/2-X,+Y,1/2+Z

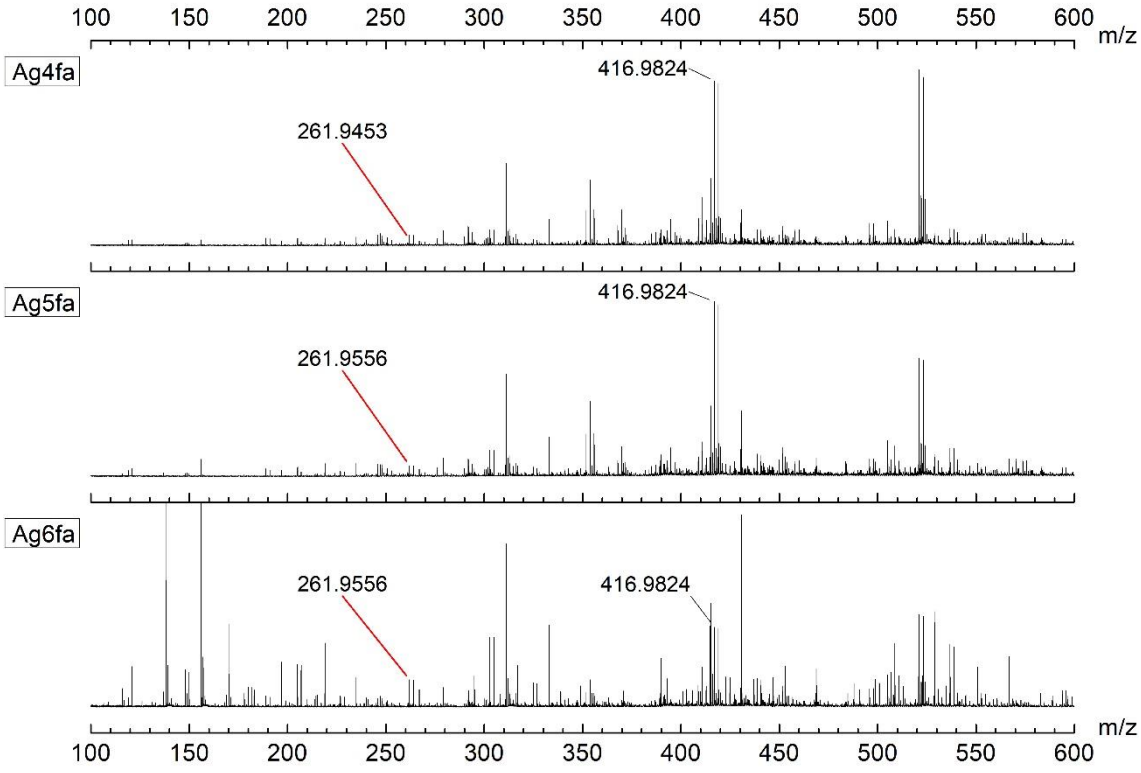

Appendix Figure 1. Full mass spectra of the complexes Ag4fa, Ag5fa and Ag6fa

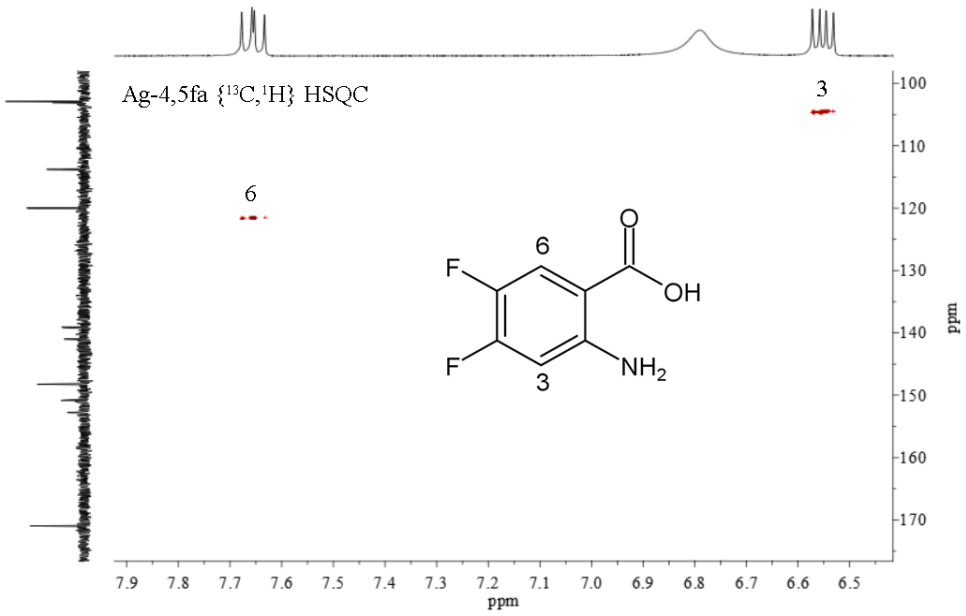

Appendix Figure 2. The {^{13}C,^{1}H} HSQC NMR spectra of Ag-4,5fa in DMSO-d^{6}.

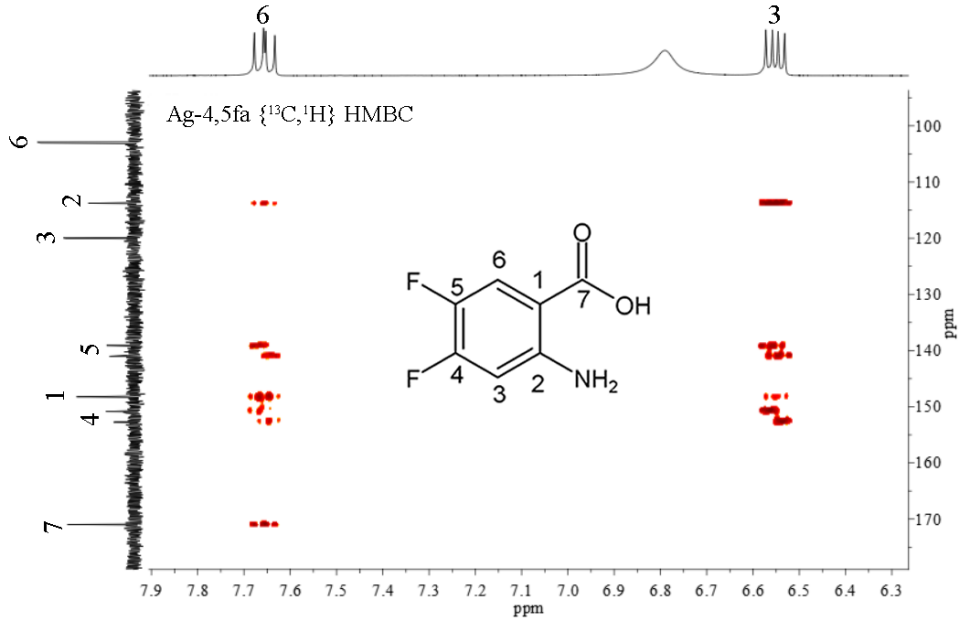

Appendix Figure 3. The {^{13}C,^{1}H} HMBC NMR spectra of Ag-4,5fa in DMSO-d^{6}.

IX. References

1 World Health Organization, *Media centre Tuberculosis*, 2016, 1–5.

2 S. V. Kumar, M. K. Deka, M. Bagga, M. S. Kala and K. Gauthaman, *European review for medical and pharmacological sciences*, 2010, **14**, 831–843.

3 N. R. Gandhi, A. Moll, A. W. Sturm, R. Pawinski, T. Govender, U. Lalloo, K. Zeller, J. Andrews and G. Friedland, *Lancet*, 2006, **368**, 1575–1580.

4 A. E. DeBarber, K. Mdluli, M. Bosman, L. G. Bekker and C. E. Barry, *Proceedings of the National Academy of Sciences of the United States of America*, 2000, **97**, 9677–82.

5 World Health Organization, *Global Tuberculosis Report*, 2020.

6 S. Tiberi, A. Scardigli, R. Centis, L. D'Ambrosio, M. Muñoz-Torrico, M. Á. Salazar-Lezama, A. Spanevello, D. Visca, A. Zumla, G. B. Migliori and J. A. Caminero Luna, *International Journal of Infectious Diseases*, 2017, **56**, 181–184.

7 B. Spellberg, *Critical Care*, 2014, **18**, 228.

8 World Health Organization, *Multidrug and extensively drug-resistant TB (M/XDR-TB): 2010 global report on surveillance and response*, 2010.

9 J. A. Caminero and A. Scardigli, *European Respiratory Journal*, 2015, **46**, 887–893.

10 J. A. Lemire, J. J. Harrison and R. J. Turner, *Nature Reviews Microbiology*, 2013, **11**, 371–384.

11 F. R. G. Bergamini, M. A. Ferreira, R. E. F. de Paiva, A. F. Gomes, F. C. Gozzo, A. L. B. Formiga, F. C. A. Corbi, I. O. Mazali, D. A. Alves, M. Lancellotti and P. Paulo. Corbi, *RSC Advances*, 2012, **2**, 10372–10379.

12 S. Pal, E. J. Yoon, S. H. Park, E. C. Choi and J. M. Song, *The Journal of antimicrobial chemotherapy*, 2010, **65**, 2134–2140.

13 G. Grass, C. Rensing and M. Solioz, *Applied and Environmental Microbiology*, 2011, **77**, 1541–1547.

14 S. B. Levy and B. Marshall, *Nature Medicine*, 2004, **10**, S122–S129.

15 S. Medici, M. Peana, V. M. Nurchi, J. I. Lachowicz, G. Crisponi and M. A. Zoroddu, *Coordination Chemistry Reviews*, 2015, **284**, 329–350.

16 S. P. Fricker, *Dalton Transactions*, 2007, 4903.

17 S. Medici, M. Peana, V. M. Nurchi and M. A. Zoroddu, *Journal of Medicinal Chemistry*, 2019, **62**, 5923–5943.

18 H. J. Klasen, *Burns : journal of the International Society for Burn Injuries*, 2000, **26**, 117–130.

19 H. J. Klasen, *Burns*, 2000, **26**, 131–138.

20 J. L. Hobman and L. C. Crossman, *Journal of Medical Microbiology*, 2015, **64**, 471–497.

21 A. Rusu, G. Hancu, A. Cristina Munteanu and V. Uivarosi, *Journal of Organometallic Chemistry*, 2017, **839**, 19–30.

22 U. O. Ozdemir, N. Ozbek, Z. K. Genc, F. İlbiz and A. B. Gündüzalp, *Journal of Molecular Structure*, 2017, **1138**, 55–63.

23 A. T. M. Fiori, D. H. Nakahata, A. Cuin, W. R. Lustri and P. P. Corbi, *Polyhedron*, 2017, **121**, 172–179.

24 U. Kalinowska-Lis, E. M. Szewczyk, L. Chęcińska, J. M. Wojciechowski, W. M. Wolf and J. Ochocki, *ChemMedChem*, 2014, **9**, 169–176.

25 J. H. B. Nunes, F. R. G. Bergamini, W. R. Lustri, P. P. de Paiva, A. L. T. G. Ruiz, J. E. de Carvalho and P. P. Corbi, *Journal of Fluorine Chemistry*, 2017, **195**, 93–101.

26 M. E. K. Stathopoulou, C. N. Banti, N. Kourkoumelis, A. G. Hatzidimitriou, A. G. Kalampounias and S. K. Hadjikakou, *Journal of Inorganic Biochemistry*, 2018, **181**, 41–55.

27 M. R. Ciol, C. M. Manzano, A. Cuin, F. R. Pavan, C. M. Ribeiro, A. L. T. G. Ruiz, E. C. S. de Oliveira, W. R. Lustri, N. F. Fregonezi, F. A. R. Nogueira and P. P. Corbi, *ChemistrySelect*, 2018, **3**, 1719–1726.

28 C. N. Banti, C. Papatriantafyllopoulou, M. Manoli, A. J. Tasiopoulos and S. K. Hadjikakou, *Inorganic Chemistry*, 2016, **55**, 8681–8696.

29 S. Dasari and P. Bernard Tchounwou, *European Journal of Pharmacology*, 2014, **740**, 364–378.

30 C. N. Banti and S. K. Hadjikakou, *Metallomics*, 2013, **5**, 569–596.

31 C. N. Banti, A. D. Giannoulis, N. Kourkoumelis, A. M. Owczarzak, M. Poyraz, M. Kubicki, K. Charalabopoulos and S. K. Hadjikakou, *Metallomics*, 2012, **4**, 545–560.

32 J. H. Bormio Nunes, P. P. de Paiva, A. L. T. G. Ruiz, J. E. de Carvalho and P. P. Corbi, *Toxicology in Vitro*, 2019, **60**, 359–368.

33 B. Rosenberg, L. van Camp and T. Krigas, *Nature*, 1965, **205**, 698–699.

34 B. Rosenberg, L. van Camp, J. Trosko and V. Mansour, *Nature*, 1969, **222**, 385–386.

35 M. G. Apps, E. H. Y. Choi and N. J. Wheate, *Endocrine-Related Cancer*, 2015, **22**, R219–R233.

36 N. J. Wheate, S. Walker, G. E. Craig and R. Oun, *Dalton Transactions*, 2010, **39**, 8113–8127.

37 G. D. de Souza, M. Aparecida Rodrigues, P. Pereira Silva, E. C. Pereira-Maia, F. Vasconcelos Botelho, T. A. de Campos, E. de Faria Franca, K. J. de Almeida and W. Guerra, *Croatica Chemica Acta*, 2013, **86**, 201–206.

38 A. Garoufis, S. K. Hadjikakou and N. Hadjiliadis, *Coordination Chemistry Reviews*, 2009, **253**, 1384–1397.

39 D. Kovala-Demertzi, M. A. Demertzis, E. Filiou, A. A. Pantazaki, P. N. Yadav, J. R. Miller, Y. Zheng and D. A. Kyriakidis, *Biometals : an international journal on the role of metal ions in biology, biochemistry, and medicine*, 2003, **16**, 411–8.

40 C. M. Manzano, F. R. G. Bergamini, W. R. Lustri, A. L. T. G. Ruiz, E. C. S. de Oliveira, M. A. Ribeiro, A. L. B. Formiga and P. P. Corbi, *Journal of Molecular Structure*, 2018, **1154**, 469–479.

41 P. A. Ajibade and O. G. Idemudia, *Bioinorganic Chemistry and Applications*, 2013, **2013**, 1–8.

42 A. M. Plutín, A. Alvarez, R. Mocelo, R. Ramos, E. E. Castellano, M. M. da Silva, W. Villarreal, F. R. Pavan, C. S. Meira, J. S. R. Filho, D. R. M. Moreira, M. B. P. Soares and A. A. Batista, *Polyhedron*, 2017, **132**, 70–77.

43 A. M. Plutín, A. Alvarez, R. Mocelo, R. Ramos, E. E. Castellano, M. M. da Silva, L. Colina-Vegas, F. R. Pavan and A. A. Batista, *Inorganic Chemistry Communications*, 2016, **63**, 74–80.

44 L. P. de Oliveira, Z. A. Carneiro, C. M. Ribeiro, M. F. Lima, D. A. Paixão, M. Pivatto, M. V. N. de Souza, L. R. Teixeira, C. D. Lopes, S. de Albuquerque, F. R. Pavan and W. Guerra, *Journal of Inorganic Biochemistry*, 2018, **183**, 77–83.

45 D. H. Nakahata, R. E. F. de Paiva, W. R. Lustri, C. M. Ribeiro, F. R. Pavan, G. G. da Silva, A. L. T. G. Ruiz, J. E. de Carvalho and P. P. Corbi, *Journal of Inorganic Biochemistry*, 2018, **187**, 85–96.

46 P. McCarron, M. McCann, M. Devereux, K. Kavanagh, C. Skerry, P. C. Karakousis, A. C. Aor, T. P. Mello, A. L. S. Santos, D. L. Campos and F. R. Pavan, *Frontiers in Microbiology*, 2018, **9**, 1–10.

47 E. R. dos Santos, R. S. Corrêa, L. v. Pozzi, A. E. Graminha, H. S. Selistre-de-Araújo, F. R. Pavan and A. A. Batista, *Inorganica Chimica Acta*, 2017, **463**, 1–6.

48 Y.-L. Wang, X. Zhang, X.-M. Meng, X. Li, C.-F. Bi and Y.-H. Fan, *Transition Metal Chemistry*, 2016, **41**, 897–907.

49 B.-E. Kim, T. Nevitt and D. J. Thiele, *Nature Chemical Biology*, 2008, **4**, 176–185.

50 W. J. Lian, X. T. Wang, C. Z. Xie, H. Tian, X. Q. Song, H. T. Pan, X. Qiao and J. Y. Xu, *Dalton Transactions*, 2016, **45**, 9073–9087.

51 C. Marzano, M. Pellei, F. Tisato and C. Santini, *Anti-Cancer Agents in Medicinal Chemistry*, 2009, **9**, 185–211.

52 F. Carvallo-Chaigneau, C. Trejo-Solís, C. Gómez-Ruiz, E. Rodríguez-Aguilera, L. Macías-Rosales, E. Cortés-Barberena, C. Cedillo-Peláez, I. Gracia-Mora, L. Ruiz-Azuara, V. Madrid-Marina and F. Constantino-Casas, *BioMetals*, 2008, **21**, 17–28.

53 C. Trejo-Solís, G. Palencia, S. Zuñiga, A. Rodríguez-Ropon, L. Osorio-Rico, S. Torres Luvia, I. Gracia-Mora, L. Marquez-Rosado, A. Sánchez, M. E. Moreno-García, A. Cruz, M. E. Bravo-Gómez, L. Ruiz-Ramírez, S. Rodríquez-Enriquez and J. Sotelo, *Neoplasia*, 2005, **7**, 563–574.

54 L. Ruiz-Ramirez, I. Gracia-Mora, Ma. E. de la Rosa, H. Sumano, C. Gomez, F. Arenas, E. Gomez, E. Pimentel and M. Cruces, *Journal of Inorganic Biochemistry*, 1993, **51**, 406.

55 A. de Vizcaya-Ruiz, A. Rivero-Muller, L. Ruiz-Ramirez, G. E. N. Kass, L. R. Kelland, R. M. Orr and M. Dobrota, *Toxicology in Vitro*, 2000, **14**, 1–5.

56 L. Ruiz-Azuara and M. E. Bravo-Gomez, *Current Medicinal Chemistry*, 2010, **17**, 3606–3615.

57 A. R. Barbosa, K. R. Caleffi-Ferracioli, C. Q. F. Leite, J. C. García-Ramos, Y. Toledano-Magaña, L. Ruiz-Azuara, V. L. D. Siqueira, F. R. Pavan and R. F. Cardoso, *Chemotherapy*, 2016, **61**, 249–255.

58 S. Shah, A. G. Dalecki, A. P. Malalasekera, C. L. Crawford, S. M. Michalek, O. Kutsch, J. Sun, S. H. Bossmann and F. Wolschendorf, *Antimicrobial agents and chemotherapy*, 2016, **60**, 5765–76.

59 D. S. Sigman, D. R. Graham, V. D'Aurora and A. M. Stern, *The Journal of biological chemistry*, 1979, **254**, 12269–72.

60 L. E. Marshall, D. R. Graham, K. A. Reich and D. S. Sigman, *Biochemistry*, 1981, **20**, 244–250.

61 L. G. F. Lopes, E. M. Carvalho and E. H. S. Sousa, *Dalton Transactions*, 2020, **49**, 15988–16003.

62 J. S. Oliveira, E. H. S. Sousa, L. A. Basso, M. Palaci, R. Dietze, D. S. Santos and I. S. Moreira, *Chemical communications (Cambridge, England)*, 2004, **4**, 312–3.

63 E. G. Salina, O. Ryabova, A. Vocat, B. Nikonenko, S. T. Cole and V. Makarov, *Journal of Infection and Chemotherapy*, 2017, **23**, 794–797.

64 B. E. Volcani, S. Sicher, E. D. Bergmann and H. Bendas, *The Journal of biological chemistry*, 1954, **207**, 411–420.

65 ElizabethW. Jones, P. B. Berget, J. M. B. III, C. Anderson, D. Asafu-Adjei, S. Avetisian, F. Barrie, R. Chen, B. Chu, S. Conroy, S. Conroy, A. Dill, W. Eimer, D. Garrity, A. Greenwood, T. Hamilton, S. Hucko, C. Jackson, K. Livesey, T. Monaco, C. Onorato, M. Otsuka, S. Pai, G. Schaeffer, S. Shung, S. Spath, J. Stahlman, B. Sweeney, E. Wiltrout, D. Yurovsky and A. Zonneveld, *Yeast*, 2008, **25**, 41–46.

66 J. H. Toyn, P. Gunyuzlu, W. H. White, L. A. Thompson and G. F. Hollis, *Yeast*, 2000, **16**, 553–560.

67 P. Prasher and M. Sharma, *Drug Development Research*, 2021, **82**, 945–958.

68 H. M. Faidallah, K. A. Khan and A. M. Asiri, *Journal of Fluorine Chemistry*, 2011, **132**, 870–877.

69 B. E. Smart, *Journal of Fluorine Chemistry*, 2001, **109**, 3–11.

70 J. P. Dalton, B. Uy, N. Phummarin, B. R. Copp, W. A. Denny, S. Swift and S. Wiles, *PeerJ*, 2016, **4**, e2717.

71 M. D. Macia, E. Rojo-Molinero and A. Oliver, *Clinical Microbiology and Infection*, 2014, **20**, 981–990.

72 K. A. Abrahams, J. A. G. Cox, K. Fütterer, J. Rullas, F. Ortega-Muro, N. J. Loman, P. J. Moynihan, E. Pérez-Herrán, E. Jiménez, J. Esquivias, D. Barros, L. Ballell, C. Alemparte and G. S. Besra, *Scientific Reports*, 2017, **7**, 9430.

73 K. Michalska, S. Wellington, P. P. Nag, R. Jedrzejczak, N. I. Maltseva, S. L. Fisher, S. L. Schreiber, D. T. Hung and A. Joachimiak, *Acta Crystallographica Section A Foundations and Advances*, 2017, **73**, a288–a288.

74 A. Castell, F. L. Short, G. L. Evans, T. V. M. Cookson, E. M. M. Bulloch, D. D. A. Joseph, C. E. Lee, E. J. Parker, E. N. Baker and J. S. Lott, *Biochemistry*, 2013, **52**, 1776–1787.

75 J. Shaun Lott, *Biochemical Society Transactions*, 2020, **48**, 2029–2037.

76 Y. J. Zhang, M. C. Reddy, T. R. Ioerger, A. C. Rothchild, V. Dartois, B. M. Schuster, A. Trauner, D. Wallis, S. Galaviz, C. Huttenhower, J. C. Sacchettini, S. M. Behar and E. J. Rubin, *Cell*, 2013, **155**, 1296–1308.

77 M. Nurul Islam, R. Hitchings, S. Kumar, F. L. Fontes, J. S. Lott, N. A. Kruh-Garcia and D. C. Crick, *ACS Infectious Diseases*, 2019, **5**, 55–62.

78 D. A. Smith, T. Parish, N. G. Stoker and G. J. Bancroft, *Infection and Immunity*, 2001, **69**, 1142–1150.

79 T. V. M. Cookson, A. Castell, E. M. M. M. Bulloch, G. L. Evans, F. L. Short, E. N. Baker, J. S. Lott and E. J. Parker, *Biochemical Journal*, 2014, **461**, 87–98.

80 F. Ali and A. J. Jarad, *Chemistry and Materials Research* , 2013, **3**, 126–134.

81 J.-W. Zheng and L. Ma, *Chinese Chemical Letters*, 2016, **27**, 627–630.

82 M. S. Suresh and V. Prakash, *International Journal of the Physical Sciences*, 2010, **5**, 1443–1449.

83 A. M. i El-Roud, A. A. M. Aly, A. A. Abd El-Gaber and M. El-Shabasy, *Croatica Chemica Acta*, 1988, **61**, 775–782.

84 A. Mehta, N. Zitzmann, P. M. Rudd, T. M. Block and R. A. Dwek, *FEBS Letters*, 1998, **430**, 17–22.

85 X. Li, C. F. Bi, Y. H. Fan, X. Zhang, X. M. Meng and L. S. Cui, *Inorganic Chemistry Communications*, 2014, **50**, 35–41.

86 Y.-L. Wang, X. Zhang, X.-M. Meng, X. Li, C.-F. Bi and Y.-H. Fan, *Transition Metal Chemistry*, 2016, **41**, 897–907.

87 P. P. Utthra, N. Pravin and N. Raman, *Journal of Photochemistry and Photobiology B: Biology*, 2016, **158**, 136–144.

88 O. v. Dolomanov, L. J. Bourhis, R. J. Gildea, J. A. K. Howard and H. Puschmann, *Journal of Applied Crystallography*, 2009, **42**, 339–341.

89 G. M. Sheldrick, *Acta Crystallographica Section A Foundations and Advances*, 2015, **71**, 3–8.

90 G. M. Sheldrick, *Acta Crystallographica Section C Structural Chemistry*, 2015, **71**, 3–8.

91 C. L. S. Institute, *M100S: Performance Standards for Antimicrobial Susceptibility Testing*, 2016.

92 J.-C. Palomino, A. Martin, M. Camacho, H. Guerra, J. Swings and F. Portaels, *Antimicrobial Agents and Chemotherapy*, 2002, **46**, 2720–2722.

93 B. Page, M. Page and C. Noel, *International journal of oncology*, 1993, **3**, 473–476.

94 M. P. Chelopo, S. A. Pawar, M. K. Sokhela, T. Govender, H. G. Kruger and G. E. M. Maguire, *European Journal of Medicinal Chemistry*, 2013, **66**, 407–414.

95 D. M. Maron and B. N. Ames, *Mutation Research/Environmental Mutagenesis and Related Subjects*, 1983, 113, 173–215.

96 F. A. Resende, W. Vilegas, L. C. dos Santos and E. A. Varanda, *Molecules*, 2012, **17**, 5255–5268.

97 S. Sreenivasa, K. E. ManojKumar, P. A. Suchetan, B. S. Palakshamurthy and K. Gunasekaran, *Acta Crystallographica Section E Structure Reports Online*, 2013, **69**, o387–o387.

98 C. R. Groom, I. J. Bruno, M. P. Lightfoot and S. C. Ward, *Acta Crystallographica Section B Structural Science, Crystal Engineering and Materials*, 2016, **72**, 171–179.

99 B. Cai, M. E. Zhu, Y. N. Meng and K. Li, *Zeitschrift fur Kristallographie - New Crystal Structures*, 2020, **235**, 543–544.

100 P. Huang, C. Y. Huang, T. C. Lin, L. E. Lin, E. Yang, C. Lee, C. C. Hsu and P. T. Chou, *Analytical Chemistry*, 2020, **92**, 7139–7145.

101 D. Di Tommaso, *CrystEngComm*, 2013, **15**, 6564–6577.

102 A. Gavezzotti, *Acta crystallographica. Section B, Structural science*, 2008, **64**, 401–403.

103 C. Janiak, *Journal of the Chemical Society, Dalton Transactions*, 2000, 3885–3896.

104 X.-Y. Dong, X. Li, B. Li, Y.-Y. Zhu, S.-Q. Zang and M.-S. Tang, *Dalton Transactions*, 2016, **45**, 18142–18146.

105 X.-Q. Fang, Z.-P. Deng, L.-H. Huo, W. Wan, Z.-B. Zhu, H. Zhao and S. Gao, *Inorganic Chemistry*, 2011, **50**, 12562–12574.

106 D. Sun, F.-J. Liu, R.-B. Huang and L.-S. Zheng, *CrystEngComm*, 2013, **15**, 1185–1193.

107 Kazuo Nakamoto, *Infrared and Raman Spectra of Inorganic and Coordination Compounds - Part A: Theory and Application in inorganic Chemistry*, John Wiley & Sons, Sixth Edit., 2009.

108 P. Melnikov, P. P. Corbi, C. Diaz Aguila, M. A. Zacharias, M. Cavicchioli and A. C. Massabni, *Journal of Alloys and Compounds*, 2000, **307**, 179–183.

109 N. Y. Gorobets, S. A. Yermolayev, T. Gurley, A. A. Gurinov, P. M. Tolstoy, I. G. Shenderovich and N. E. Leadbeater, *Journal of Physical Organic Chemistry*, 2012, **25**, 287–295.

110 J.-X. Yu, R. R. Hallac, S. Chiguru and R. P. Mason, *Progress in Nuclear Magnetic Resonance Spectroscopy*, 2013, **70**, 25–49.

111 W. K. Jung, H. C. Koo, K. W. Kim, S. Shin, S. H. Kim and Y. H. Park, *Applied and environmental microbiology*, 2008, **74**, 2171–2178.

112 S. Chernousova and M. Epple, *Angewandte Chemie International Edition*, 2013, **52**, 1636–1653.

113 R. E. F. de Paiva, C. Abbehausen, A. F. Gomes, F. C. Gozzo, W. R. Lustri, A. L. B. Formiga and P. P. Corbi, *Polyhedron*, 2012, **36**, 112–119.

114 C. L. Fox and S. M. Modak, *Antimicrobial agents and chemotherapy*, 1974, **5**, 582–588.

115 B. S. Atiyeh, M. Costagliola, S. N. Hayek and S. A. Dibo, *Burns*, 2007, **33**, 139–148.

116 C. M. Manzano, D. H. Nakahata, J. C. Tenorio, W. R. Lustri, F. A. Resende Nogueira, N. A. Aleixo, P. S. da Silva Gomes, F. R. Pavan, J. A. Grecco, C. M. Ribeiro and P. P. Corbi, *Inorganica Chimica Acta*, 2020, **502**, 119293.

117 J. P. Dalton, B. Uy, N. Phummarin, B. R. Copp, W. A. Denny, S. Swift and S. Wiles, *PeerJ*, 2016, **4**, e2717.

118 D. F. Segura, A. V. G. Netto, R. C. G. Frem, A. E. Mauro, P. B. da Silva, J. A. Fernandes, F. A. A. Paz, A. L. T. Dias, N. C. Silva, E. T. de Almeida, M. J. Marques, L. de Almeida, K. F. Alves, F. R. Pavan, P. C. de Souza, H. B. de Barros and C. Q. F. Leite, *Polyhedron*, 2014, **79**, 197–206.

119 M. Altaf, H. Stoeckli-Evans, A. Cuin, D. N. Sato, F. R. Pavan, C. Q. F. Leite, S. Ahmad, M. Bouakka, M. Mimouni, F. Z. Khardli and T. ben Hadda, *Polyhedron*, 2013, **62**, 138–147.

120 S. A. da Silva, C. Q. F. Leite, F. R. Pavan, N. Masciocchi and A. Cuin, *Polyhedron*, 2014, **79**, 170–177.

121 A. Cuin, A. C. Massabni, G. A. Pereira, C. Q. F. Leite, F. R. Pavan, R. Sesti-Costa, T. A. Heinrich and C. M. Costa-Neto, *Biomedicine & Pharmacotherapy*, 2011, **65**, 334–338.

122 M. Cavicchioli, C. Q. F. Leite, D. N. Sato and A. C. Massabni, *Archiv der Pharmazie*, 2007, **340**, 538–542.

123 G. A. Pereira, A. C. Massabni, E. E. Castellano, L. A. S. Costa, C. Q. F. Leite, F. R. Pavan and A. Cuin, *Polyhedron*, 2012, **38**, 291–296.

124 S. Consalvi, C. Scarpecci, M. Biava and G. Poce, *Bioorganic and Medicinal Chemistry Letters*, 2019, **29**, 126731.

125 L. Vila, R. Marcos and A. Hernández, *Nanotoxicology*, 2017, **11**, 1–10.

126 A. Oberemm, U. Hansen, L. Böhmert, C. Meckert, A. Braeuning, A. F. Thünemann and A. Lampen, *Journal of Applied Toxicology*, 2016, **36**, 404–413.

127 M. van der Zande, A. K. Undas, E. Kramer, M. P. Monopoli, R. J. Peters, D. Garry, E. C. Antunes Fernandes, P. J. Hendriksen, H. J. P. Marvin, A. A. Peijnenburg and H. Bouwmeester, *Nanotoxicology*, 2016, **10**, 1431–1441.

128 M. A. Iqbal, R. A. Haque, S. F. Nasri, A. A. Majid, M. B. K. Ahamed, E. Farsi and T. Fatima, *Chemistry Central Journal*, 2013, **7**, 27–43.

129 D. J. Beck and R. R. Brubaker, *Journal of bacteriology*, 1973, **116**, 1247–52.

130 D. Wang and S. J. Lippard, *Nature Reviews Drug Delivery*, 2005, **4**, 307–320.

131 H. S. Rosenkranz and S. Rosenkranz, *Antimicrobial Agents and Chemotherapy*, 1972, **2**, 373–383.

132 K. Nakamoto, *Infrared and Raman Spectra of Inorganic and Coordination Compounds - Part B: Application in Coordination, Organometallic and Bioinorganic Chemistry*, John Wiley & Sons, Sixth Edit., 2009.

133 A. Filippi, C. Fraschetti, F. Grandinetti, M. Speranza, A. Ponzi, P. Decleva and S. Stranges, *Physical Chemistry Chemical Physics*, 2015, **17**, 25845–25853.

134 G. A. Prosser and L. P. S. De Carvalho, *ACS Medicinal Chemistry Letters*, 2013, **4**, 1233–1237.

135 M. A. Arbex, M. de C. L. Varella, H. R. de Siqueira and F. A. F. de Mello, *Jornal Brasileiro de Pneumologia*, 2010, **36**, 641–656.

136 S. Batson, C. de Chiara, V. Majce, A. J. Lloyd, S. Gobec, D. Rea, V. Fülöp, C. W. Thoroughgood, K. J. Simmons, C. G. Dowson, C. W. G. Fishwick, L. P. S. de Carvalho and D. I. Roper, *Nature Communications*, 2017, **8**, 1939.

137 A. Vora, *The Journal of the Association of Physicians of India*, 2010, **58**, 267–8.

138 S. David, *Journal of Antimicrobial Chemotherapy*, 2001, **47**, 203–206.

139 C. Preti, G. Tosi and P. Zannini, *Z. anorg. allg. Chem.*, 1979, **453**, 173–184.

140 H. Sakurai, C. Shibata, H. Matsuura and T. Yoshimura, *Inorganica Chimica Acta*, 1981, **56**, 25–26.

141 P. Buglyó, T. Kiss, L. S. Erre, G. Micera, H. Kozlowski and S. Djemil, *Journal of Inorganic Biochemistry*, 1992, **46**, 49–66.

142 P. O'Brien, *Inorganica Chimica Acta*, 1983, **78**, L37–L38.

143 M. M. Shoukry and A. K. A. Hadi, 1989, **62**, 67–72.

144 F. Forghieri, C. Preti, G. Tosi and P. Zannini, *Australian Journal of Chemistry*, 1983, **36**, 1125.

145 C. Preti and G. Tosi, *Australian Journal of Chemistry*, 1980, **33**, 57.

146 B. Jayaram and N. M. M. Gowda, *Analytica Chimica Acta*, 1985, **173**, 381–386.

147 C. v. Barra, F. v. Rocha, L. Morel, A. Gautier, S. S. Garrido, A. E. Mauro, R. C. G. Frem and A. V. G. Netto, *Inorganica Chimica Acta*, 2016, **446**, 54–60.

148 P. P. Corbi and A. C. Massabni, *Spectrochimica Acta Part A: Molecular and Biomolecular Spectroscopy*, 2006, **64**, 418–419.

149 H.-H. Lee, N. Takeuchi, H. Senda, A. Kuwae and K. Hanai, *Spectroscopy Letters*, 1998, **31**, 1217–1231.